

NAVAL POSTGRADUATE SCHOOL

Monterey, California



THESIS

ANALYSIS OF SYMMETRIC REINFORCEMENT OF
QUASI-ISOTROPIC GRAPHITE-EPOXY PLATES
WITH A CIRCULAR CUTOUT UNDER UNIAXIAL
TENSILE LOADING

by

David H. Pickett and Patrick D. Sullivan

December 1983

Thesis Advisor:

M.H. Bank

Approved for public release; Distribution Unlimited.

T218322

REPORT DOCUMENTATION PAGE		READ INSTRUCTIONS BEFORE COMPLETING FORM
1. REPORT NUMBER	2. GOVT ACCESSION NO.	3. RECIPIENT'S CATALOG NUMBER
4. TITLE (and Subtitle) Analysis of Symmetric Reinforcement of Quasi-Isotropic Graphite-Epoxy Plates With a Circular Cutout under Uniaxial Tensile Loading		5. TYPE OF REPORT & PERIOD COVERED Master's Thesis; December 1983
7. AUTHOR(s) David H. Pickett and Patrick Sullivan		6. PERFORMING ORG. REPORT NUMBER
8. CONTRACT OR GRANT NUMBER(s)		
9. PERFORMING ORGANIZATION NAME AND ADDRESS Naval Postgraduate School Monterey, California 93943		10. PROGRAM ELEMENT, PROJECT, TASK AREA & WORK UNIT NUMBERS
11. CONTROLLING OFFICE NAME AND ADDRESS Naval Postgraduate School Monterey, California 93943		12. REPORT DATE December 1983
		13. NUMBER OF PAGES 111
14. MONITORING AGENCY NAME & ADDRESS (if different from Controlling Office)		15. SECURITY CLASS. (of this report) Unclassified
		15a. DECLASSIFICATION/DOWNGRADING SCHEDULE
16. DISTRIBUTION STATEMENT (of this Report) Approved for public release; distribution unlimited.		
17. DISTRIBUTION STATEMENT (of the abstract entered in Block 20, if different from Report)		
18. SUPPLEMENTARY NOTES		
19. KEY WORDS (Continue on reverse side if necessary and identify by block number) Composite Materials Stress Concentration Strain Field Finite Element Analysis Graphite/Epoxy Reinforcement		
20. ABSTRACT (Continue on reverse side if necessary and identify by block number) An experimental and computational analysis was made of the strain field around a reinforced circular hole in four HMF330/34 graphite/epoxy (G/Ep) panels under uniaxial tensile loading. The basic panel was a 10.0" wide, 26.0" long, eight ply, quasi-isotropic [0/+45/90] _s cloth laminate. Each panel was reinforced during manufacture by co-curing two circular plies of the same material to each side of the panel.		

#20 - ABSTRACT - (CONTINUED)

A circular one inch hole was drilled concentrically through the laminate to provide a stress concentration. Four different reinforcement geometries were used: a combination of [$+45, \dots$] or [$0/90, \dots$] additional plies with a total reinforcement^s volume equalling 163 or 203% of the removed hole volume. A prior investigation of similar, but asymmetrically reinforced panels demonstrated only a 5 to 12% improvement in ultimate strength over a similar but unreinforced panel with a cutout. The symmetric reinforcement reported here provided an improvement of 29 to 40% in ultimate strength over a similar but unreinforced panel under the same loading conditions. Test results indicated that panel failure would occur when the fibers in the dominating orientation (either $+45^\circ$ or $0/90^\circ$) were strained approximately 1%. There appeared to be a significant load transfer within the laminate at high strains from the failed $0/90^\circ$ to the $+45^\circ$ fibers. A finite element analysis was made and found in excellent agreement with experimental results.

Approved for Public Release; Distribution Unlimited

Analysis of Symmetric Reinforcement of Quasi-Isotropic
Graphite-Epoxy Plates with a Circular
Cutout under Uniaxial Tensile Loading

By

David H. Pickett
Captain, United States Army
B.S. United States Military Academy, 1973

and

Patrick Sullivan
Commander, United States Navy
B.S. United States Naval Academy, 1969

Submitted in partial fulfillment of the
requirements for the degree of

MASTER OF SCIENCE IN AERONAUTICAL ENGINEERING

from the

NAVAL POSTGRADUATE SCHOOL
/ December 1983

D. J. ...
M. ...
... 113

ABSTRACT

An experimental and computational analysis was made of the strain field around a reinforced circular hole in four HMF330/34 graphite/epoxy panels under uniaxial tensile loading. The basic panel was a 10.0x26.0 in. eight ply, quasi-isotropic $0/\pm 45/90_s$ cloth laminate. Each panel was reinforced during manufacturing by co-curing two circular plies of the same material to each side of the panel. A circular one inch hole was drilled concentrically through the laminate to provide a stress concentration. Four different reinforcement geometries were used: a combination of $[\pm 45, \dots]_s$ or $[0, 90, \dots]_s$ additional plies with the total reinforcement volume equalling 163 or 203% of the removed hole volume. A prior investigation of similar, but asymmetrically reinforced panels demonstrated only a 5 to 12% improvement in ultimate strength compared to an unreinforced panel. The symmetric reinforcement reported here provided an improvement of 29 to 40%. A finite element analysis was made and found to be in excellent agreement with the experimental results.

TABLE OF CONTENTS

I.	INTRODUCTION	12
	A. RECENT RESEARCH	14
II.	OBJECTIVES AND SCOPE	17
	A. PANEL REINFORCEMENT CONFIGURATION	18
III.	COMPUTATIONAL ANALYSIS	22
	A. LAMINATED PLATE ANALYSIS	22
	B. FINITE ELEMENT ANALYSIS	24
	1. Finite Element Mesh Generation	25
	2. Material Definition	27
	3. Post-Processing	27
IV.	EXPERIMENTAL ANALYSIS	30
	A. PANEL SELECTION AND CONSTRUCTION	30
	B. TEST APPARATUS AND PROCEDURES	32
	1. Apparatus	32
	2. Instrumentation	34
	3. Test Procedures	39
	C. EXPERIMENTAL RESULTS	40
	1. Assymetric Reinforcement Results	40
	2. Symmetrically Reinforced Panels Results	40
V.	DISCUSSION OF RESULTS	49
	A. SYMMETRIC REINFORCEMENT RESULTS	49
	1. 0/90° Reinforcement Orientation	49
	2. ±45° Reinforcement Orientation	50
	3. Asymmetric Round Reinforcements	51
	B. COMPARISON OF COMPUTATIONAL AND EXPERIMENTAL RESULTS	52
	C. FAILURE PREDICTION	52

VI.	SUMMARY AND CONCLUSIONS	54
A.	GENERAL	54
B.	SUGGESTED FURTHER RESEARCH	55
APPENDIX A:	PANEL 1A	56
APPENDIX B:	PANEL 1B	67
APPENDIX C:	PANEL 2A	80
APPENDIX D:	PANEL 2B	94
LIST OF REFERENCES	107
INITIAL DISTRIBUTION LIST	111

LIST OF TABLES

I.	Material Properties of HMF 330/34 Cloth	23
II.	Material Properties of The Laminate	24
III.	Comparison of Finite Element Computed Strain	29
IV.	Experimental Results: Failure Values	47
V.	Experimental Results: Failure Comparisons	48
VI.	Panel 1A: Strain Gage Locations and Strain at 10,000 psi (Far Field)	58
VII.	Panel 1B: Strain Gage Locations and Strain at 10,000 psi (Far Field)	69
VIII.	Panel 2A: Strain Gage Locations and Strain at 10,000 psi (Far Field)	82
IX.	Panel 2B: Strain Gage Locations and Strain at 10,000 psi (Far Field)	96

LIST OF FIGURES

2.1	Reinforcement Configuration, Type 1	19
2.2	Reinforcement Configuration, Type 2	21
3.1	Panels 1A and 1B Shell Element Mesh	26
3.2	Shell Elements Near the Cut-Out	28
4.1	Basic Panel Dimensions (in inches)	31
4.2	Test Apparatus	33
4.3	Tension Attachment Device with Panel 1A	35
4.4	Photoelastic Reflection Polariscopes	38
4.5	Panel 2B: Load Comparison	46
A.1	Panel 1A: Strain Gage Locations	57
A.2	Panel 1A: Strain Along X Axis at 10,000 psi	59
A.3	Panel 1A: Microstrain vs. Tensile Load	60
A.4	Panel 1A: Photoelastic Panel at 5,000 psi	61
A.5	Panel 1A: Photoelastic Panel at 10,000 psi	61
A.6	Panel 1A: Photoelastic Panel at 15,000 psi	62
A.7	Panel 1A: Photoelastic Panel at 20,000 psi	62
A.8	Panel 1A: Fracture Line	63
A.9	Panel 1A: $\epsilon_{ps}-Y$ ($\times 10^6$) Contours Near Cutout	64
A.10	Panel 1A: $\epsilon_{ps}-X$ ($\times 10^6$) Contours Near Cutout	65
A.11	Panel 1A: $\epsilon_{ps}-XY$ ($\times 10^6$) Contours Near Cutout	66
B.1	Panel 1B: Strain Gage Locations	68
B.2	Panel 1B: Strain Along X Axis at 10,000 psi	70
B.3	Panel 1B: Microstrain vs. Tensile Load	71
B.4	Panel 1B: Photoelastic Panel at 5,000 psi	72
B.5	Panel 1B: Photoelastic Panel at 10,000 psi	72
B.6	Panel 1B: Photoelastic Panel at 15,000 psi	73
B.7	Panel 1B: Photoelastic Panel at 20,000 psi	73
B.8	Panel 1B: Photoelastic Panel at 25,000 psi	74
B.9	Panel 1B: Photoelastic Panel at 30,000 psi	74
B.10	Panel 1B: Photoelastic Panel at 35,000 psi	75

B.11	Panel 1B: Photoelastic Panel at 40,000 psi . . .	75
B.12	Panel 1B: Fracture Line	76
B.13	Panel 1B: Eps-Y ($\times 10^6$) Contours Near Cutout . .	77
B.14	Panel 1B: Eps-X ($\times 10^6$) Contours Near Cutout . .	78
B.15	Panel 1B: Eps-XY ($\times 10^6$) Contours Near Cutout . .	79
C.1	Panel 2A: Strain Gage Locations	81
C.2	Panel 2A: Strain Along X Axis at 10,000 psi . .	83
C.3	Panel 2A: Microstrain vs. Tensile Load	84
C.4	Panel 2A: Photoelastic Panel at 5,000 psi . . .	85
C.5	Panel 2A: Photoelastic Panel at 10,000 psi . . .	86
C.6	Panel 2A: Photoelastic Panel at 15,000 psi . . .	87
C.7	Panel 2A: Photoelastic Panel at 20,000 psi . . .	87
C.8	Panel 2A: Photoelastic Panel at 25,000 psi . . .	88
C.9	Panel 2A: Photoelastic Panel at 30,000 psi . . .	88
C.10	Panel 2A: Photoelastic Panel at 35,000 psi . . .	89
C.11	Panel 2A: Photoelastic Panel at 40,000 psi . . .	89
C.12	Panel 2A: Fracture Line	90
C.13	Panel 2A: Eps-Y ($\times 10^6$) Contours Near Cutout . .	91
C.14	Panel 2A: Eps-X ($\times 10^6$) Contours Near Cutout . .	92
C.15	Panel 2A: Eps-XY ($\times 10^6$) Contours Near Cutout . .	93
D.1	Panel 2B: Strain Gage Locations	95
D.2	Panel 2B: Strain Along X Axis at 10,000 psi . .	97
D.3	Panel 2B: Microstrain vs. Tensile Load	98
D.4	Panel 2B: Photoelastic Panel at 5,000 psi . . .	99
D.5	Panel 2B: Photoelastic Panel at 10,000 psi . . .	99
D.6	Panel 2B Photoelastic Panel at 15,000 psi . .	100
D.7	Panel 2B Photoelastic Panel at 20,000 psi . .	100
D.8	Panel 2B Photoelastic Panel at 25,000 psi . .	101
D.9	Panel 2B: Photoelastic Panel at 30,000 psi . .	101
D.10	Panel 2B: Photoelastic Panel at 35,000 psi . .	102
D.11	Panel 2B: Photoelastic Panel at 45,000 psi . .	102
D.12	Panel 2B: Fracture Line	103
D.13	Panel 2B: Eps-Y ($\times 10^6$) Contours Near Cutout .	104

D.14	Panel 2B: Eps-X ($\times 10^6$) Contours Near Cutout .	105
D.15	Panel 2B: Eps-XY ($\times 10^6$) Contours Near Cutout .	106

ACKNOWLEDGEMENTS

The authors wishes to express their most grateful appreciation to Professor Milton Bank for his guidance and enthusiasm and Drs. J.A. Bailie and N. Cyr of Lockheed Missiles and Space Company for their infinite patience and words of wisdom. The value of the technical assistance provided by Robert A. Besel, Ted B. Dunton, and Glenn A. Middleton in the manufacturing of test aparatus, set-up of test equipment, and data taking was immeasurable. Funding, without which this study would not have been possible, was provided by the U.S Navy Strategic Systems Project Office, for which the authors extend their thanks.

I. INTRODUCTION

In the 1980's high modulus, advanced composite materials are seeing more use in aerospace structural applications than ever before. Their superiority to the metals they replace has been well documented. However, until quite recently designers have been reluctant to use the most valuable characteristic of laminated composites: their directional properties. When faced with typical design unknowns, the choice is usually to take a weight penalty and add additional laminate plies. This added weight can be very costly in some applications; other methods must be sought if composites are to fulfill their potential.

Advanced composite materials, carbon/epoxy (C/Ep) and graphite/epoxy (G/Ep) in particular, are seeing increased use in the production of aircraft, missiles and space vehicles primarily due to advantages in weight, stiffness and thermal properties. A few hundred pounds of saved weight in a commercial airliner or military tactical jet can be worth millions of dollars in reduced life-cycle cost. Additional weight reductions are possible by using the directional properties of composites and by placing reinforcement properly at areas of stress concentrations. This report examines one aspect of using these geometric and directional properties applied to reinforcing around cutouts in G/Ep plates under uniaxial tension.

Difficulties in development, manufacture and quality control have been the primary factors responsible for the high cost of composites. As pointed out by Delmonte [Ref. 1], the decreasing cost of the composite prepreg material is approaching the increasing cost of aircraft grade metals. The F-18 and AV-8B are examples of flight vehicles with

significant percentages of primary structure fabricated from composites. The decrease in overall weight and increase in performance and life-cycle savings offset their higher initial cost. A significant further weight saving, even in these aircraft, could have been accomplished with a more aggressive design. It will take a number of years and, no doubt, a few mistakes to fully utilize composite materials' potential. The Army's Advanced Composite Airframe Program (ACAP) is an example of advanced design with composites. Well over 90% of the primary and secondary structure of the two current competing designs are either Kevlar, fiberglass or carbon/graphite composites [Ref. 2 & 3].

Until recently the majority of applications of composites has been limited to those in which the laminate properties closely resemble those of homogeneous, isotropic materials such as metals. Simple geometric designs utilizing quasi-isotropic laminates have been preferred, according to Tsai [Ref. 4], because they are easier to understand and their behavior is easier to predict than that of directionally oriented composites. The inability to accurately predict every loading condition has made designs very conservative. These safety considerations have resulted in an overdesign of parts in order to guarantee adequate strength under "unpredictable" circumstances [Ref. 5 & 6].

In aircraft construction it has always been necessary to have holes and cutouts in load carrying structure. An aircraft wing spar, for example, requires access holes for control rods, fuel lines, and electrical wiring. The presence of these stress concentrators requires that either the entire member be designed accept the increase in local stress or that reinforcement be applied around the areas experiencing higher stress. The first method requires an excessive increase in weight, the second, more expensive and

time-consuming analysis and manufacturing techniques. This report examines the effect of reinforcing around a hole to reduce the local stress. In applications where light weight and high strength are required at some cost in ease of manufacture, this seems to be a promising avenue of research.

A. RECENT RESEARCH

When the current research into the effects of stress concentrations in composite materials was reviewed little could be found in the area of reinforcement of holes or cutouts. There are, however, a number of related reports covering the effect of loaded and unloaded holes in composite plates.

Several studies by Rowlands, Daniels and Whiteside [Refs. 7-9] have found that the manner of diffusion of strain around a hole in a composite panel was dependent on the material properties of the laminate. It was noted that the nondimensional hole-diameter-to-panel-width ratio (d/b) did not affect the maximum value of the stress concentration factor (SCF), but it did affect the slope of the stress gradient near the hole. Smaller d/b ratios have higher stress gradients close to the hole. The effect of the stress concentration dies off more rapidly with decreasing hole size. The laminate's stacking sequence was found to have a major effect on the diffusion of stress around a cutout in a orthotropic panel. Konish [Ref.10] also noted that the SCF for a quasi-isotropic material was approximately three; however, he states that SCF is not an adequate measure of strength of a composite laminate containing a circular cutout. He pointed out that for a laminate with plies only in the direction of the applied load the theoretical SCF approached seven. Further he states that the strength of a composite plate with a hole appears to be

related to the "in-plane elastic stress within a region adjacent to the hole boundary".

The hole-size effect is also discussed by Daniel, et al [Ref. 7], and Waddoups, et al [Ref. 11]. They show that a hole diameter of 1.0 inch in a panel with dimensions to produce d/b of less than 0.4 reduces the SCF in composites. This reduction is somewhat misleading because it comes from increasing the far field stress rather than reducing stress next to the cutout. Smaller holes increase the SCF, while larger holes increase the d/b ratio which reduces the area over which the stress can diffuse around the hole, thus reducing the SCF.

Due to their inherently brittle nature advanced composites tend to be highly sensitive to stress raisers. They have demonstrated, however, higher than predicted ultimate strength. This is generally attributed to load transfer among fibers during strain induced failure and interlaminar shear behavior. Garbo states [Ref. 12] that his panel strengths were 25 to 50% higher than theoretical stress concentrations would indicate. For other than uniaxial loads failure was shown to initiate at locations away from peak stress concentrations. He stated "...laminate failure is predicted by comparing elastic stress distributions with material failure criteria on a ply-by-ply basis at a characteristic dimension away from the hole boundary." Whitney [Ref. 13] discusses the characteristic distance (d_0) which is the distance away from the discontinuity where the strength is equal to that of the unnotched panel. This distance is sufficient to contain an "inherent flaw" in the material where failure can initiate; and therefore, the concept of predicting the strength of a brittle material at a single point seems questionable. A study by Bailie, et al [Ref. 14], showed that strain gages near a hole demonstrated nonlinear responses at 80% of the failure stress which were associated with "highly localized fiber and resin damage".

The inherent nonhomogeneity (acting somewhat like flaws in metal) of multi-directional composite laminates suggests to Kim [Ref. 15] that the first ply failure (FPF) is dependent on the type laminate, material properties, and residual stresses within the laminate. Premature FPF can be caused by residual stresses remaining from the curing process, but the FPF does not lead immediately to panel failure. The ultimate panel failure is invariably preceded by the failure of weaker plies, plies oriented in the direction of load, and interlaminar load transfer when possible.

The reinforcement of notches in composite panels by the use of G/Ep rings has been investigated by McKinzie [Ref. 16]. Some of the problems associated with asymmetric reinforcement and separate curing of panels and reinforcements were discussed. Whiteside, Rowlands and Daniel [Ref. 7] investigated the benefits of different materials, lay-ups, panel thickness, and compared effects of circular to elliptic holes as well as the effects of hole edge roughness. The actual use of reinforcement was not studied; however, they showed that doubling of thicknesses for panels with holes produced improvements of only 20% in strength over single thickness panels. A study of the effects of asymmetric (one side only) reinforcement of panels with cutouts under tension was made by O'Neill [Ref. 17]. His work led directly to this study, and will be discussed below.

II. OBJECTIVES AND SCOPE

The objective of this investigation was to determine the benefits of symmetric reinforcement of a quasi-isotropic G/Ep panel containing a stress concentration due to a drilled circular hole. This study was suggested as a continuation of an investigation of asymmetric reinforcement of the same type panels by O'Neill [Ref. 17]. Initially, asymmetric reinforcement was considered desirable from the point of view of the ease of manufacture. Reinforcing only one side of the panel circumvents some problems in mating it to other parts and allows manufacturing (layup) of panels on flat metal sheets. The strength of the asymmetrically reinforced, notched panel was found to be only 5 to 12% greater than that of a similar but unreinforced panel. This small improvement, in light of the small sample size and possible experimental error, may represent very little actual improvement. Certainly, based on any cost (of manufacture) to benefit ratio, there was no improvement. The concept of cutout reinforcement was narrowed to symmetric (both sides of a panel) by O'Neill.

From the standpoint of weight, a reinforcement should be a small percentage of the component's total weight. A good measure of weight reduction is the ratio of reinforced to unreinforced panel weight for the same stress (or strain) concentration around a cutout. Obviously adding additional plies over the whole surface will increase the area over which the load must act and reduce average stress. This, however, puts a lot of material where it is not needed. By selectively adding material around the the hole stress should be reduced with only a small increase in weight. This approach would seem to have merit only if there is

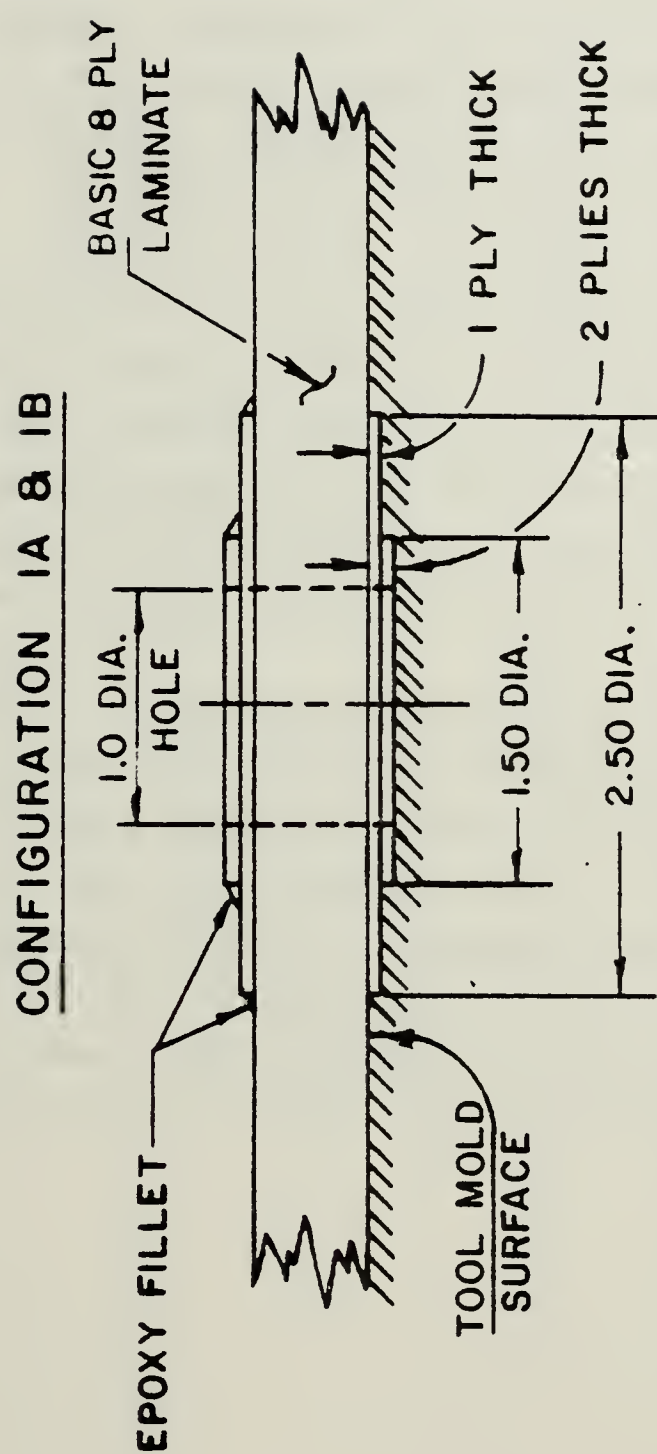
significant stress reduction, due to the increase in manufacturing and quality assurance costs. Any competitive design must satisfy the scrutiny of a cost/benefit analysis.

O'Neill attributed asymmetric reinforcement's small effectiveness to possible delamination near the ultimate load due to induced curvature [Ref. 17: pp 93-4]. He found significant differences between front and back surface strains close to the notch, indicating that the panels deflect away from the reinforced side at the hole. The reinforced side being stiffer than the unreinforced (back) side caused this bowing of the panel. The stress gradient through the thickness of the panel at the edge of the hole was from high tensile stress on the back side to lower tensile stress on the reinforced side. This induced an additional interlaminar shear superimposed over that expected due to differing adjacent ply orientations.

To avoid the induced curvature and associated premature delamination problem, symmetry was recommended. Symmetry for this investigation was achieved by co-curing identical reinforcements on both sides of the panels. Submerging the reinforcement layers below layers of the laminate to gain symmetry was considered, but the added problems of verifying the reinforcement ply orientation and the curvature of the outer layers over the reinforcements caused rejection of this option in favor the "wedding cake" geometry.

A. PANEL REINFORCEMENT CONFIGURATION

This investigation considered four configurations of reinforcement. These circular reinforcements consisted of two small, circular, concentric plies added to each side of a basic quasi-isotropic G/Ep panel with a centrally located one inch diameter hole through the thickness of the panel.



CONFIGURATION IA HAS ITS REINFORCING PLATES AT 0°
 CONFIGURATION IB HAS ITS REINFORCING PLATES AT $\pm 45^\circ$

Figure 2.1 Reinforcement Configuration, Type 1.

The center of the hole was designated the axis origin. The X axis extends horizontally across the width of the panel; the Y axis extends vertically upward in the direction of the applied tension. The reinforcing plies were centered on the hole center. Figures 2.1 and 2.2 show the cross-sections of the two reinforcement configurations. In each case the reinforcements consisted of two plies on each side of the panel. The reinforcing ply next to the base panel surface had a 1.25 inch radius. For Type 1 reinforcements, the outer ply had a 0.75 inch radius, while the Type 2 reinforcements had an outer radius of 1.0 inch. Each type of reinforcement was manufactured with two reinforcement orientations: "A" reinforcements were oriented $\pm 45^\circ$ to the load axis, while "B" reinforcements were oriented 0/90°. O'Neill analyzed these configurations, but did not test them experimentally.

Computational and experimental methods were used which closely (if not exactly) followed procedures used in Reference 17. Where deviations have occurred, they are noted and explained. This investigation did not try to reiterate theoretical and computational analysis previously done, but does reference materials published since that study was made and elaborates upon areas researched further. Panel dimensions and construction details are discussed in Section IV.A.

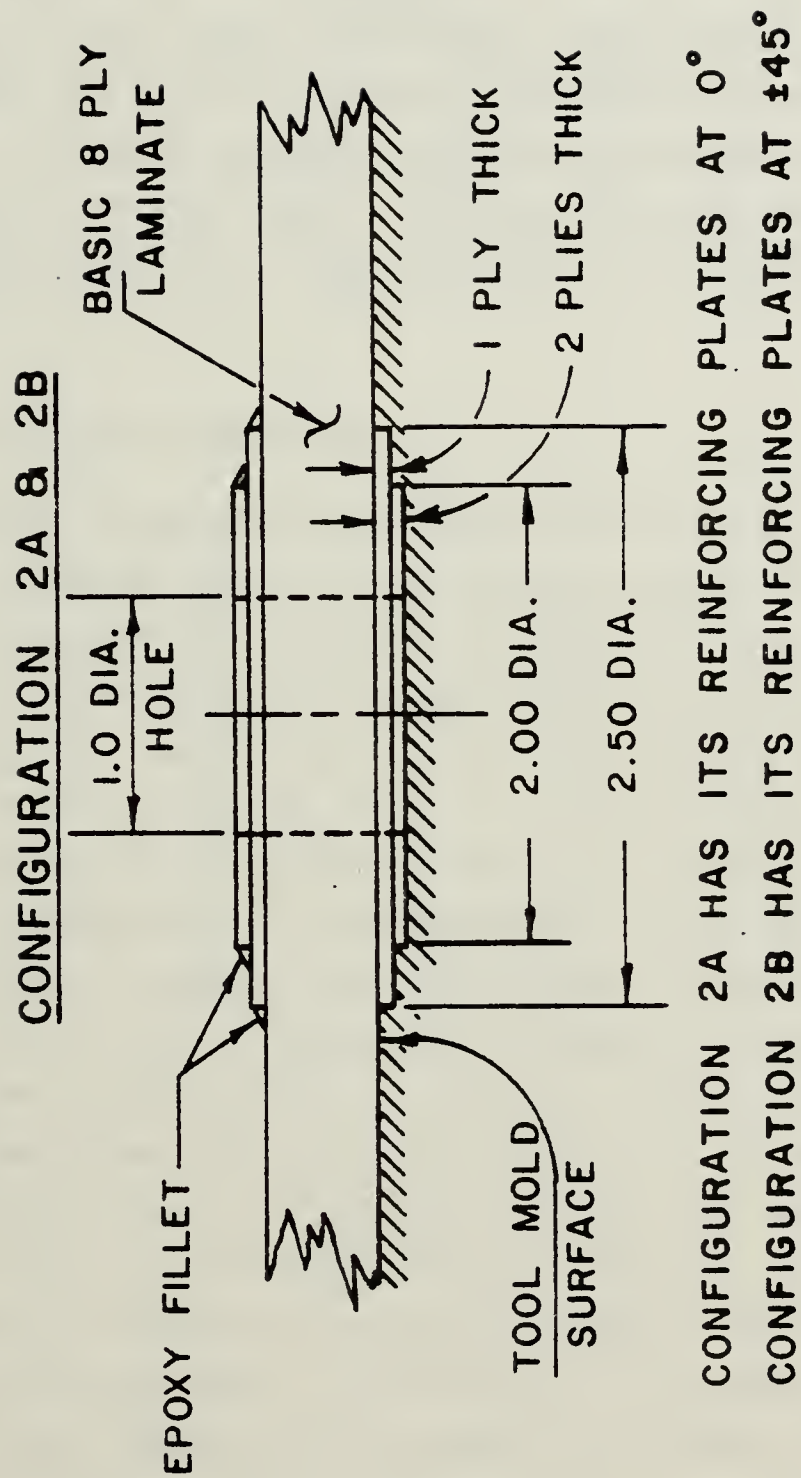


Figure 2.2 Reinforcement Configuration, Type 2.

III. COMPUTATIONAL ANALYSIS

The panel laminate was analyzed using both open and closed form methods. Standard laminate analysis using Tsai's approach [Ref. 4] determined the material properties of the panel in the quasi-isotropic (far-field) area and in the area close to the hole which included the co-cured reinforcement. A finite element analysis was made of each of the four panels using DIAL, a versatile code developed by Lockheed Missile & Space Company (LMSC), Sunnyvale, CA [Ref. 18].

A. LAMINATED PLATE ANALYSIS

The material properties of cured HMF 330/34 graphite/epoxy cloth prepreg used in the computational and experimental analysis are given in Table I. It should be noted that E_1 and E_2 refer to the moduli in the principal ply direction (1) and 90° to it (2) in the ply coordinate system, and that E_x and E_y refer to the laminate coordinates. The material properties of cloth differ markedly from those of tape 90° to the principal axis due to the influence of the crossply (woven) fibers. Even in cloth material there is some difference between E_1 and E_2 , primarily determined by the fiber to matrix ratio and the weaving process. Composite cloth prepreg is not, in itself, quasi-isotropic despite the nearly equal moduli E_1 and E_2 . The shear modulus (G) is too low; quasi-isotropic properties in composites are a result of an equal angular distribution of ply principal directions: $[0, \pm 45, 90]_s$ or $[0, \pm 60]_s$.

The four test panels were supplied by LMSC who also provided preliminary data on the material. Subsequent testing demonstrated that the cured panels had a slightly lower modulus (about 9%) than LMSC predicted. The initial

material properties were revised and subsequently demonstrated excellent correlation between closed and open form analysis and the experimental results. Any effect of the

TABLE I
Material Properties of HMF 330/34 Cloth

Tension	E1: 9.8×10^6 psi	E2: 8.8×10^6 psi
Compression	E1: 8.5×10^6 psi	E2: 8.1×10^6 psi
Shear	G12: 1.0×10^6 psi	
Poisson	ν_{12} : 0.09	

differences between tensile and compressive moduli was not taken into consideration. The areas of compressive strain did little to cause panel failure.

The analysis of the basic laminate was made using the computer program RSQ adapted by Sullivan [Ref. 19] from a earlier program developed by General Dynamics, Fort Worth. The laminate properties are listed in Table II. The characteristics of the laminates are apparent. It can be seen that the unreinforced portion (far-field) $[0, \pm 45, 90]_s$ is quasi-isotropic. This is the 8 ply laminate forming the basic panel. The other two configurations represent the basic panel combined with reinforcement plies close to the cutout. Panels 1A and 2A ($[0, 90, \pm 45, 90]_s$) have higher moduli except in shear. Panels 1B and 2B ($[\pm 45, 0, \pm 45, 90]_s$) have equal moduli in the X and Y direction but are much stiffer in shear. This difference in shear modulus may be seen in the photoelastic photographs of each panel under stress as well as the finite element generated contours of strain in Appendices A through D.

TABLE II
Material Properties of The Laminate

Laminate	No. of Plies		E_x	E_y	G_{xy}	ν_{xy}	Remarks
	0/90°	±45°					
[0,±45,90]s	4	4	7.03	7.03	2.83	0.244	Base Panel
[0,90,0,±45,90]s	8	4	8.06	7.74	2.22	0.154	"A" Config.
[±45,0,±45,90]s	4	8	6.00	6.00	3.43	0.354	"B" Config.

(Modulus x10⁶ psi)

Note: The base panel properties exist everywhere on the panel except at the reinforcement around the cutout. The "A" and "B" configurations are the properties immediately next to the cutout where the reinforcement is two plies thick on each side.

Because of the discontinuities in material properties and laminate thickness it is not currently possible to analyze these panels using the closed form mathematics presented by Garbo and Ogonowski for plain panels with circular cutouts [Ref. 12].

B. FINITE ELEMENT ANALYSIS

Experimental tests are both expensive and time consuming. If it can be shown that panel reinforcement can be successfully modeled, then optimization can be accomplished using numerical methods and only the final configurations need to be built and validated experimentally. It has been pointed out that closed form solutions do not exist for laminated panels in these reinforced configurations. Finite element analysis was required to predict the panels' response to a uniaxial tensile load. A finite element analysis system named DIAL developed by LSMC Structures Organization was used in this analysis.

DIAL is a general purpose two- and three-dimensional finite element analysis system. It consists of a family of independent programs (executable modules) called processors. The processors read and write to a data base established for each problem. The processors are executed in a logical order and may be rerun individually without restarting the analysis from the beginning. DIAL's library of elements consists of multi-order isoparametric solid and corresponding degenerate curved shell and plate elements. The material library can handle general anisotropic linear materials, isotropic elastic-plastic, nonlinear elastic orthotropic, isotropic incompressible, etc. An extensive library of post-processing routines allow for analysis of developed data and plotting in a wide number of modes. The analysis required for a notched panel under uniaxial tension was relatively simple. The panels' geometry was defined by generating a "mesh", the material properties of each ply were specified, the loading conditions were applied and the results tabulated and plotted.

1. Finite Element Mesh Generation

A two-dimensional modified thick shell isoparametric quadrilateral element was chosen as the best in terms of accuracy and computer time to develop the mesh. The element has a node at each of the four corners and one on each element side allowing a parabolic representation. This mesh was an improved version of the one O'Neill developed. An effort was made to keep the interior angles of the element as equal as possible to increase the accuracy. Figure 3.1 shows a typical mesh for the panel. Taking advantage of symmetry, only the upper right quadrant of each panel was modeled. Figure 3.2 is the mesh closer to the cutout showing the node numbering method and the element modeling.



Figure 3.1 Panels 1A and 1B Shell Element Mesh.

In order to increase the density of the mesh without drastically increasing run times nodal degrees of freedom were reduced. Since the panels were symmetric through the thickness, out of plane deflections (Z direction) were suppressed. Several test runs demonstrated that nodal rotation was virtually nil. Suppressing these rotations reduced run time by about 80%.

2. Material Definition

Material definition follows the method of superposition. The material properties of a single ply of G/Ep cloth are first defined (see Table I). Then the number of plies and ply orientation for each element is combined using linear laminate theory. This is done in the DIAL "MATL" processor. In this manner each element of the mesh may be assigned specific properties.

3. Post-Processing

The parabolic isoparametric element produces stress and strain reactions at four Gauss points in the element interior. These points were somewhat off the true X axis. A DIAL routine was used to extrapolate values at the Gauss points to nodes on the X axis ($Y=0$). The strain field in each panel was calculated and plotted using contours of strain in the X direction, Y directions and in shear (ϵ_{ps-X} , ϵ_{ps-Y} and ϵ_{ps-XY}). These contour plots are included in Appendices A through D, Figures A.9-11, B.13-15, C.13-15 and D.13-15. Table III lists the maximum and minimum values of micro-strain in each panel as calculated by the finite element program. It is interesting to note that the "A" configuration (0/90° reinforcement) induces relatively high shear strains. Also, note that the difference in maximum tensile strain in the Y direction between the 163% and 206% reinforced cutouts in both the "A" and "B" configurations is less than 2%.

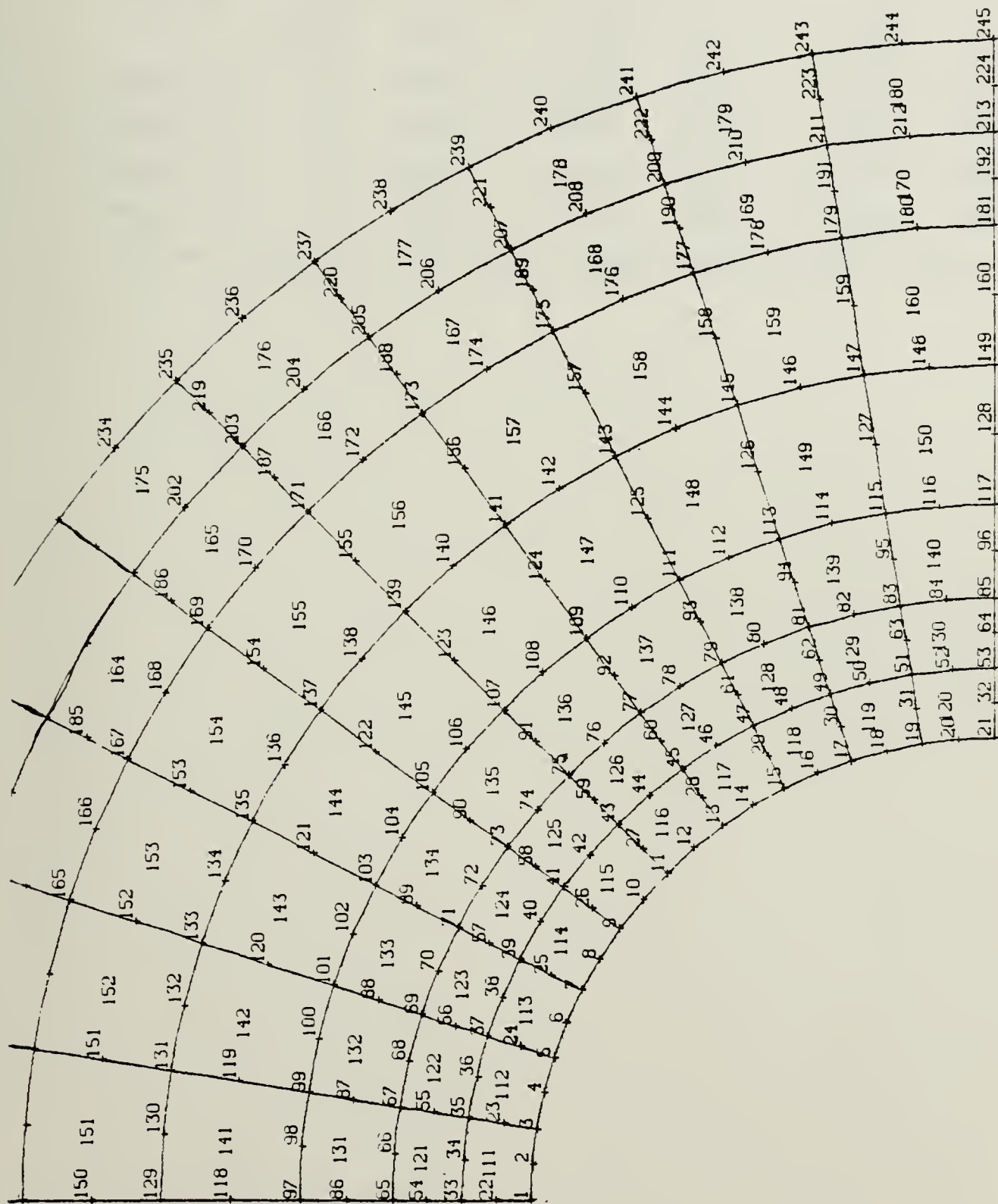


Figure 3.2 Shell Elements Near the Cut-Out.

TABLE III
Comparison of Finite Element Computed Strain

Strain:	eps-Y		eps-X		eps-XY	
	MIN	MAX	MIN	MAX	MIN	MAX
Panel 1A	0	3400	-1145	325	-681	3226
Panel 1B	0	3575	-1559	368	-439	2235
Panel 2A	0	3335	-1134	317	-675	3150
Panel 2B	0	3525	-1526	360	-444	2202

Note: Strain is shown in micro-strain (eps x 10⁶)

IV. EXPERIMENTAL ANALYSIS

The objectives of the experimental testing were to verify analytical and computational results. A comparison could then be made between computational and experimental results for the symmetric and asymmetric methods of reinforcement. All four of the symmetric reinforcement configurations analyzed by the DIAL finite element program were experimentally tested.

A. PANEL SELECTION AND CONSTRUCTION

The basic panel dimensions and layup were replicas of the panels tested or analyzed by O'Neill [Ref. 17: p 56]. The dimensions are shown in Figure 4.1. The layup of the basic panel consisted of eight layers of HMF 330/34 graphite epoxy cloth. The orientations of the plies was $[0/\pm 45/90]_s$, to produce a thin, high strength panel with quasi-isotropic properties. The panel dimensions (thickness, length and width) and hole size were chosen so as to be the same order of magnitude as an actual airframe component. The reinforcement plies were of the same material, and were co-cured along with the basic panels during manufacture. This was done in lieu of reinforcing a cured specimen in order to avoid bonding problems and the possibility of non-uniform curing of the reinforcement plies. A tooled surface was necessary during the manufacture of the panels to allow the placement of the reinforcement on the underside of the panel. A flat steel plate was machined to the required depth and geometry. This method produced a panel with a smooth (plate side) surface on one side and a rougher (bag side) surface on the other. The dimensions of the

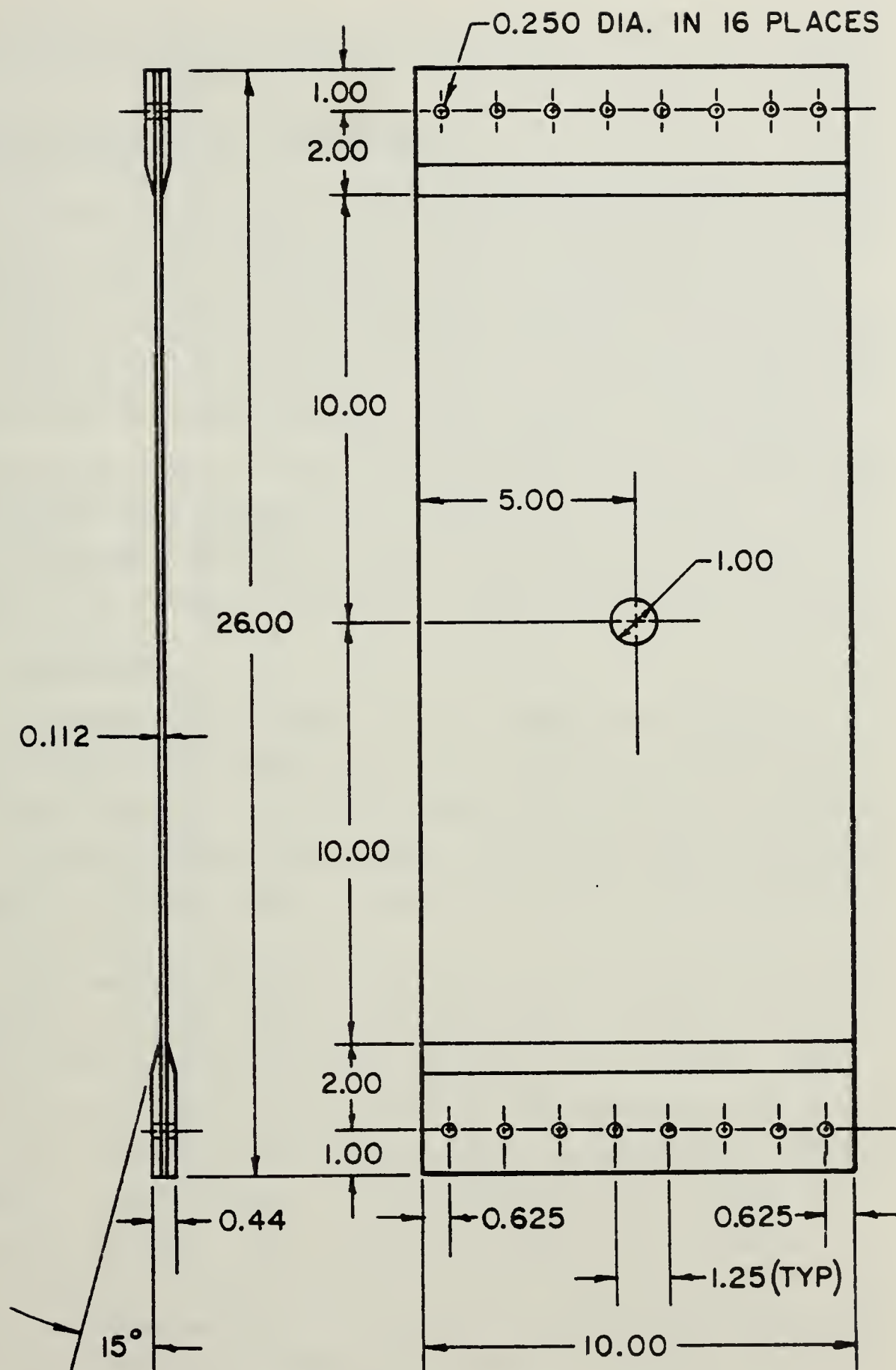


Figure 4.1 Basic Panel Dimensions (in inches).

reinforcements were cut into the steel plate at right angles into the surface (see Figs. 2.1 and 2.2).

B. TEST APPARATUS AND PROCEDURES

The testing procedures and equipment setup were designed to produce the same conditions used in O'Neill's tests of the asymmetrically reinforced panels. One difference in testing was the use of a photoelastic plastic coating on one side of the panel. The panels were all loaded in the test machine below the level of any fiber failure for several repetitions in order to take preliminary data and experiment with the photoelastic material measuring procedures. The number of loading cycles in each case was less than ten, well below the number which might cause any fatigue damage.

1. Apparatus

A Riehle PS 300 test machine was used to apply uniaxial tension to each panel. To distribute the load across the width of the panel's top and bottom a "whiffle tree" attachment device was used. The device was designed and built by O'Neill and was used in an identical manner (see Fig. 4.3).

The test panels were bolted to the whiffle tree and then secured in the Riehle's tension jaws. Eight bolts torqued to 100 in-lbs held the plates to the panels, and four bolts transferred the load from the whiffle tree to the plates. The whiffle tree was designed to withstand 100,000 lbs load in order to test the unnotched panel during the asymmetric testing. The unnotched sample was expected to fail at around 67,000 lbs and actually failed at 65,000 lbs allowing for greater than 50% safety margin. The attachment device was constructed using 4130 Steel, and all the bolts were high strength, close tolerance steel bolts.

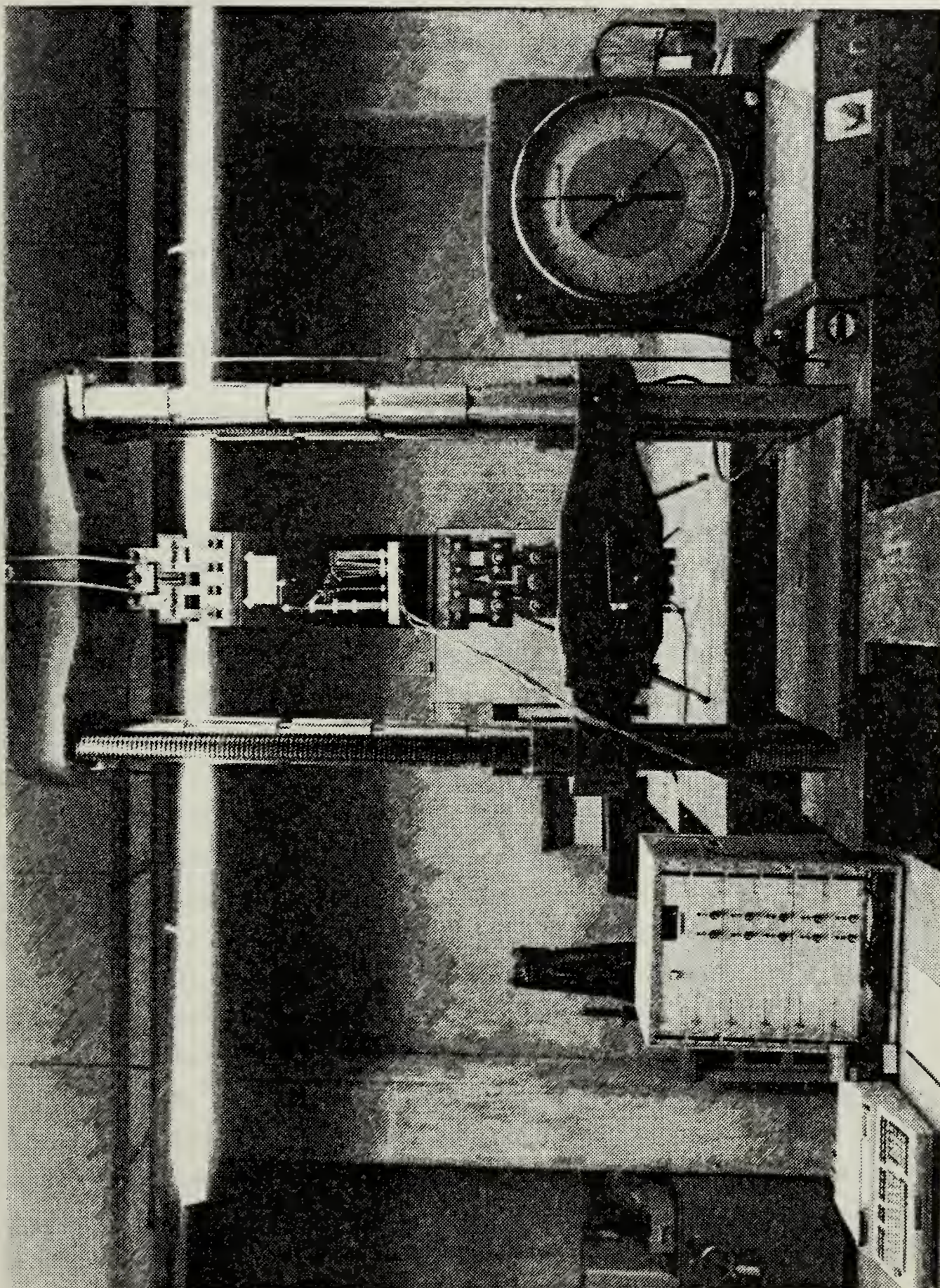


Figure 4.2 Test Apparatus.

2. Instrumentation

Two methods of acquiring strain data from the test panels were used. Strain gages were applied to one side of the panel and contourable photoelastic plastic was bonded to the other. It was thought that the redundancy of data obtained would provide a cross-check to verify the results. The photoelastic coating would also provide photographic evidence of the strain distribution around the cutout.

a. Strain Gages

Vishay Micro-Measurements 120, 350 and 5000 ohm strain gages were used to measure the strain at points of interest. O'Neill's study showed that asymmetric reinforcement configurations had induced curvature near the hole, with a resultant strain gradient through the thickness. For this study, since both the base panels and the reinforcements were symmetric there were no out-of-plane deflections, and strain was constant through the thickness at any point. Thus strain gages could be applied to only one side of the panel without loss of data.

Strain gages were concentrated along the X axis, (perpendicular to the load direction), primarily oriented in the load direction (see Figs. A-D.1 and Tables VI-IX in the appendices). Small strain gages (0.08 in. along a side) having 5,000 ohm resistance were placed closest to the hole and on the reinforcement layers. The 5,000 ohm gages were chosen to minimize problems due to self-heating and apparent strain drift. Sullivan discusses this phenomena in his study of plates under compressive loading [Ref. 21]. The small gage length was chosen because the overall error for integrating strain gradient is proportional to the gage's length. Reference 22 discusses methods of measuring high strain gradients around stress concentrations and the errors which may occur.

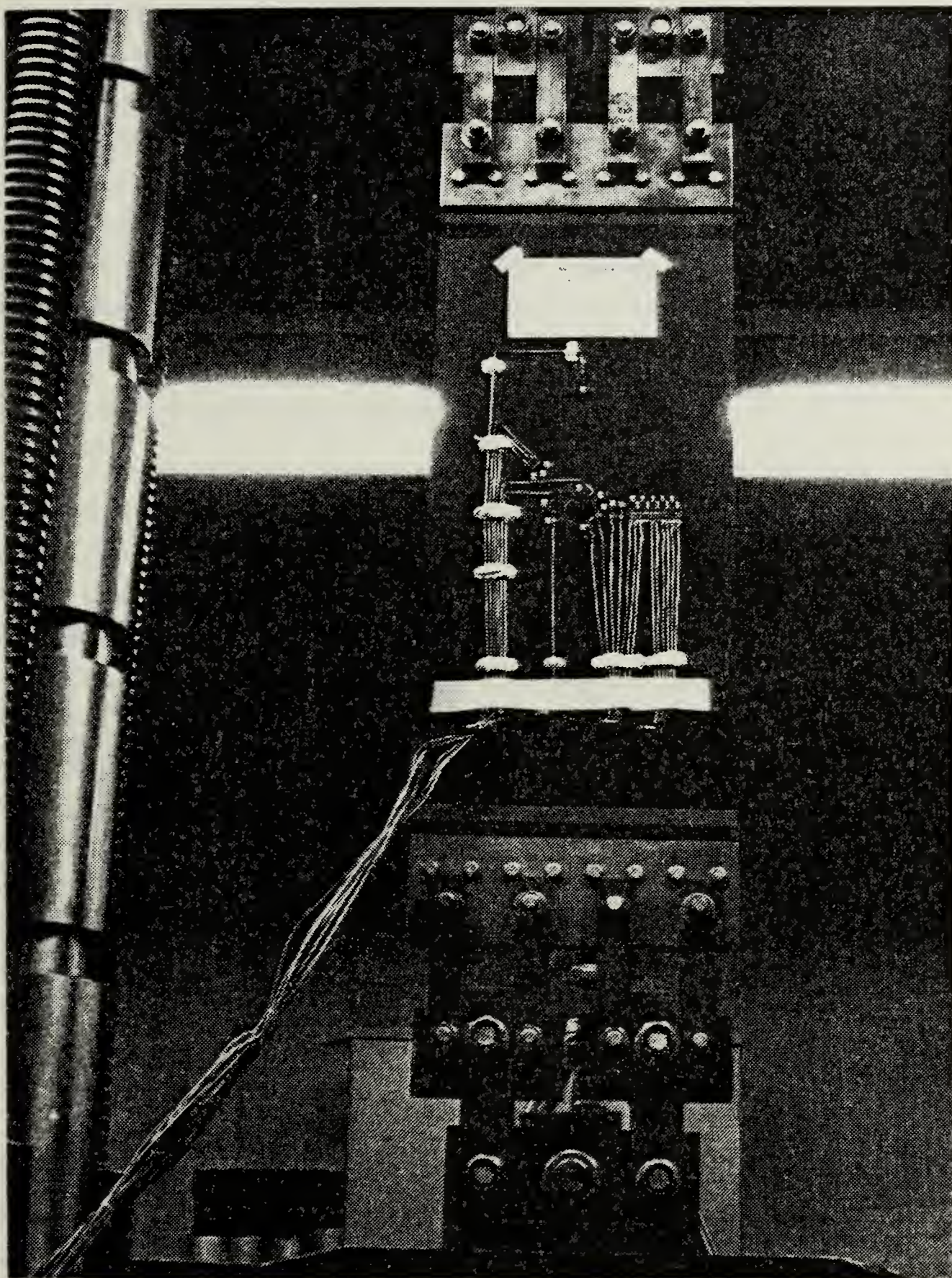


Figure 4.3 Tension Attachment Device with Panel 1A.

The number of gages, their type and location varied with each panel. As experience was gained from the preceding panels, the best location and type gage was sought for the strain distribution and laminate layup. Standardization of strain gage locations among the panels was not used due to different reinforcement sizes and layup. A close approximations of gage locations was attempted to facilitate comparison of data. The information for each panel gage layout is given in Tables VI-IX, and Figures A-D.1, in the appropriate appendix.

b. Strain Gage Measurements

A Vishay Measurements Group System 4000 was used for strain gage scanning, data recording and reduction. The system consisted of a Hewlett-Packard 9825T desktop computer with a controlling software program, and five Vishay Measurements Group Model 4270 Strain Gage Scanners mounted in parallel resulting in a one hundred channel capability (see Fig. 4.2). The system was used with automatic temperature compensation channels for the different types of strain gages. Channel assignment and gage factors for all the gages were initialized, and all rosettes designated. The system recorded and reduced all data when commanded. It is capable of automatic (at set time intervals) data recording, but that feature was not utilized for this experiment. Instead, data was taken on command at fixed load intervals.

c. Photoelastic Coating

Due to the reinforcement geometry around the hole it was necessary to use a contourable photoelastic coating. Its thickness was chosen to give a good color definition and not significantly add to the reinforcement. The material has a nominal modulus of 420,000 psi. The procedures specified by the manufacturer for casting and

application were followed [Ref. 23]. The thickness of the photoelastic coating was kept to a minimum to prevent any significant reinforcement to the composite material. The first two panels, 1A and 2A, received coatings approximately 0.080 in. thick, while the last two panels' coatings were reduced to 0.060 in. as the experimenters' abilities increased with experience. The photoelastic plates were bonded to the panels with a reflective, epoxy glue.

d. Photoelastic Measurement Equipment

A Photoelastic Reflective Polariscopes, Model 030, from Photoelastic Inc. was used to make strain measurement from the photoelastic coating. The Basic Analyzer, Model 031, consists of two ball bearing mounted Polarizer-Quarter Wave Plate Assemblies attached to a common frame, and mechanically connected so as to rotate in unison. The assembly was equipped to receive the (polarized) light source and accessories for measurements of strain (see Figure 3.7). The Basic Analyzer measures three major pieces of data:

1. The directions of the principal strains or stress.
2. The magnitude and sign of the tangential stress at free boundaries, or in any region of uniaxial stress condition.
3. The magnitude of the difference of the principal strains.

In order to separate the principal strains, an Oblique Incidence Adapter, Model 033, was used. The Oblique Incidence Adapter attached directly to the Basic Analyzer. With the two measurements obtained (normal and oblique incidence) and the two unknown principal strains, the equations can be solved for principal strains as is detailed in Reference 24.

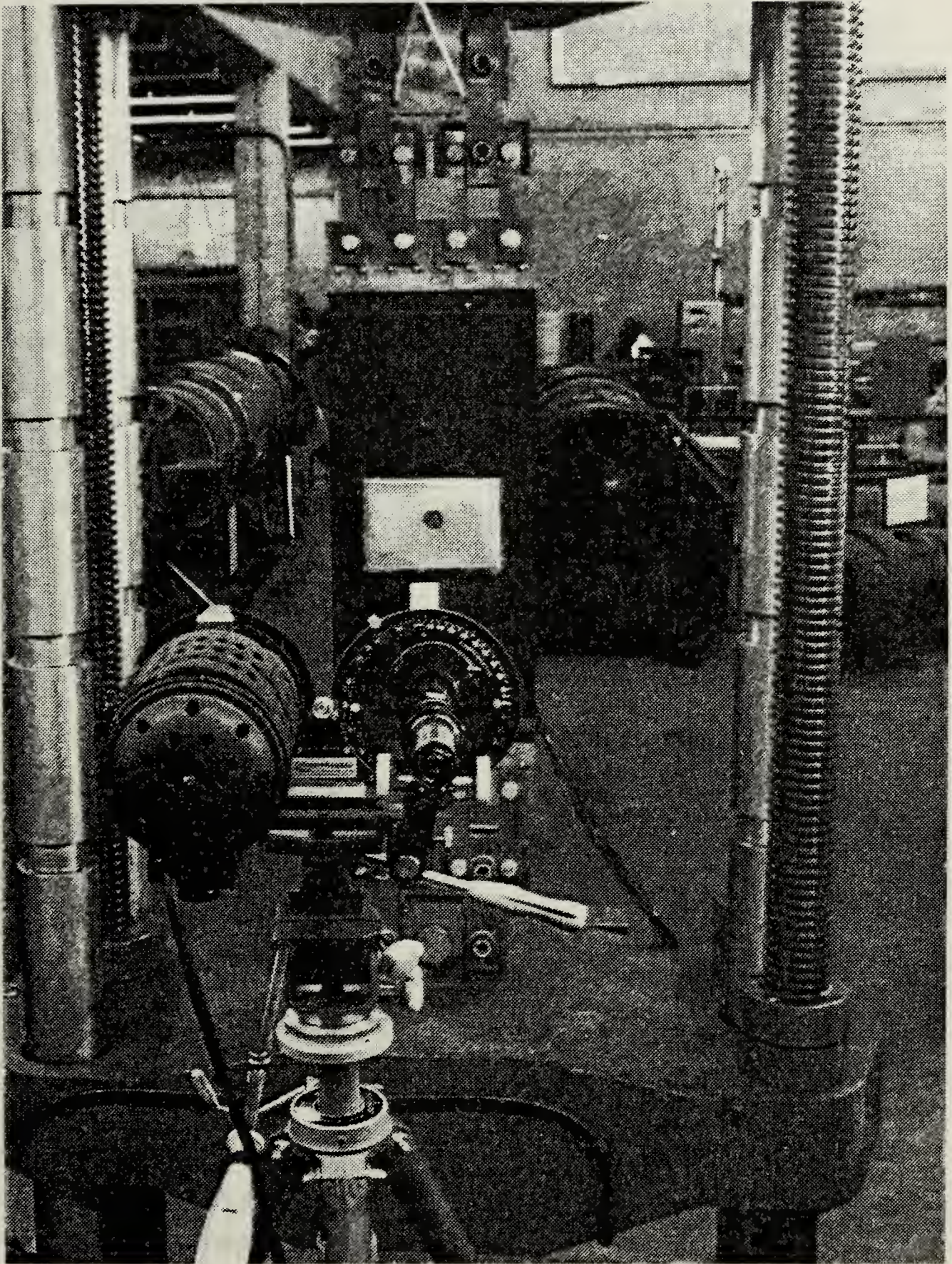


Figure 4.4 Photoelastic Reflection Polariscope.

3. Test Procedures

The procedures used to obtain data for each of the four panels are outlined below. These were identical to those used in the asymmetric panel testing with the exception of the photoelastic procedures.

1. The whiffle trees were attached to the panel to be tested. The upper whiffle tree was clamped in the top jaws of the Riehle Machine, and the strain gage lead wires connected to the System 4000. With the panel hanging freely, initial gage calibration and zero strain readings were recorded. The photoelastic coating was examined to insure that a uniform, zero loading was present.
2. The lower whiffle tree was clamped into the Riehle Machine, and the panel was slowly loaded to 2,500 psi. Any slippage or slack was taken out of the system and the load set to an initial 2,500 psi.
3. As load was increased, strain gage readings and color pictures of the photoelastic coating were taken every 2,500 psi. The panels were slowly loaded until the first audible breaking of fibers in the panel was heard.
4. The load was reduced to 2,500 psi and the camera reloaded with black and white film for pictures with a monochromatic filter.
5. The panels were again loaded in 2,500 psi increments. As the strain near the edge of the hole approached 1% (the anticipated upper limit of the strength of the panel), data was recorded every 1,000 lbs without stopping between load increments.

6. The load level of first audible fiber breaking and any other significant information were recorded.

7. The loading continued in 2,500 PSI increments until failure occurred.

Since the panel was not of uniform thickness it was decided to normalize the load by area to pounds per square inch (psi) rather than use the pounds per inch (stress resultant) normally referred to in plate theory. The pounds per square inch loading refers to the load applied along the top and bottom of the panel. The same problem arose when trying to relate stress over a plate cross section whose thickness was varying (at the cutout 90° to the applied load) to the strain gradients. Since strain is the quantity easiest to measure experimentally it was used as the principal means to compare the panels.

C. EXPERIMENTAL RESULTS

1. Assymetric Reinforcement Results

The average failure load for the two unnotched samples tested by O'Neill was 65,000 lbs. (58,036 psi.). The average failure load for the two notched but unreinforced panels was 36,000 lbs. (32,143 psi far field stress) with the extrapolated strain at the edge of the hole being about 10,000 microstrain or 1% elongation. The ratio of the failure load for a panel with a cutout but not reinforced to the failure load for the unnotched panel (P/P_0) was about 55%.

2. Symmetrically Reinforced Panels Results

The symmetric reinforcements provided significantly greater reinforcement than the asymmetric. No visible signs of deformation or buckling during loading were evident in

any of the panels; however, uneven loading was noted on panel 2B as indicated by the photoelastic coatings and strain gage data. Like the asymmetric panels from Ref. 17, the panels from this study had the characteristic fiber cracking noises, but the onset was delayed somewhat. The first audible cracking occurred around 21,500 psi for all the panels. This cracking in the asymmetric panels started between 18,750 and 20,500 psi. The first indication was a loud "pop", much louder than subsequent noises. The initial fiber (possibly an entire tow) failure was followed by softer but steady "pings" of fiber failure. This noise level varied from low to moderate with sharp spikes of noise from loud "pops" of fiber breaking at occasional, seemingly random intervals.

All the panels failed suddenly with separation beginning at the point of maximum strain, at the edge of the hole 90° to the direction of applied load. There was evidence of delamination at that point extending $1/3$ to $1/2$ of an inch into the laminate. Failures progressed from the edge of the hole horizontally to the outer edge of the panel. The failure lines were fairly straight, coinciding with the X axis, except for two 30 degree crack diversions (see Figs. A.8 and C.12). These are not considered significant, but are more indicative of the basic inhomogeneity of composite materials.

The strain gage data was essentially linear to failure for all gages. Several of the 5,000 ohm gages near the hole failed prior to final panel failure. It appears that the backing material of these gages is too stiff and can not reliably accept more than about 7000 microstrain. Linear extrapolations were made for these gages to the point of final panel failure. It should be noted, however, that some non-linear behavior was demonstrated for gages in similar locations that did not fail just prior to panel fracture.

The photoelastic coatings provided excellent data on strain behavior near the stress concentration. Prior to failure, two of the coatings started to pull free around the edges of the panel but still provided good photographic results close to the cutout. Problems in obtaining accurate readings when using the Oblique Incidence Adapter prevented the measurement of the principal strains from the photoelastic coatings at different locations on the panel surface. Not enough contrast could be developed to accurately identify the isochromatic lines. Monochromatic photographs did provide valuable evidence of the strain gradient near the cutout.

a. Reinforcement Configuration 1A

Panel 1A had the smaller of the reinforcement configurations with all layers oriented in the direction of the applied load ($0/90^\circ$). The panel failed at 42,590 psi which is a 33% increase over the unreinforced panel and gives a P/P_c ratio of 73.4%. The strain gages functioned properly throughout the testing of this panel, and gave reliable data all the way to failure. The results shown in Fig. A.3 display a linear plot of strain versus load for all gages until the fracture point is approached. Extrapolating data to the edge of the hole shows the strain to be approximately 10,000 microstrain or about 1% elongation. The gages located at points of high stress gradients, i.e. near the hole or a reinforcement edge, have strain vs. load curves that appear to flatten out near fracture. Figure A.2 plots the strain versus location along the X-axis at 10,000 psi far field stress. The plot shows a standard strain curve increasing rapidly close to the edge of the hole.

The photoelastic material remained bonded to panel 1A throughout the testing. Photographs of fringe progression are provided in Appendix A, Figures A.4-7.

During this initial test, monochromatic photographs were made first and then color photographs were taken to failure. Monochromatic pictures were taken only up to the point of first fiber failure (21,200 psi), after which color photos were taken. In subsequent testing, the order of color to black and white photography was reversed so that more pictures closer to failure could be included in this report.

b. Reinforcement Configuration 2A

Panel 2A had the larger of the two reinforcement configurations with all layers oriented in the 0/90° direction. This reinforcement provided a 40% increase in strength with a failure at a load of 44,940 psi. P/P_0 for panel 2A was 77.4%. The first audible fiber breaking occurred at 21,512 psi.

The strain gage closest to the hole failed during loading between 25,000 and 27,500 psi (last recorded data for gage no. 1 is at 25,000 psi). The data from that gage was questionable throughout the loading sequence, and was not used for this analysis. Its initial readings showed a lower strain than the next neighboring gage which was farther from the hole. Estimated strain data for a gage in the same position provided in Fig. B.3. Extrapolating the more reliable data from other gages and the finite element solution to the edge of the hole shows that the strain was again about 10,000 microstrain or 1% elongation for the 0/90° reinforcement orientation. Plots of the data for this panel are provided in Figures B.2-3.

In this test, the photoelastic coating started to separate from the composite panel in the upper and lower right corners, and separation progressed toward the stress concentration as the load increased. This detachment did not reach or affect the regions with high stress gradients, and therefore photoelasticity provided good data for

analysis. The photographs may be found in Appendix B, Figures B.4-11.

c. Reinforcement Configuration 1B

Panel 1B had the smaller of the reinforcement configurations with $\pm 45^\circ$ orientations. The panel failed at 42,500 psi which represents a 32% increase over the unreinforced panel, and gives a P/P_o of 73.2%. The first audible fiber breaking occurred at 21,339 psi.

Again problems occurred with premature gage failures. Gages 1 and 13 failed during initial testing at loads below 15,000 psi. Testing was stopped, and the gages were replaced. Gage 1 failed again at over 11,047 microstrain, between 35,000 and 35,715 psi. The data provided to that point appears to be valid. Gage 4 failed after only 5864 microstrain (between 40,000 and 40,279 psi), but its data also appears valid up to the point of failure. Extrapolation of the data to the edge of the hole shows the strain at failure to be approximately 13,500 microstrain. Plots of these data are given in Figures C.2-3.

The photoelastic coating also started to separate from the panel in this case. It started separating from the lower right corner at 30,000 psi and progressed toward the hole. The separation did progress into the area of high stress gradient after loads of 35,000 psi, thus invalidating any further data from its photographs (see Figure C.10). Photoelastic photographic results are provided in Appendix C, Figures C.4-11.

d. Reinforcement Configuration 2B

Panel 2B had the larger reinforcement configuration with $\pm 45^\circ$ ply orientation. This reinforcement provided a 29% increase in strength with a failure at 41,429 psi. The P/P_o was 71.4% for this panel. The first audible fiber

breaking occurred at 21,650 psi. Strain gage and photoelastic data indicate that this panel was not evenly loaded.

Strain gage failures prior to final panel failure were a problem with this panel also. Gage 2 failed after 7595 microstrain between 25,000 and 27,500 psi. Gages 1 and 3 failed after 7885 and 5484 microstrain respectively which was between 27,500 and 30,000 psi load on the panel. Data from all three gages appeared to be valid up to the failure point. Extrapolation of the data to the hole's edge indicated that the panel failed when the strain at that point reached approximately 12,500 microstrain, corresponding to about 1% elongation for the $\pm 45^\circ$ orientation. Plots of strain gage data are provided in Figures D.2 and D.3.

A comparison of strains at different stress levels was made of panel 2B. Figure 4.6 shows the strain gradient at 10, 20, 30 and 40,000 psi far field load on the panel. The gradients show that the panel behaves almost perfectly linearly. Within the accuracy of the strain gages ($\pm 5-6\%$) the strain at 40,000 psi, at all locations, is a multiple of four of the strain at 10,000 psi. It is interesting to note that the slight variations in strain at 1.7" and 2.3" from the hole are maintained and linearly increase with load.

The photographic data provided excellent material for analysis of fringe progression near the stress concentration. Figures D.4-11 in Appendix D show the fringe progression.

Tables IV and V provide a summary of the experimental results. In Table IV the various failure values are compared. The failure load refers to the total panel failure, the load at which it came apart. Failure strain is the strain in the Y direction at the edge of the cutout, 90° to the direction of the applied load. The values of

Panel 2B: 45 Degree, 206 Percent Reinforcement
 10,000-40,000 PSI Tensile Load (+Py comparison)
 Micro-Strain Along Horizontal Axis of Symmetry

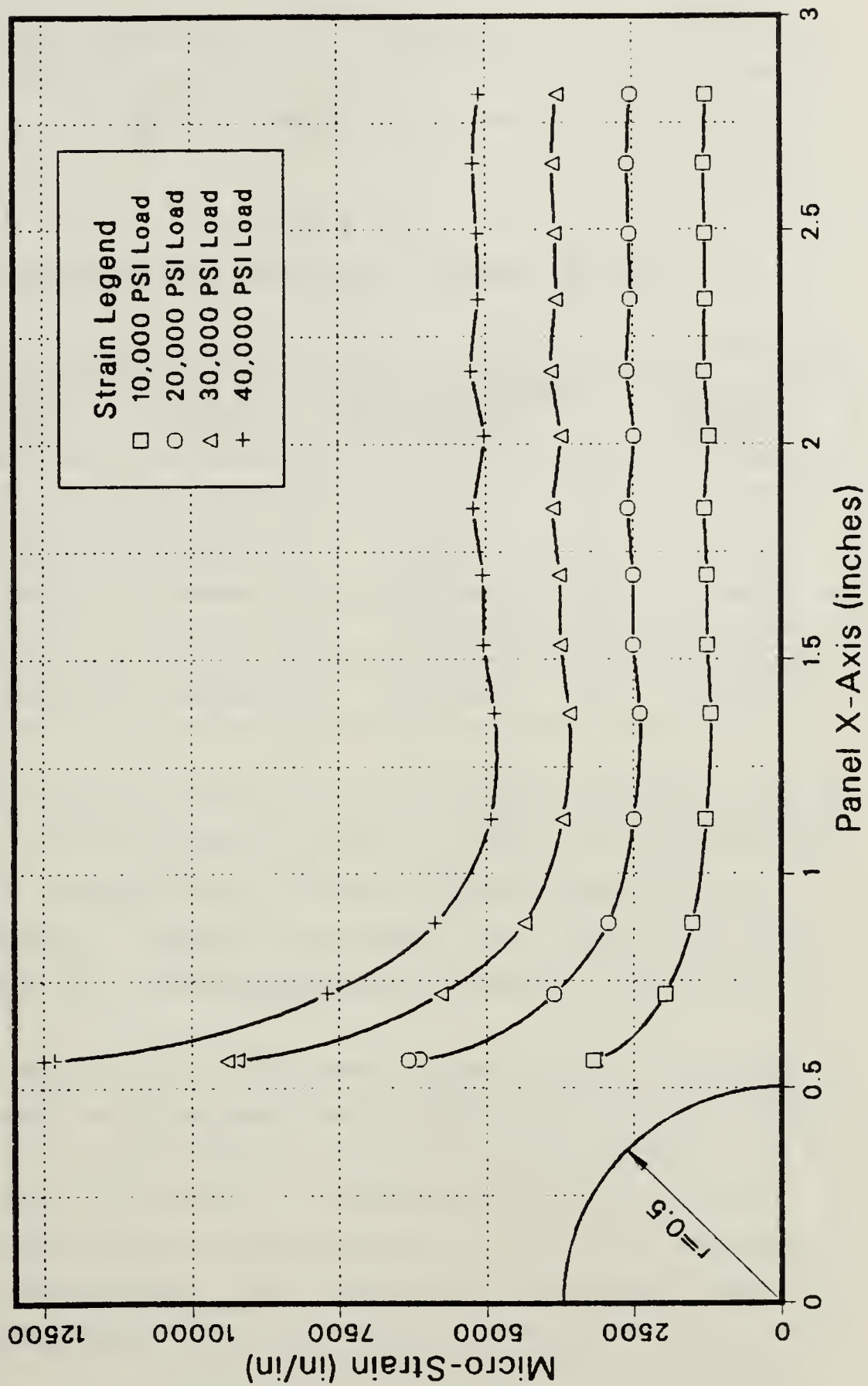


Figure 4.5 Panel 2B: Load Comparison.

microstrain are higher for the B (primarily 45°) configuration, but represent approximately 1% strain of the fibers in the ply axis. It is interesting to note that the first

TABLE IV
Experimental Results: Failure Values

Panel No.	Failure Load (psi)	Failure Strain (micro)	First Audible Fiber Failure Load (PSI)	Failure Load Ratio (P/Po)
1A	42,590	10,000	21,200	73.4%
2A	44,940	10,000	21,512	77.4%
1B	42,500	13,500	21,339	73.2%
2B	41,429	12,500	21,650	71.4%

audible fiber failure occurred at virtually the same load for each panel. The failure load ratio (P/Po) is a measure of the ultimate strength ratio of the notched panel to an un-notched panel. Ideally, the goal is to regain all the lost strength with reinforcement and reach a P/Po ratio of 100%.

Table V is a further comparison and analysis of panel failure. As discussed above the reinforcement weight was compared to the volume of material removed from the 1.0 in. dia. cutout. In the "1" configuration 162% of the volume was replaced as reinforcement; in the "2" configuration 206% was replaced. The "Increase in Failure Load" and "Percent Improvement" refers to the increase over an unreinforced panel with 1.0 inch diameter hole. The "Specific Improvement" refers to the result of dividing the "Percent Improvement" by the percent of hole volume represented by

TABLE V
Experimental Results: Failure Comparisons

Panel No.	Reinf. Weight (% hole volume)	Increase in Failure Load (PSI)	Percent Improvement	Specific Improvement
1A	162.5%	10,447	32%	0.200
2A	206.3%	12,797	40%	0.193
1B	162.5%	10,357	32%	0.198
2B	206.3%	9,286	29%	0.140

the the reinforcement; using panel 1A for example:
 $32\% / 162.5\% = 0.200$. The significance of these results is discussed in detail in Chapter V.

V. DISCUSSION OF RESULTS

A. SYMMETRIC REINFORCEMENT RESULTS

The failure of all the panels occurred at the predicted location of the highest stress concentration, i.e. the point on the cutout 90° to the applied tensile load. They failed catastrophically, without warning or visible signs of imminent fracture. Consistent with the nature of composite (brittle) materials, there was no visible hole distortion. Continual micro-fiber breaking was evident audibly from its initiation at approximately 21,500 psi until final failure, but there was no sudden change in noise level just prior to failure.

1. 0/90° Reinforcement Orientation

The "A" configurations, which had reinforcements in the direction of the applied load ($0/90^\circ$), appeared to have a predictable failure level. That is, when the point with maximum stress concentration (the point on the edge of the cutout 90° to the direction of the applied load) reached approximately 10,000 micro-strain or 1% elongation, the panel failed. Reinforcement reduced the stress around the hole by increasing the cross sectional area over which the load was distributed. It allowed a higher load to be applied before the material next to the cutout elongated 1%. It would be expected that increasing the cross sectional area in regions of high stress concentration would increase the ultimate strength of the panel. The results comparing specific gain in strength (% gain in strength / % added weight) in table IV seem to point toward another conclusion. The total applied volume of reinforcement would appear to be

the principal factor in the improvement in ultimate strength. Obviously, however, this result based upon such a small sample is hardly sufficient to do anything other than point out the need for further testing.

2. $\pm 45^\circ$ Reinforcement Orientation

The "B" configurations with reinforcements oriented in the $\pm 45^\circ$ directions have results that do not appear to be as easily characterized as the "A" configuration. The apparent strain at the edge of the hole and the failure load were both less for configuration 2B (the larger size reinforcement) than for 1B. Both of the "B" configurations did allow more strain at the edge of the hole than either of the "A" configurations. The primarily $\pm 45^\circ$ orientation makes the material more compliant and allows higher strain before panel failure.

The 2B configuration failed at a load lower than would have been expected considering the response of the other three panels. There is some evidence both in the strain gage readings and the photoelastic photographs to indicate that the load was not uniformly distributed across the width of the panel. Figures D.4-11 show slightly higher strain gradients on the left side of the hole. Figure D.2 shows the strain gage values at 10,000 psi. The variation between the two values at about 1.3 inches is the difference in strain between gages 7 and 8 (see Fig. D.1). The two gages are almost equidistant from the hole center, but on opposite sides of the panel. The difference in strain indicates an unequal loading condition. This panel failed at a load ratio (P/P_o) 6% less than the 2A configuration. This early failure is what would be expected considering the load condition.

The ability of the primarily $\pm 45^\circ$ (around the cutout) laminate to exhibit more compliance with apparently little loss in ultimate strength (compare failure loads of panels 1A and 1B) is significant. This orientation may provide designers more flexibility to design lighter structures when the load direction is known. The $0/90^\circ$ orientation provides its maximum reinforcement when applied load is parallel to the Y axis. Any other load orientation would produce higher strain and earlier failure.

3. Asymmetric Round Reinforcements

The asymmetric reinforcement schemes used by O'Neill [Ref. 17] did not provide significant increases in strength over the basic notched panel. Although only a small number of specimens was tested, in no case was the improvement more than 12%. The computational results for O'Neill's configurations 1A and 2A ($\pm 45^\circ$ orientation) showed that for a 10,000 lbs (8,929 psi) load the micro-strain for the point closest to the hole at the 90 degree from the tensile stress was:

	<u>Front</u>	<u>Back</u>	<u>Average</u>
1A:	1700	3300	2500
2A:	2250	3200	2225

The strain gradient through the thickness of the panel at the hole edge was very steep, and could cause delamination due to the interlaminar shear forces, which would contribute significantly to early panel failure. Thus it is to be expected that symmetric reinforcements, which do not have this problem, should out-perform asymmetric reinforcement.

B. COMPARISON OF COMPUTATIONAL AND EXPERIMENTAL RESULTS

The strain distribution along the X axis predicted by the finite element analysis is plotted with the strain gage measured values in the appendicies (Figs. A through D.2) The finite element solution is very close to the experimental results. Very close to the hole the analytical solution predicts a very high strain gradient. This is exceptionally difficult to measure with any accuracy [Ref. 22]. At strains approaching 1% there is probably some strain relief provided by matrix cracking and load transfer within the laminate and some local deformation. The instrumentation utilized was not accurate enough detect these reactions. The finite element code used does not account for these nonlinear behaviors. More than about 0.05 inches from the cutout the analytical solution almost exactly matches the experimental results. Further comparisons might be more economically done computationally until an optimal configuration was found. This geometry could then be validated experimentally.

C. FAILURE PREDICTION

The failure of the panels with 0/90° reinforcement ply orientation occurred when the apparent strain at the edge of the hole reached 1% elongation. The reinforcements reduced the stress in the region near the hole and thus allowed the panel to withstand a higher load before failing. The principal fibers failed at 1% elongation and panel fracture initiated.

The $\pm 45^\circ$ reinforcements failed when the panel strain at the same point was considerably higher. However, when the indicated strain at the 90 degree point of the cutout is approximately 14,150 micro-strain, the strain on the individual 45° fibers (in the ply 1-2 axes) is 10,000

micro-strain (1% elongation). Therefore, the panels failed at approximately the point where the reinforcement fibers were strained beyond capacity. Beyond 1.1% elongation the 0/90° fibers in the base panel had probably all failed and the stress was being carried by the reinforcement fibers. Panel failure occurred when these $\pm 45^\circ$ fibers were strained to their limit (1%).

While definitive predictor of failure for this type panel is not possible without further testing it is obvious from even the few specimens that the ply strain limit of this material is about 1%. Damage to the panel (however minor) begins at about one-half the limit load and progresses steadily until failure. This damage, in itself, does not appear to be the primary cause of failure in low cycle applications. The presence of symmetric reinforcement around a cutout reduces the stress and increases the load carrying ability of the notched panel. This increased ability to carry a load, up to almost 75% of the unnotched panel strength, merits consideration in future weight-critical designs. Alternate reinforcing geometries such as increasing the thickness next to the cutout may yield even better results.

VI. SUMMARY AND CONCLUSIONS

A. GENERAL

Symmetric reinforcement of cutouts graphite-epoxy panels is a viable method of significantly reducing the strain in the vicinity of a stress raiser and thus increasing panel strength when the panel is subjected to uniaxial tensile stresses. The best reinforcement configuration for this loading condition cannot be determined with the limited results of this study. Some general observations can be made, however:

1. The 0/90° ply reinforcement provided the best strain reduction; the panel was made stiffer.
2. Strain reduction due to 0/90° degree reinforcement increased proportionally to the amount of reinforcement added.
3. The increase in panel failure stress per unit weight of reinforcement was approximately constant for three of the four specimens.
4. The ±45° reinforcements allowed 25 to 35 percent more flexibility (compliance) than the 0/90° reinforcements.
5. A strain of 1% for the fibers of a symmetric reinforcement (no induced curvature) appears to be a good predictor of panel failure.
6. Symmetric reinforcement provided a 29-40% improvement over the unreinforced notched panel, versus the 5-12% improvement given by asymmetric reinforcement.

9. The DIAL finite element program provides accurate results that correlate well with experimental data.

These conclusions are based on the small number of specimens tested in this study. The data for these samples do appear to be reliable and accurate.

B. SUGGESTED FURTHER RESEARCH

Further research in this area would appear to be of significant value. An attempt to verify the apparently direct relationship between added reinforcement volume (weight), and increase ultimate failure stress would seem to be the next step. If this relationship is of limited applicability, then the question of reinforcement thickness (three or more plies) seems to be the logical next step. Additional questions which could be addressed include:

1. Is there an optimum reinforcement area? That is, is there a reinforcement-diameter-to-hole-diameter ratio that provides the most efficient reinforcement?
2. Which increases the reinforcement effect more efficiently: a large diameter reinforcement or a greater thickness?
3. Is 1% fiber elongation an adequate failure criterion, especially in the region of highest strain gradient, near the hole?
4. Do the data from analysis and tests of this type composite material loaded in uniaxial tension apply to other types of loading?

Another possible study would be the investigation of submerging the reinforcement under one or more plies of the laminate.

APPENDIX A
PANEL 1A

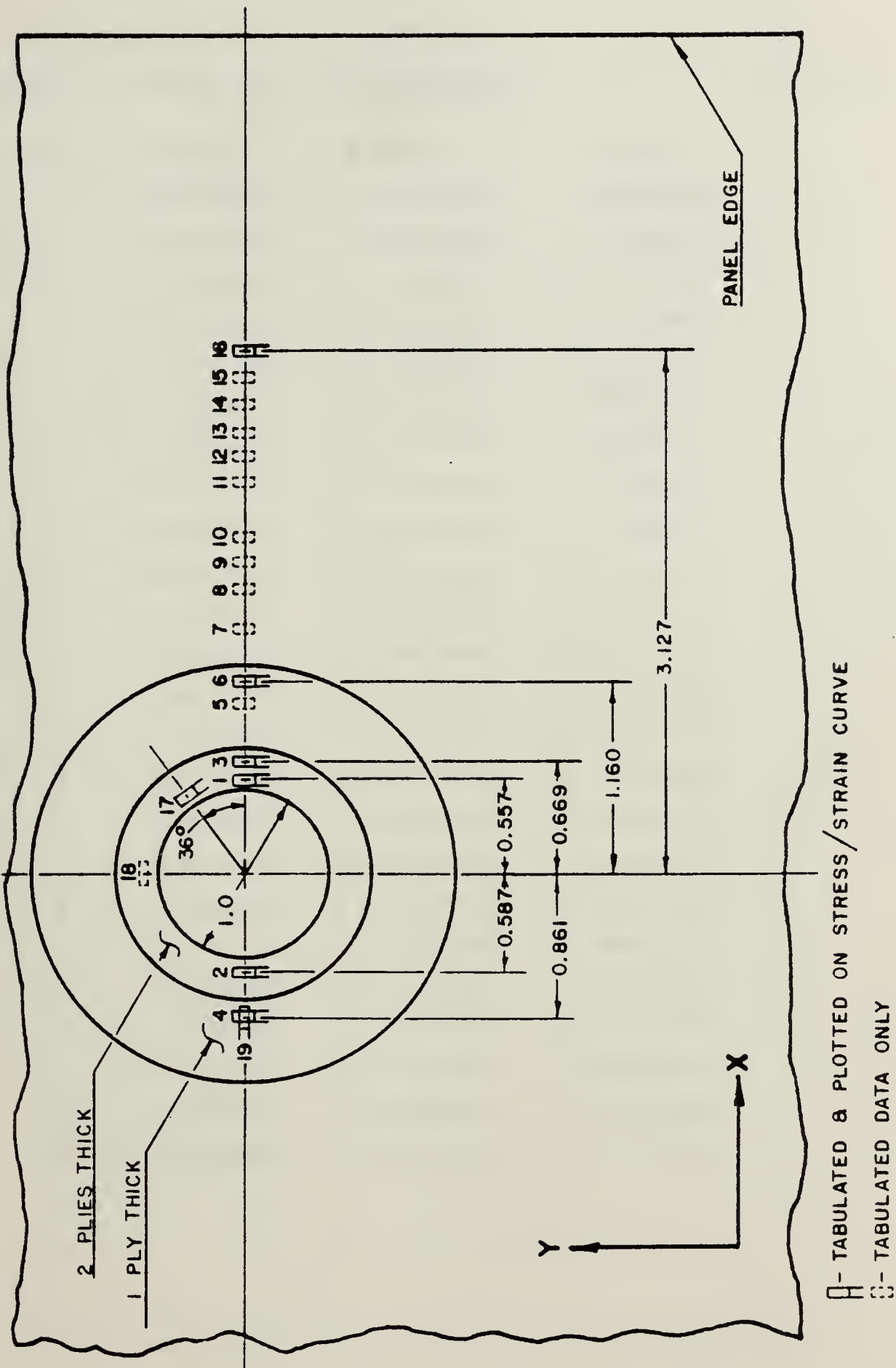


Figure A.1 Panel 1A: Strain Gage Locations.

TABLE VI

Panel 1A: Strain Gage Locations and Strain at 10,000 psi
(Far Field)

G#	X-Coord.	Y-Coord.	Strain
1	0.5570E+00	0.0008E+00	0.2061E-02
2	0.5870E+00	0.0920E+00	0.1742E-02
3	0.6690E+00	0.0120E+00	0.1392E-02
4	0.8610E+00	0.0470E+00	0.1210E-02
5	0.1021E+01	0.0820E+00	0.1054E-02
6	0.1160E+01	0.0410E+00	0.1006E-02
7	0.1472E+01	0.0740E+00	0.1052E-02
8	0.1703E+01	0.0080E+00	0.1142E-02
9	0.1856E+01	0.0080E+00	0.1135E-02
10	0.2013E+01	0.0110E+00	0.1162E-02
11	0.2343E+01	0.0180E+00	0.1165E-02
12	0.2495E+01	0.0180E+00	0.1231E-02
13	0.2647E+01	0.0180E+00	0.1182E-02
14	0.2810E+01	0.0210E+00	0.1251E-02
15	0.2972E+01	0.0210E+00	0.1199E-02
16	0.3127E+01	0.0230E+00	0.1260E-02
17	0.4840E+00	0.3480E+00	0.1644E-02
18	-0.0190E+00	0.5970E+00	-0.3660E-03
19	-0.8610E+00	0.0470E+00	-0.3800E-04
20	0.5050E+00	-0.0320E+00	-0.6570E-03
21	-0.1477E+01	0.1365E+01	-0.4800E-03
22	-0.1413E+01	0.1431E+01	0.3980E-03
23	-0.1369E+01	0.1493E+01	0.1433E-02
23	-0.0170E+00	0.4578E+01	0.1217E-02

Panel 1A: 0/90 Degree, 163 Percent Reinforcement
 Far Field 10,000 PSI Tensile Load (+Py)
 Micro-Strain Along Horizontal Axis of Symmetry

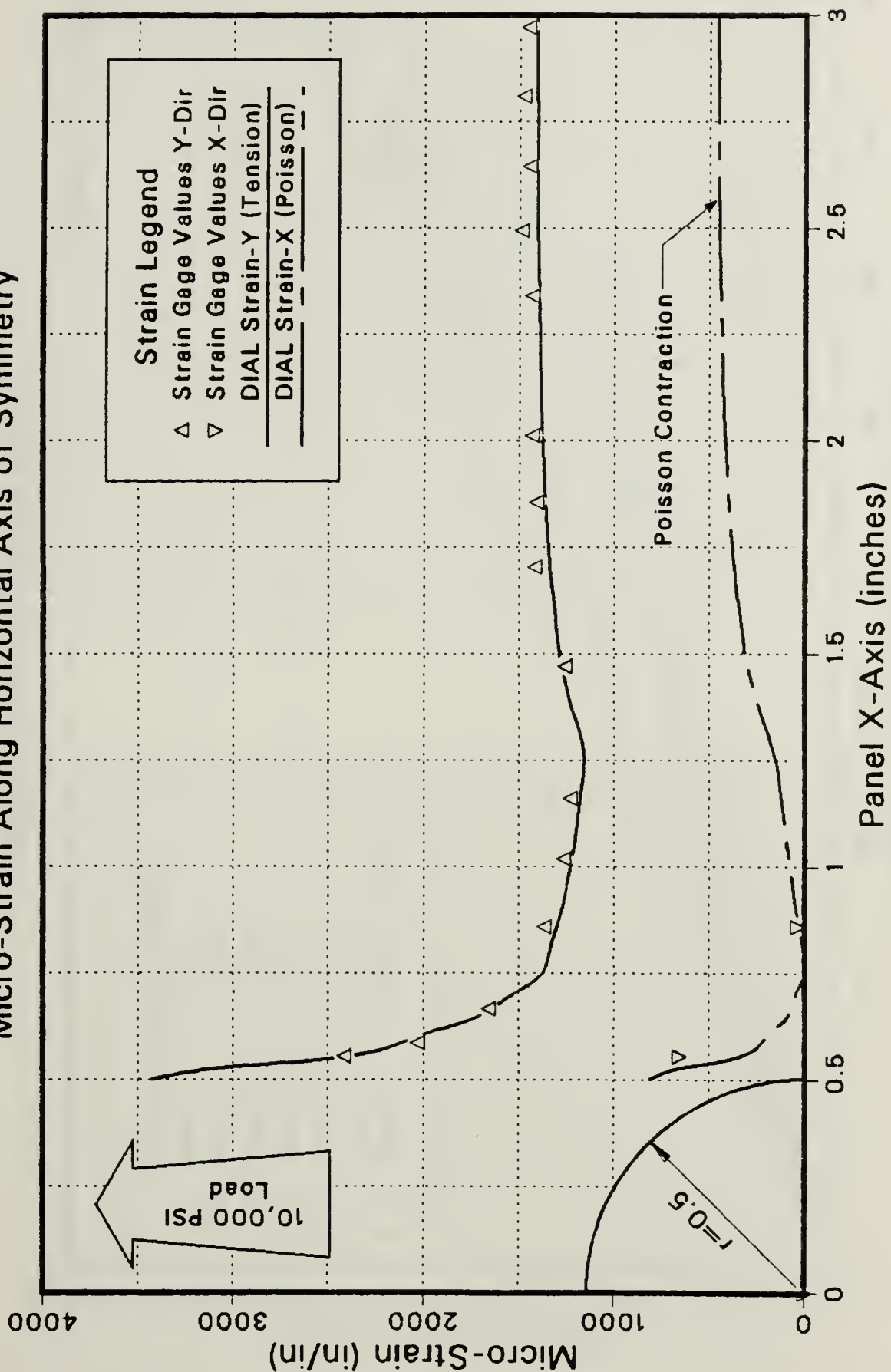


Figure A.2 Panel 1A: Strain Along X Axis at 10,000 psi.

Panel 1A: 0/90 Degree, 163 Percent Reinforcement
Micro-Strain vs Tensile Load

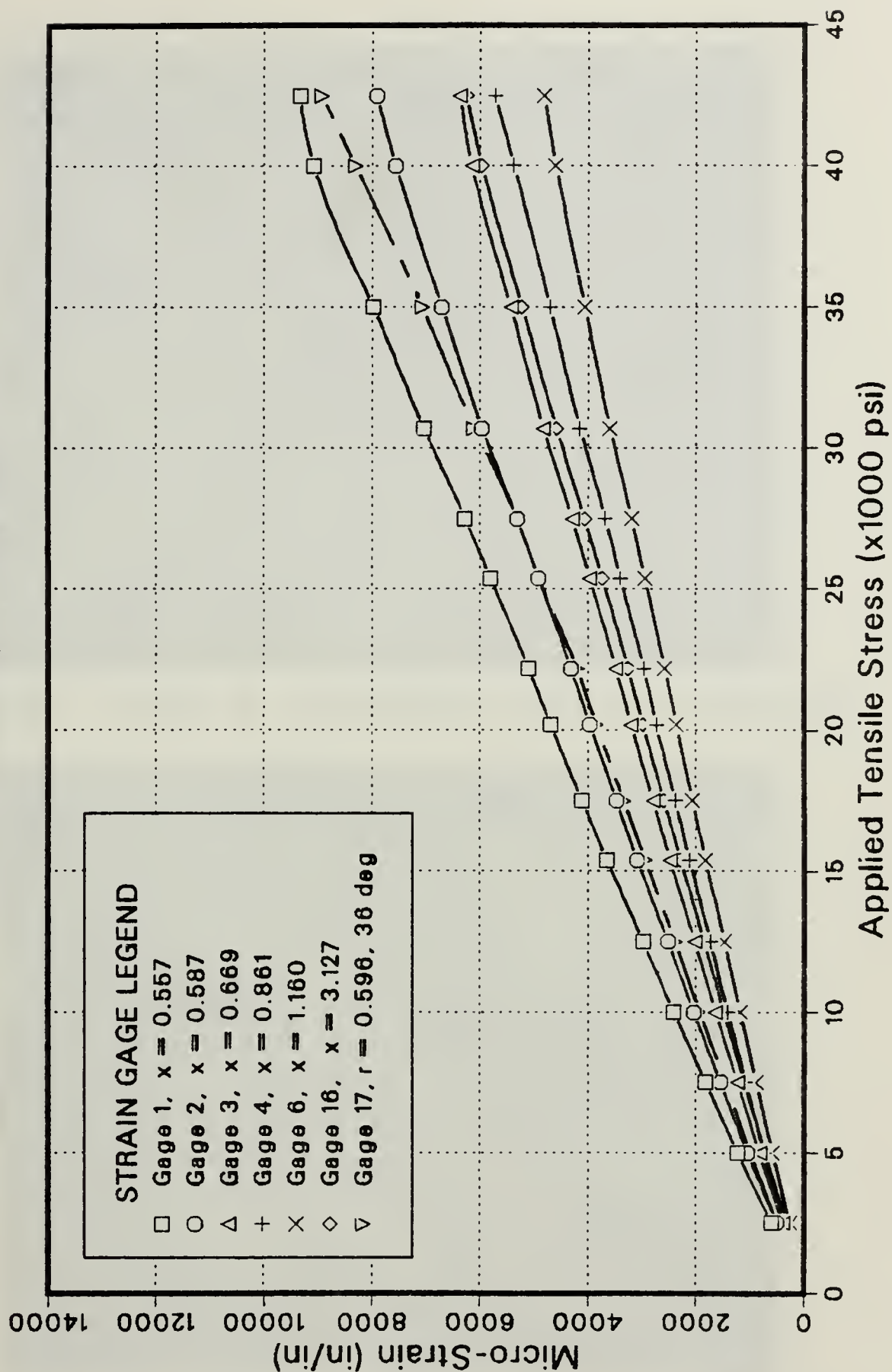


Figure A.3 Panel 1A: Microstrain vs. Tensile Load.

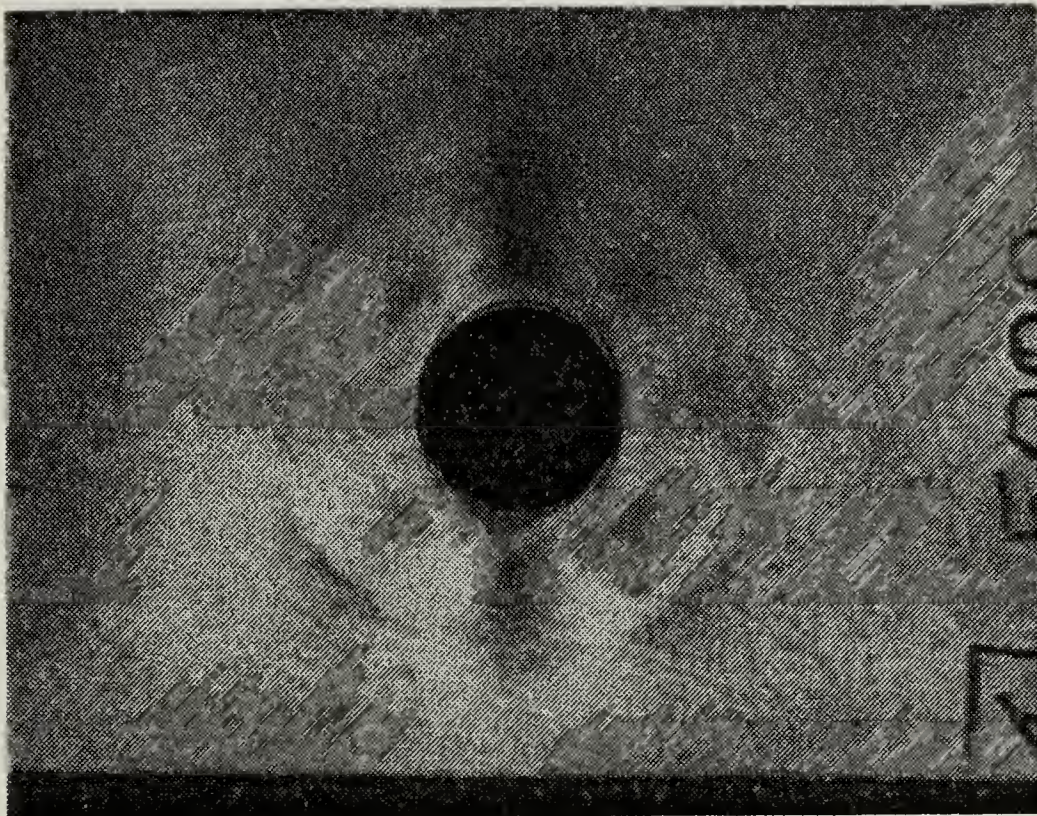


Figure A.4 Panel 1A: Photoelastic Panel at 5,000 psi.

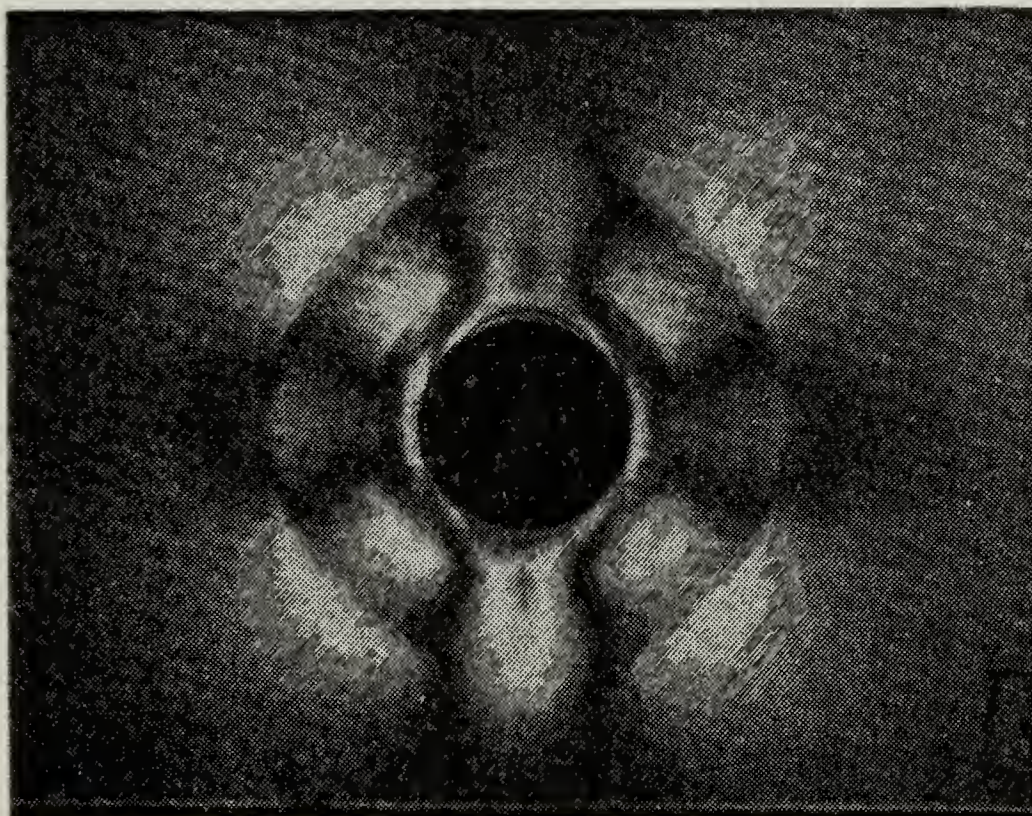


Figure A.5 Panel 1A: Photoelastic Panel at 10,000 psi.

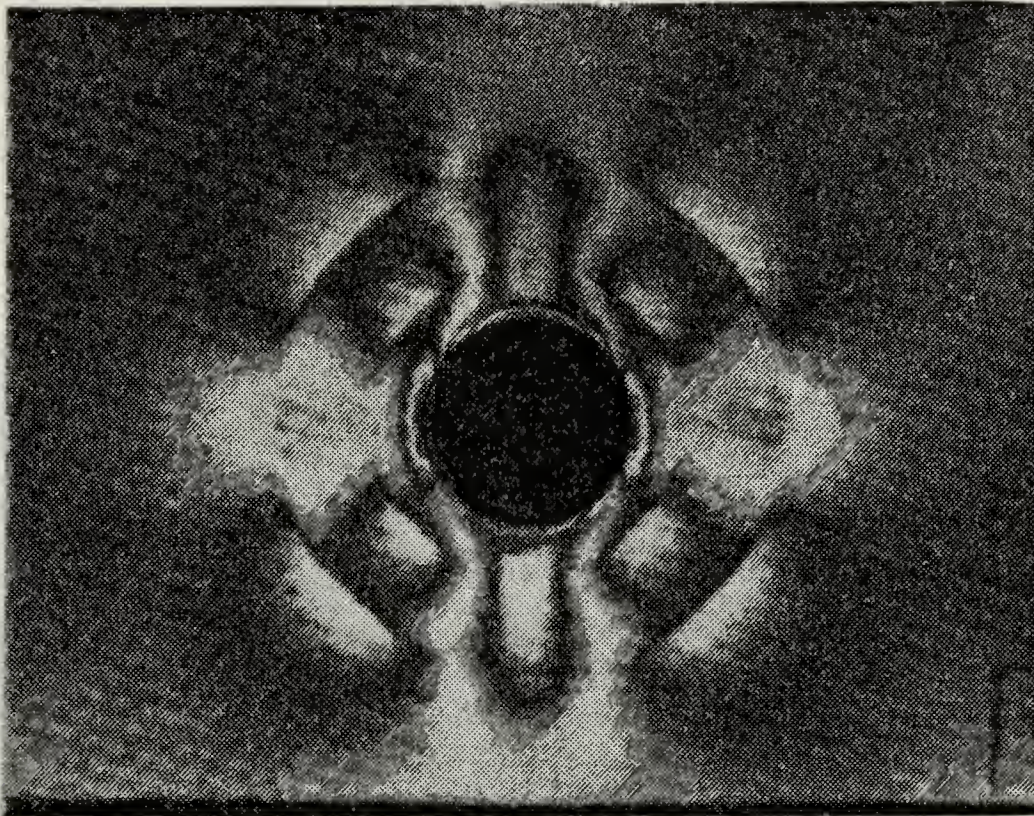


Figure A.6 Panel 1A: Photoelastic Panel at 15,000 psi.

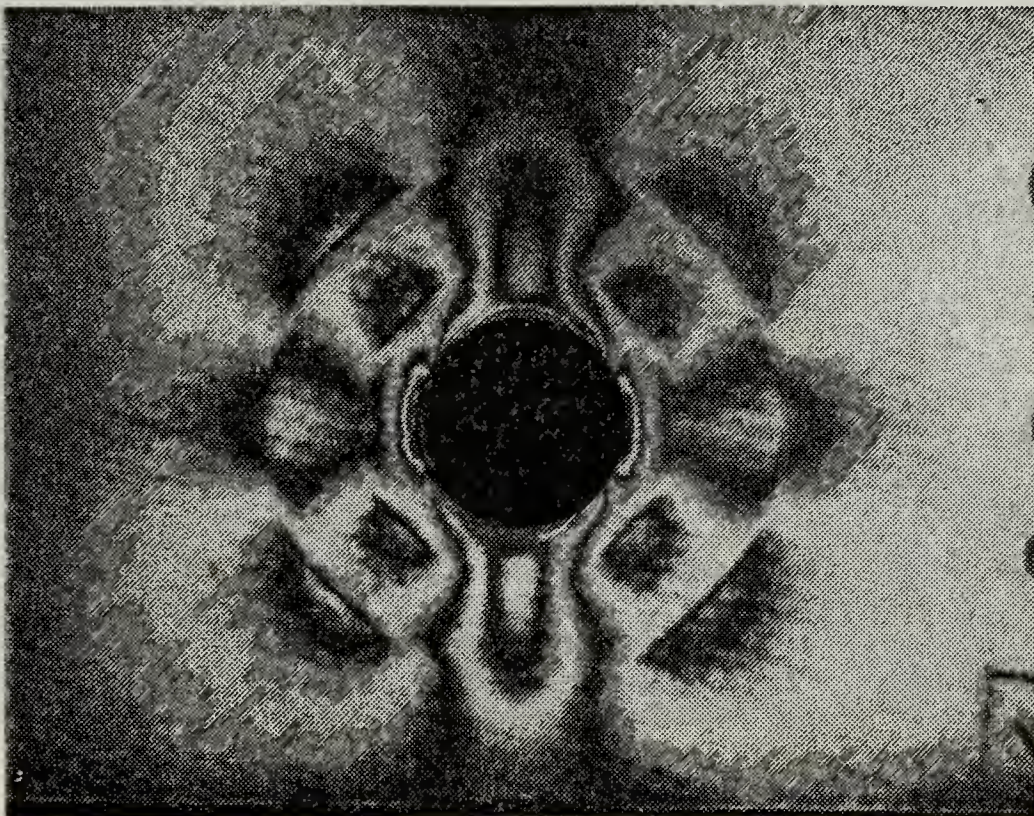


Figure A.7 Panel 1A: Photoelastic Panel at 20,000 psi.

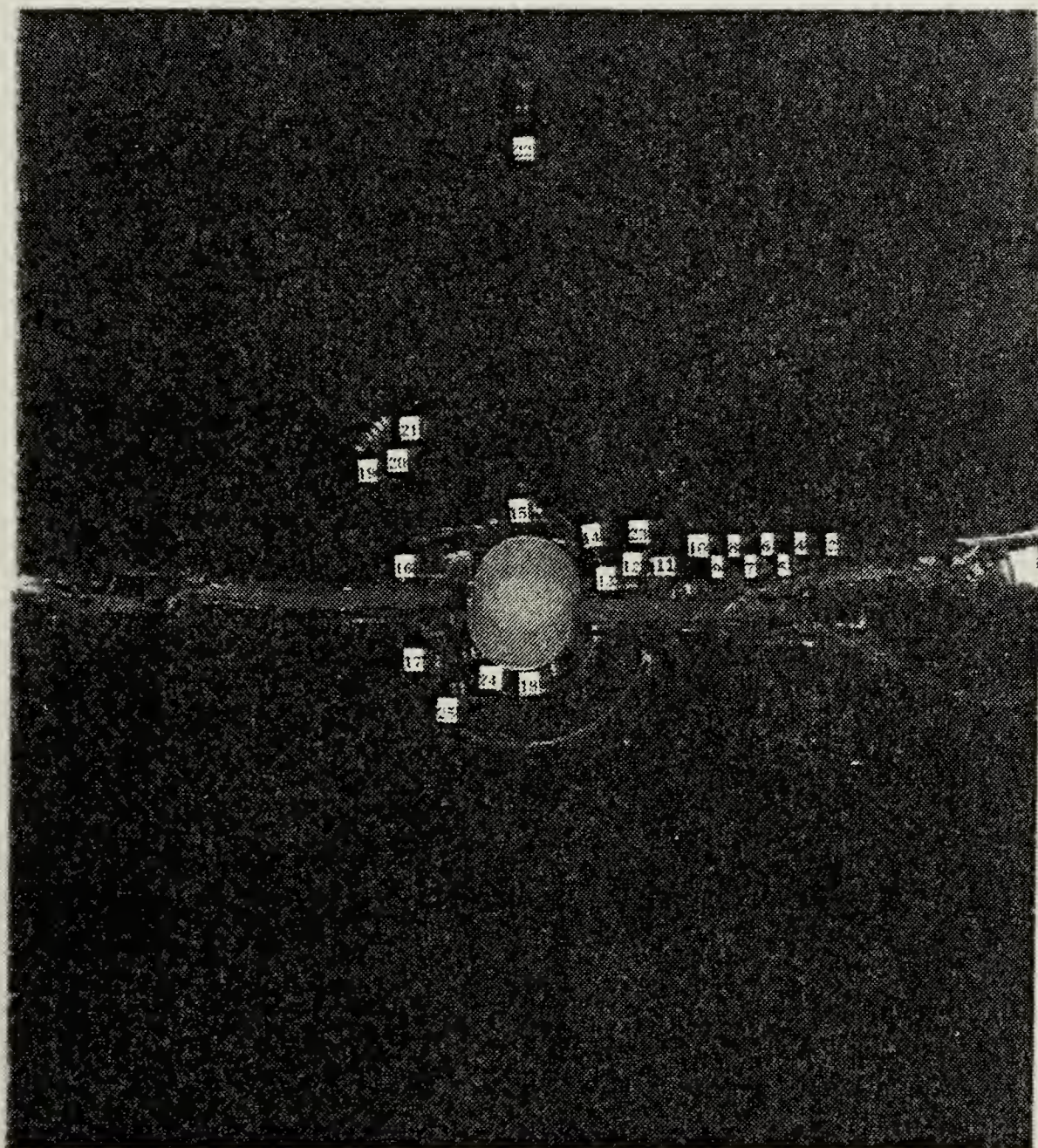


Figure A.8 Panel 1A: Fracture Line.

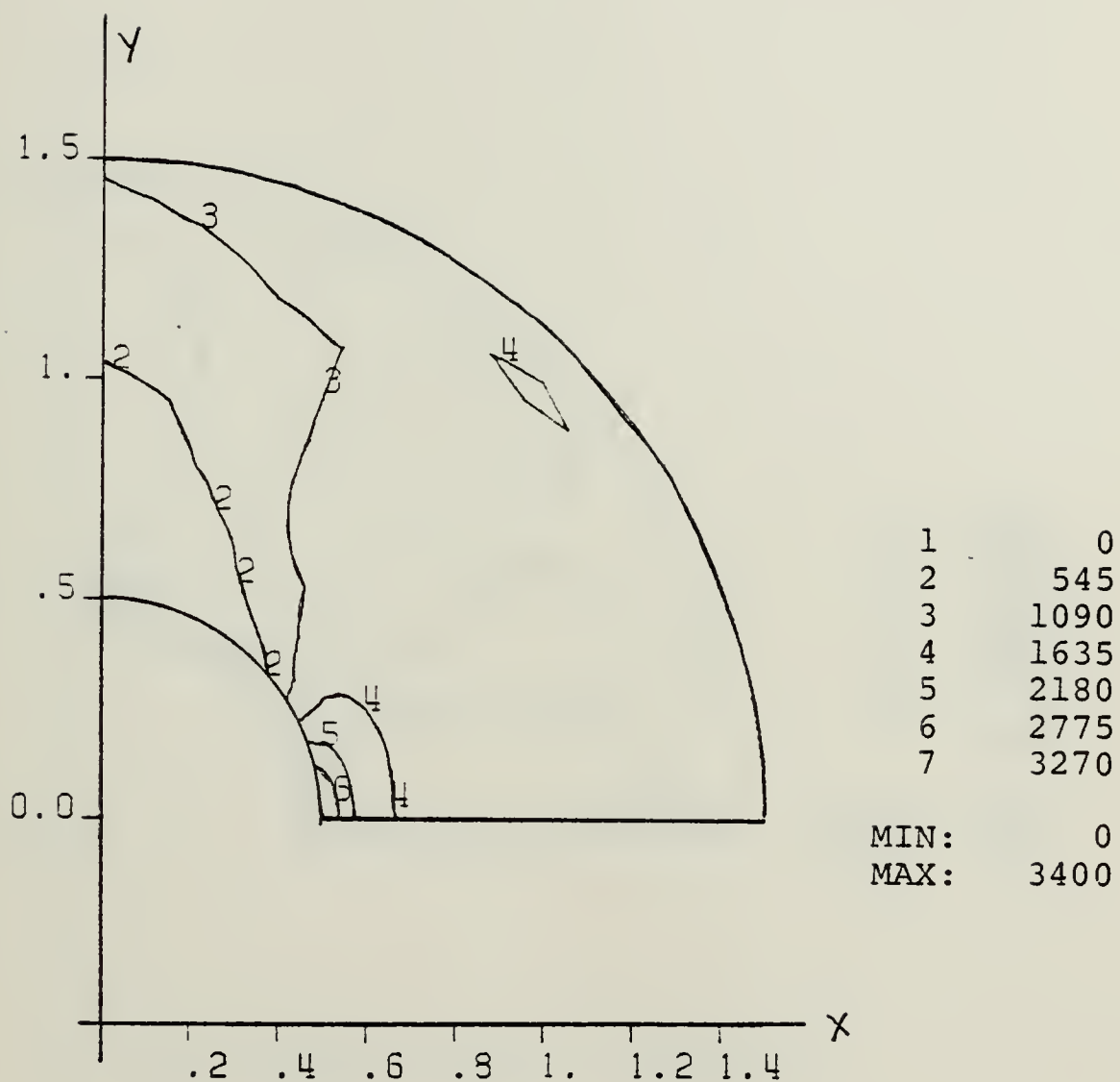


Figure A.9 Panel 1A: Eps-Y ($\times 10^6$) Contours Near Cutout.

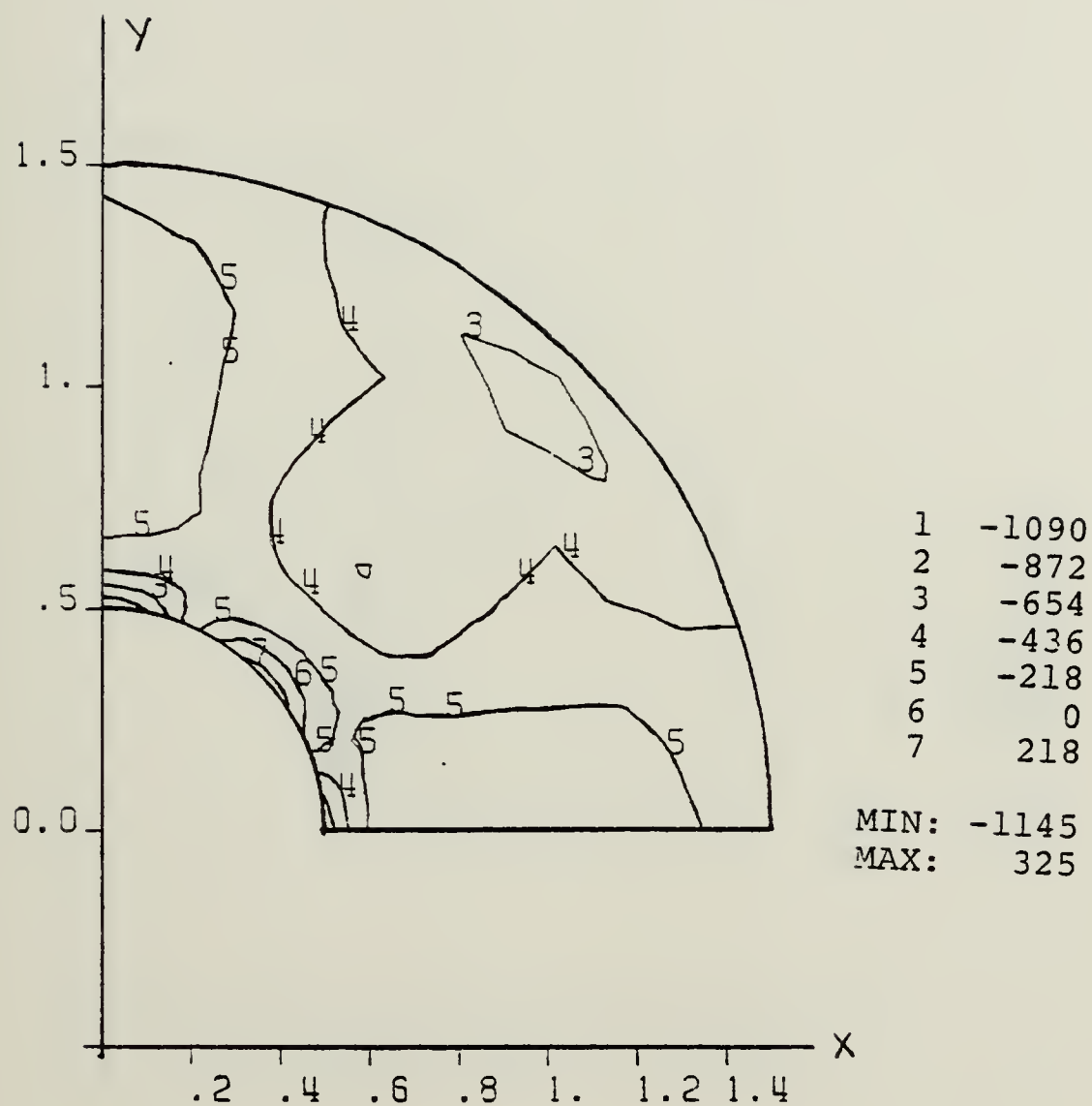


Figure A.10 Panel 1A: Eps-X (x 10⁶) Contours Near Cutout.

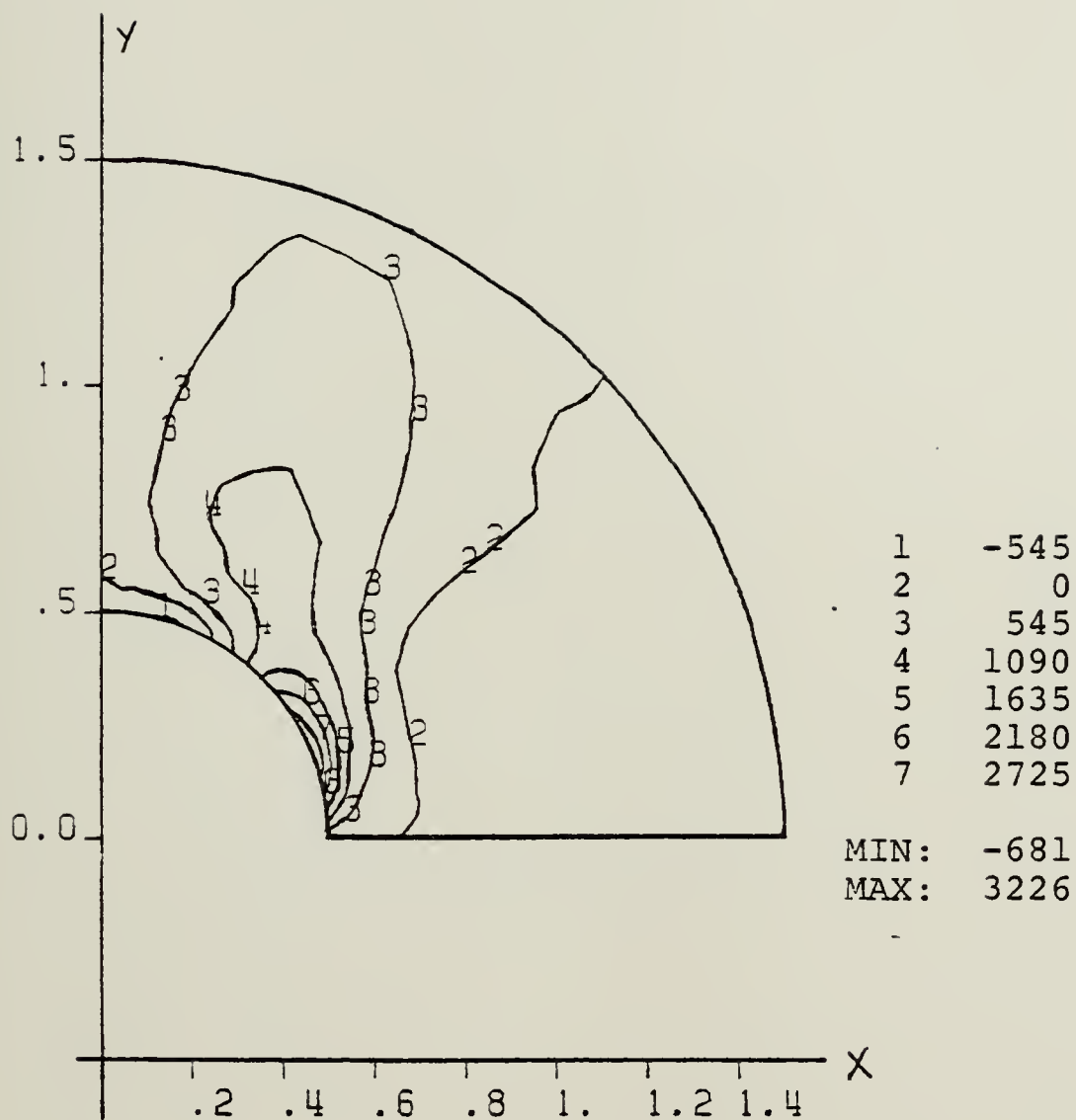


Figure A.11 Panel 1A: Eps-XY (x 10⁶) Contours Near Cutout.

APPENDIX B
PANEL 1B

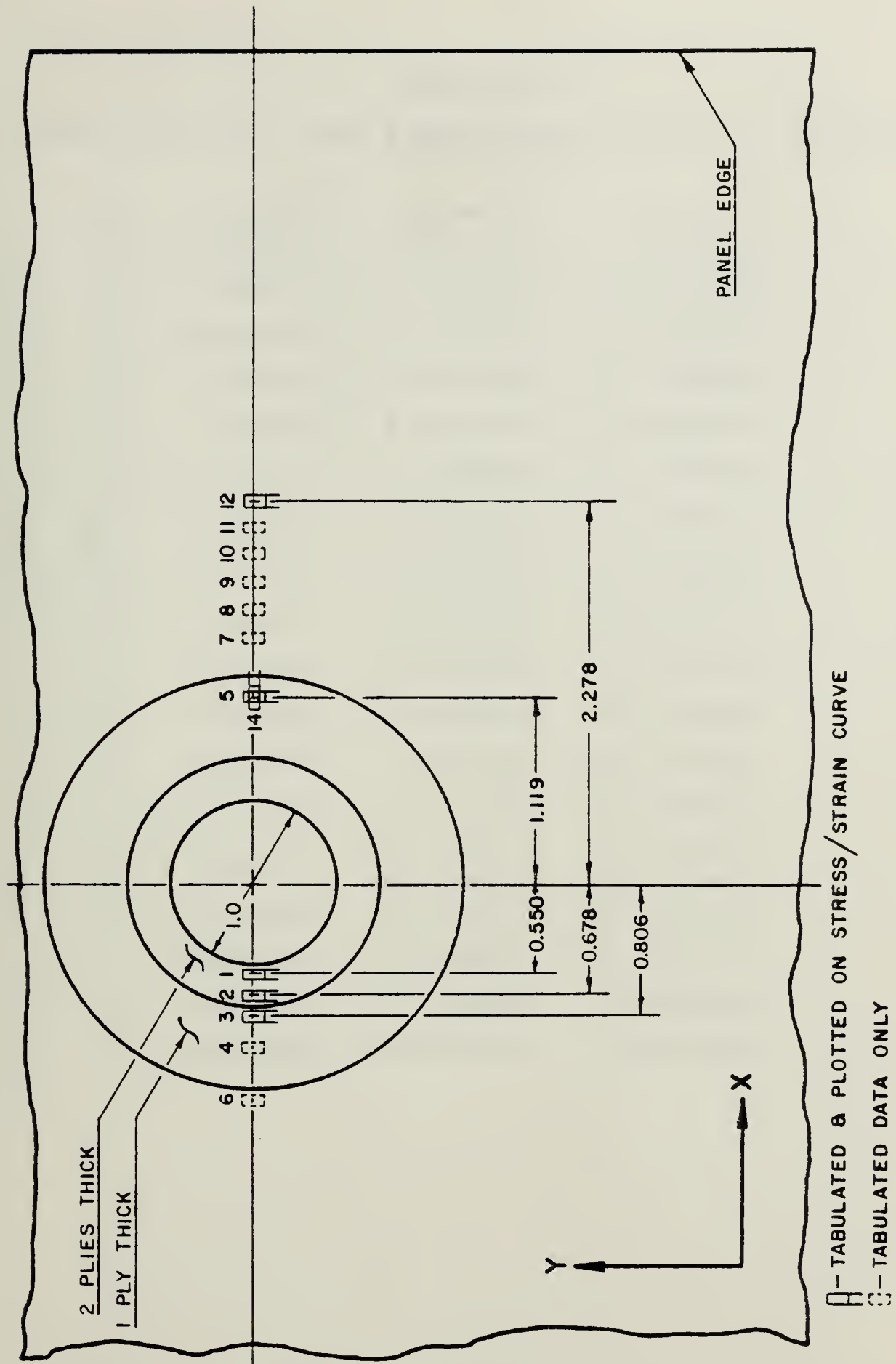


Figure B.1 Panel 1B: Strain Gage Locations.

TABLE VII

Panel 1B: Strain Gage Locations and Strain at 10,000 psi
(Far Field)

G#	X-Coord.	Y-Coord.	Strain
01	-0.5505E+00	0.0060E+00	0.3111E-02
02	-0.6785E+00	0.0125E+00	0.2158E-02
03	-0.8065E+00	0.0030E+00	0.1606E-02
04	-0.9795E+00	0.0010E+00	0.1473E-02
05	0.1195E+01	0.0210E+00	0.1398E-02
06	-0.1300E+01	0.0225E+00	0.1350E-02
07	0.1476E+01	0.0075E+00	0.1236E-02
08	0.1636E+01	0.0065E+00	0.1287E-02
09	0.1801E+01	0.0050E+00	0.1279E-02
10	0.1960E+01	0.0030E+00	0.1322E-02
11	0.2124E+01	-0.0020E+00	0.1338E-02
12	0.2278E+01	-0.0065E+00	0.1346E-02
13	0.5555E+00	0.0070E+00	-0.1789E-02
14	0.1120E+01	0.0210E+00	-0.2180E-03
15	-0.1915E+01	0.0220E+00	-0.1920E-03
16	0.0380E+00	0.5520E+00	-0.6050E-03
17	-0.0075E+00	-0.5760E+00	0.3250E-03
18	0.1515E+00	0.7728E+01	0.1604E-02
19	0.0840E+00	0.7794E+01	0.5830E-03
20	0.0195E+00	0.7871E+01	-0.2860E-03

Panel 1B: 45 Degree, 163 Percent Reinforcement
 Far Field 10,000 PSI Tensile Load (+Py)
 Micro-Strain Along Horizontal Axis of Symmetry

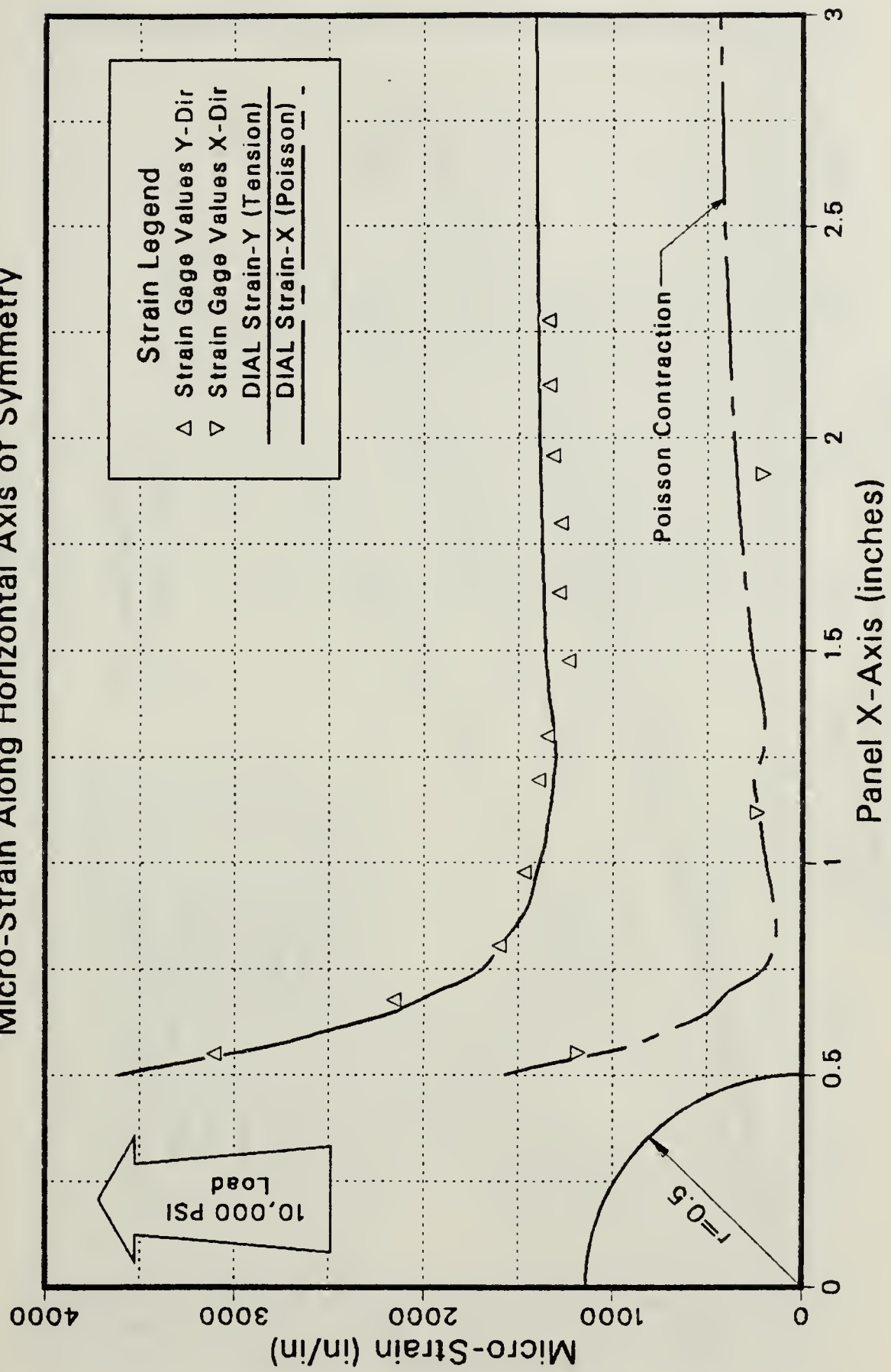


Figure B.2 Panel 1B: Strain Along X Axis at 10,000 psi.

Panel 1B: 45 Degree, 163 Percent Reinforcement

Micro-Strain vs Tensile Load

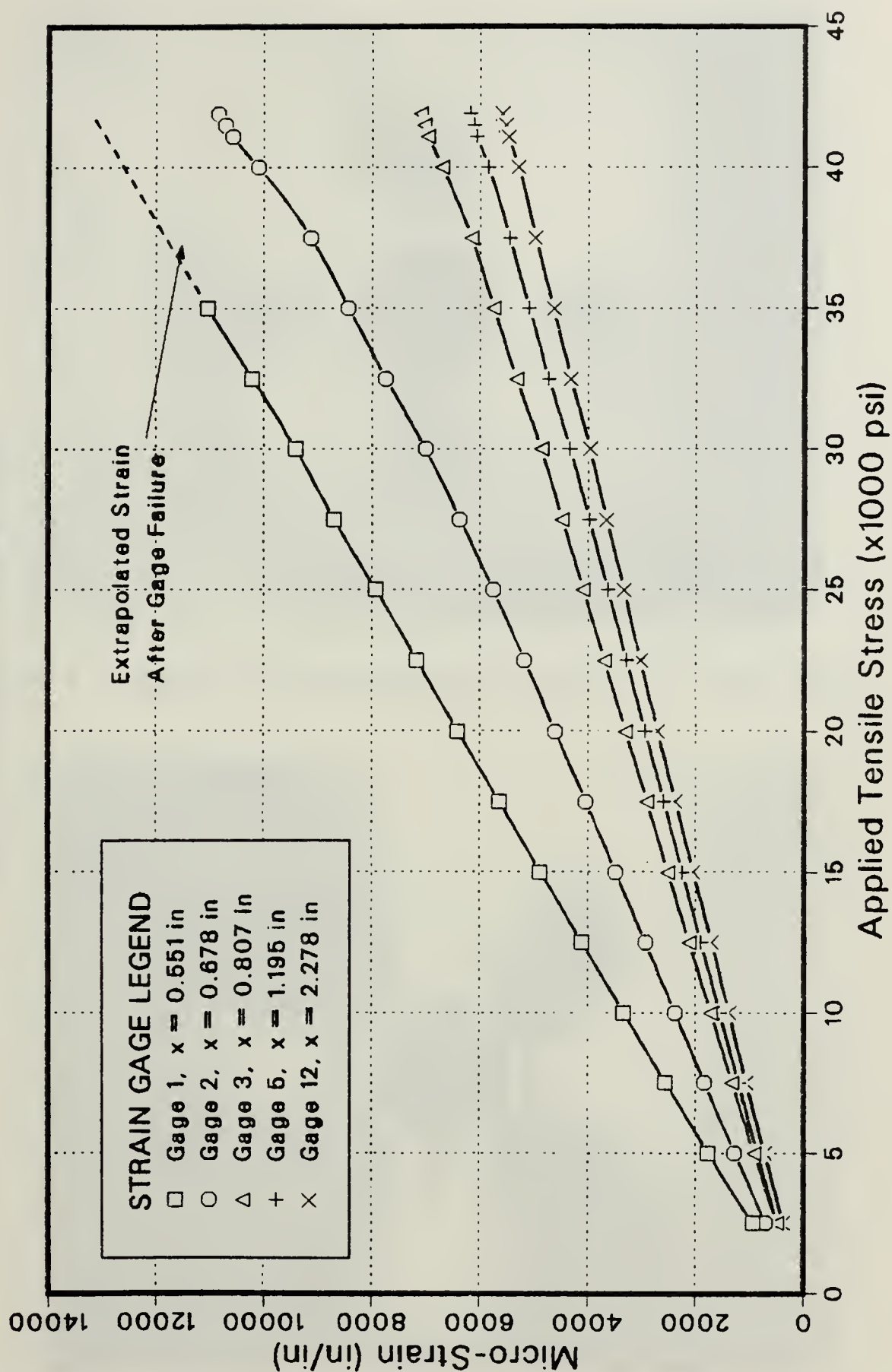


Figure B.3 Panel 1B: Microstrain vs. Tensile Load.

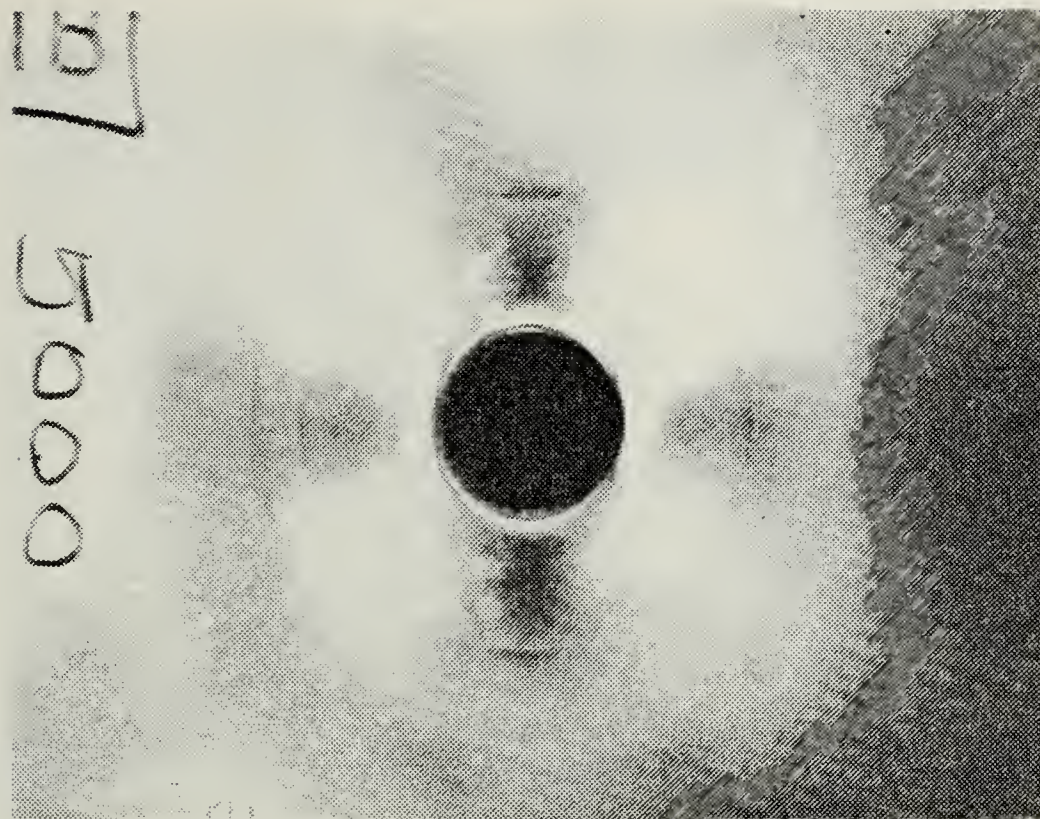


Figure B.4 Panel 1B: Photoelastic Panel at 5,000 psi.

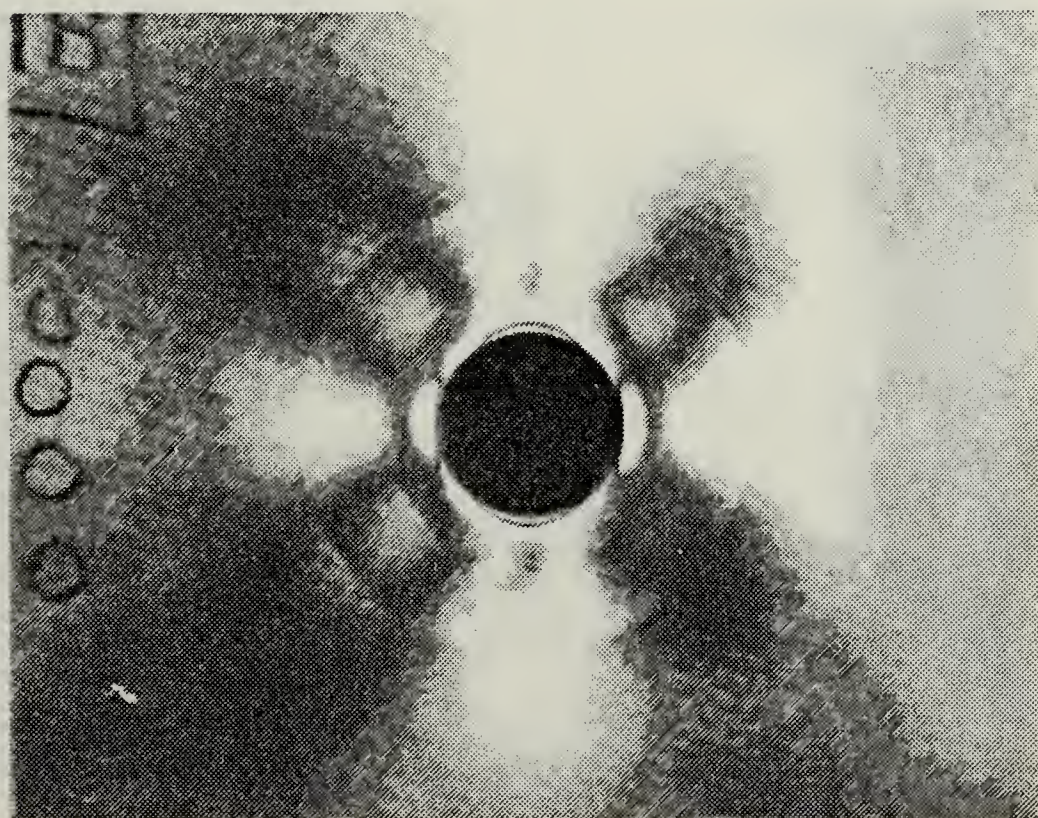


Figure B.5 Panel 1B: Photoelastic Panel at 10,000 psi.

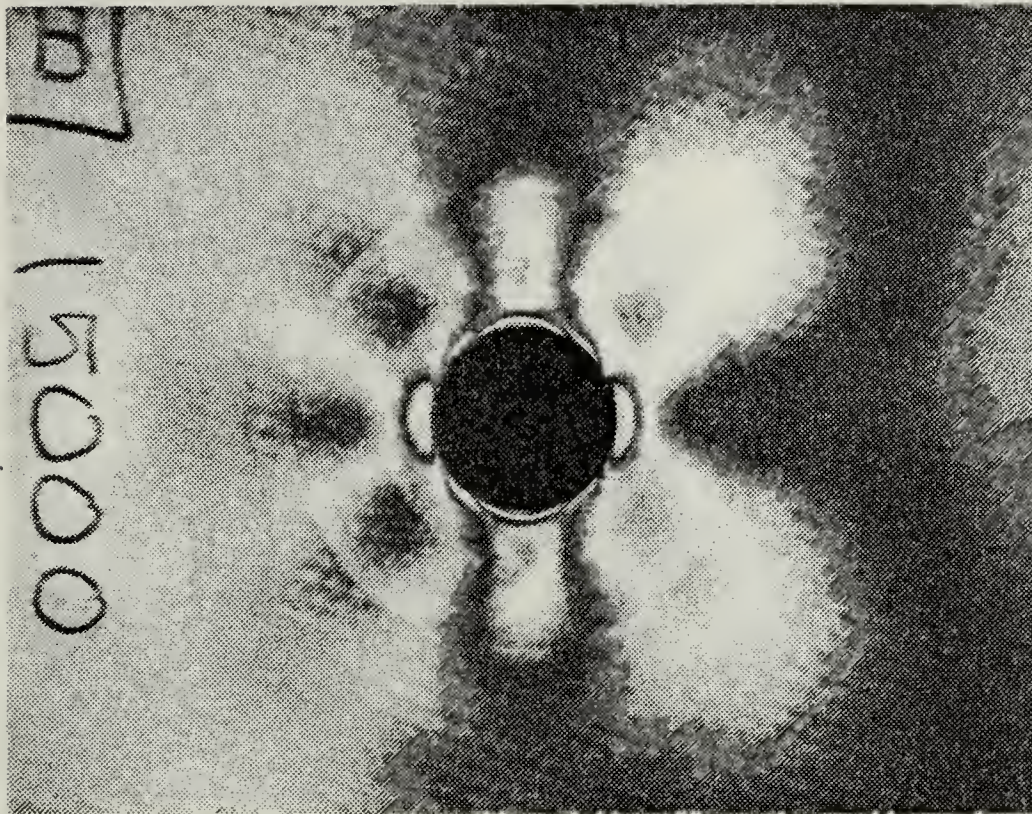


Figure B.6 Panel 1B: Photoelastic Panel at 15,000 psi.

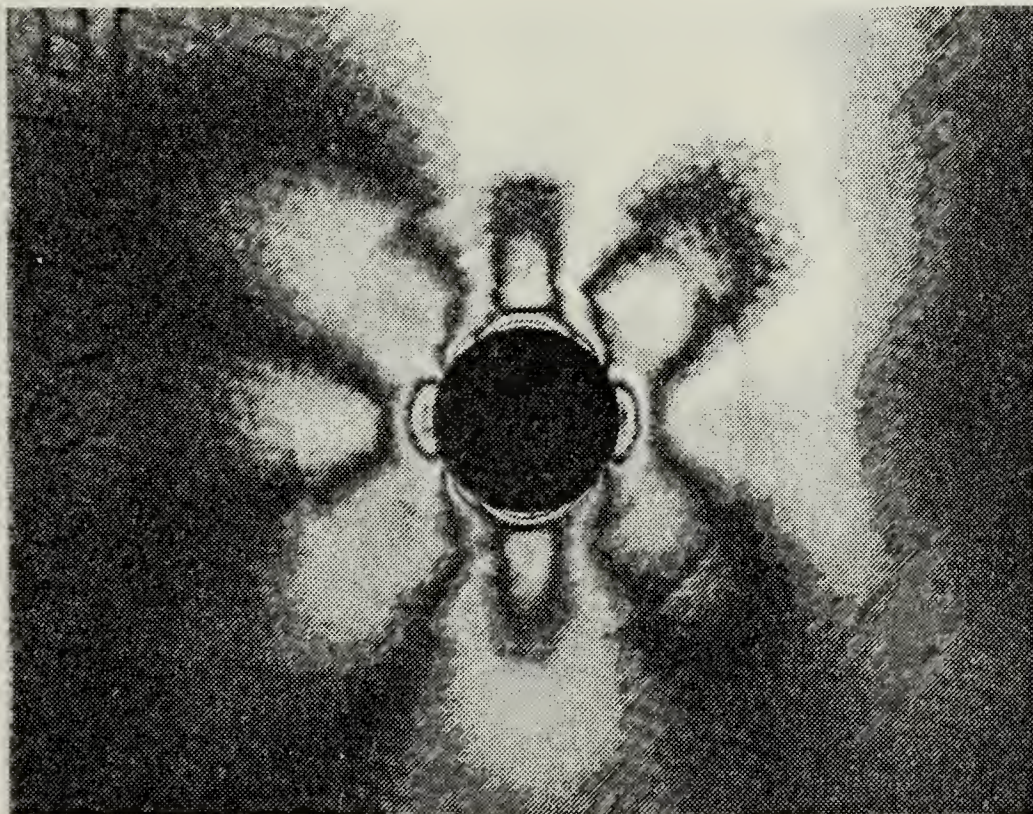


Figure B.7 Panel 1B: Photoelastic Panel at 20,000 psi.

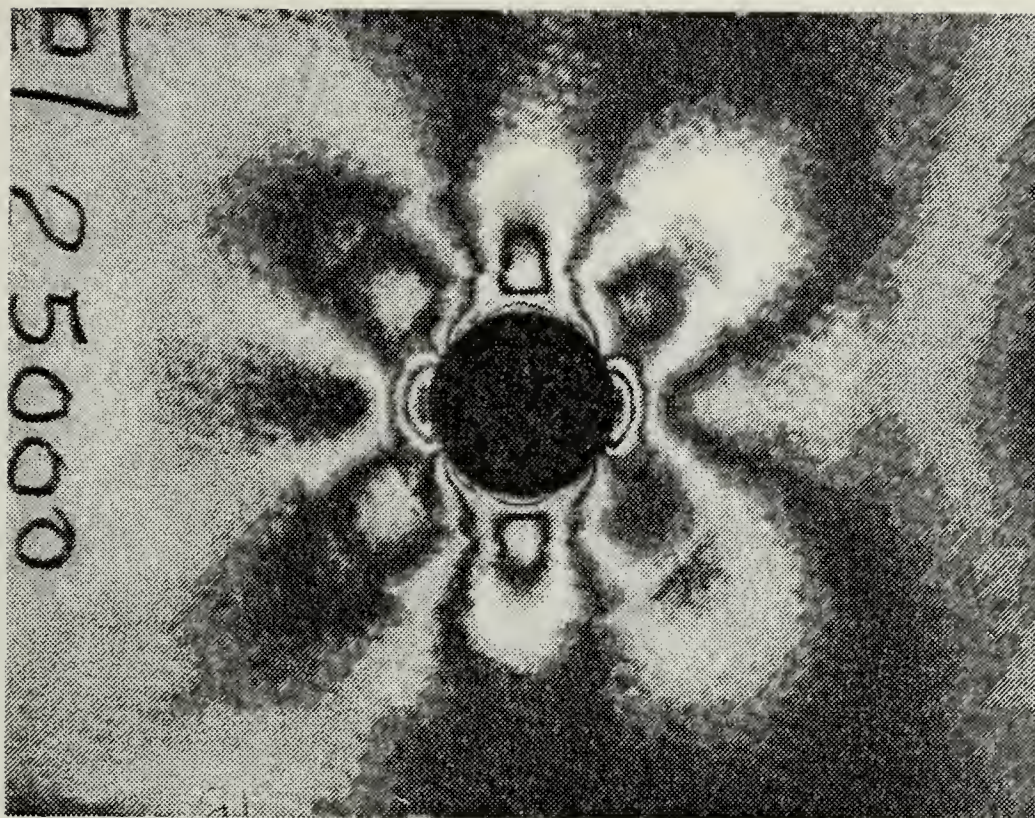


Figure B.8 Panel 1B: Photoelastic Panel at 25,000 psi.

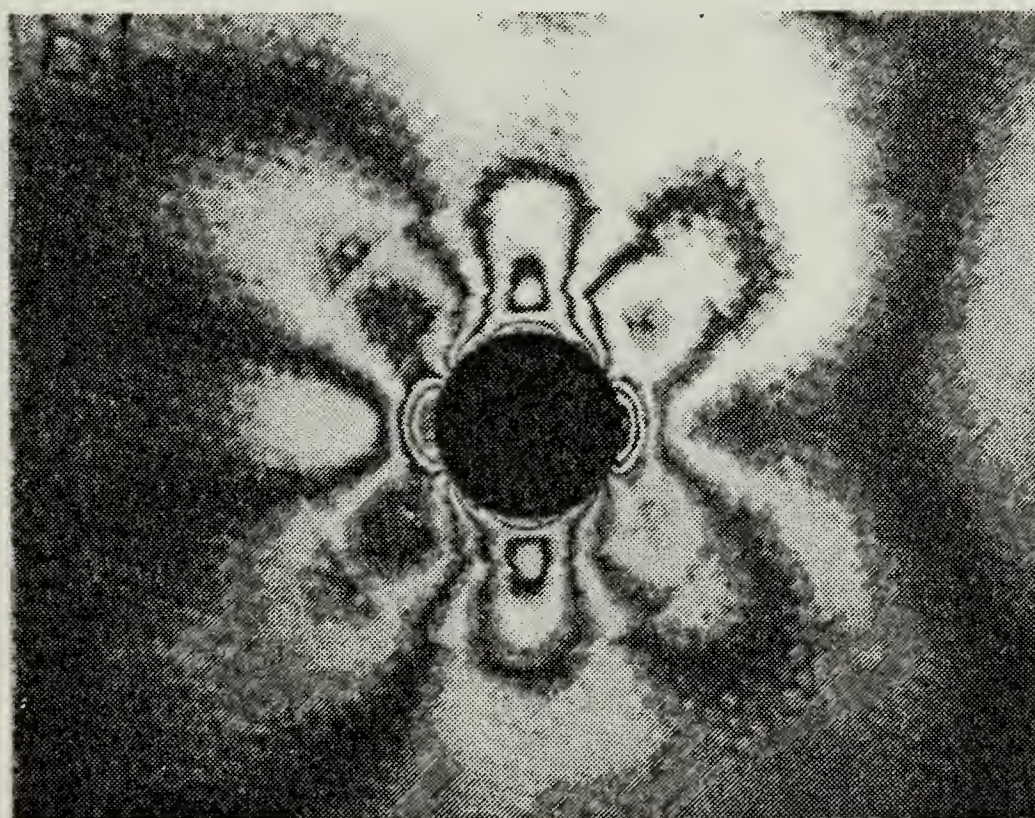


Figure B.9 Panel 1B: Photoelastic Panel at 30,000 psi.

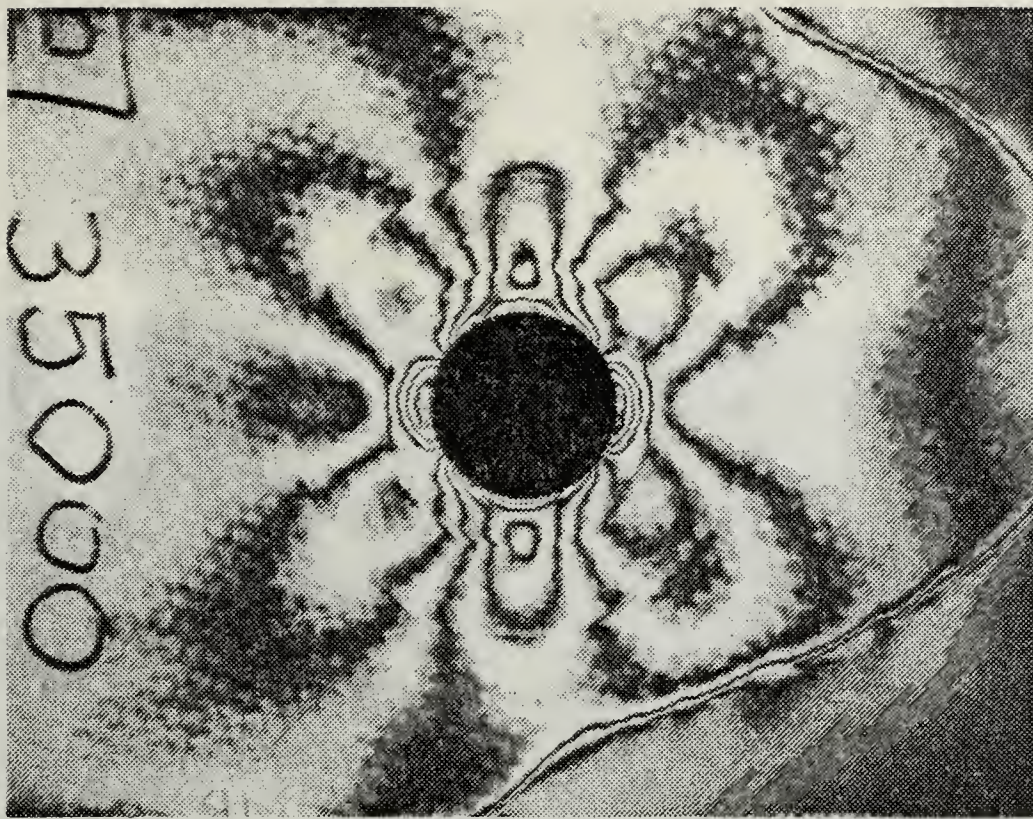


Figure B.10 Panel 1B: Photoelastic Panel at 35,000 psi.

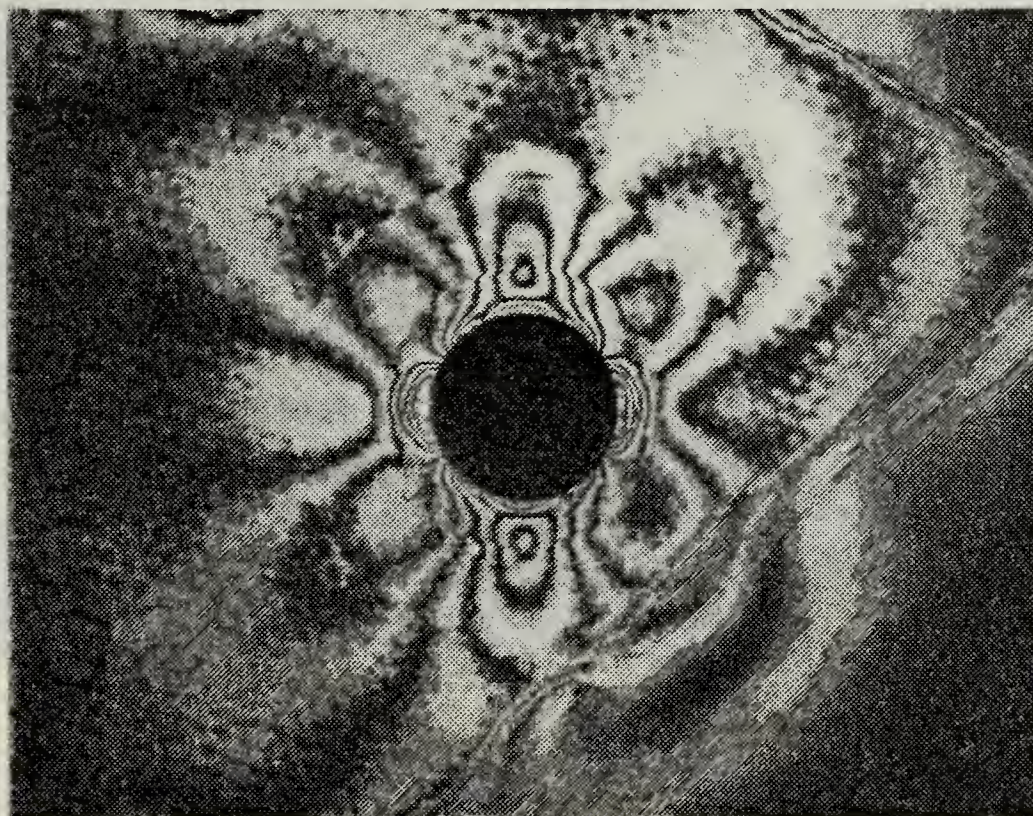


Figure B.11 Panel 1B: Photoelastic Panel at 40,000 psi.

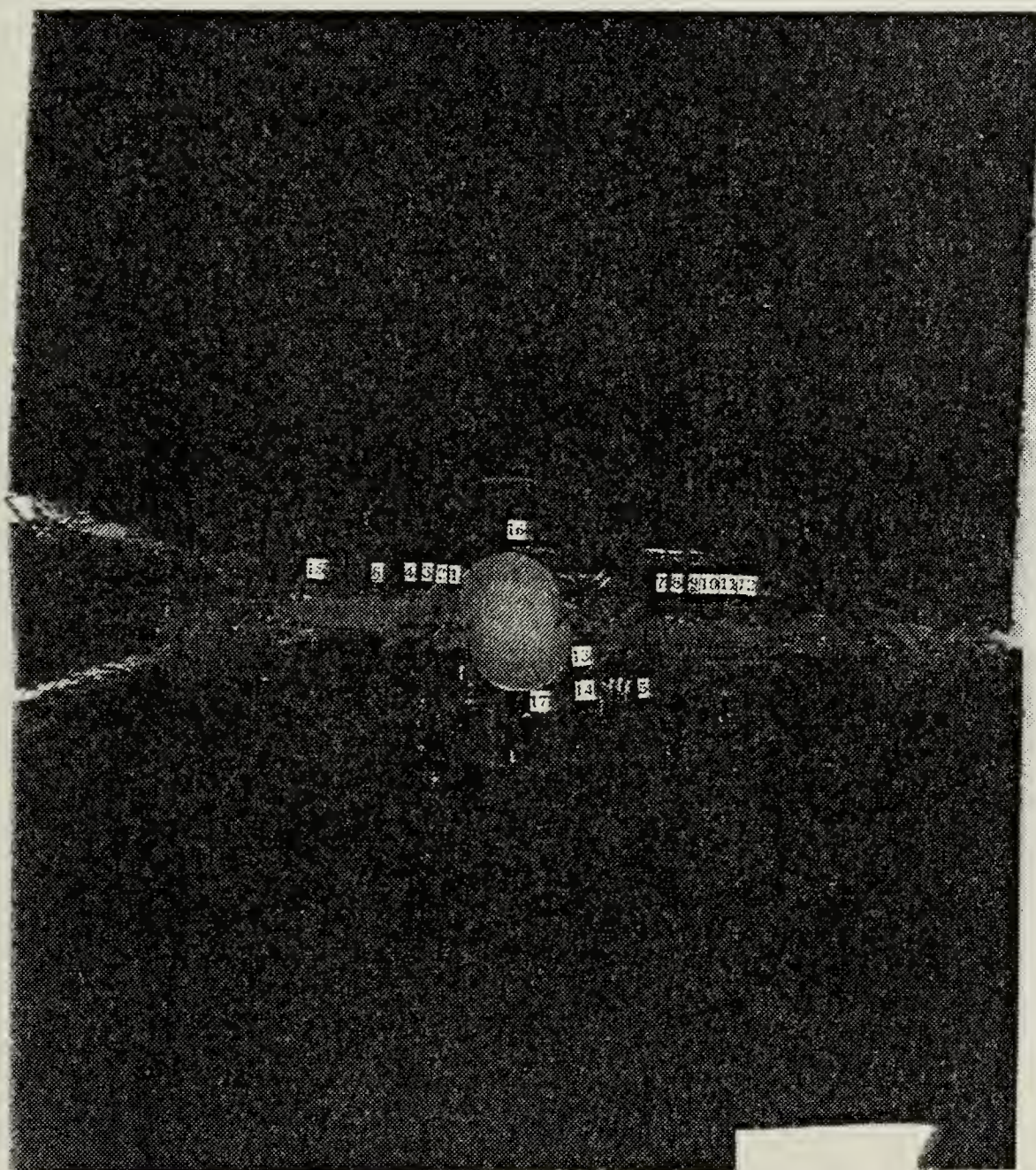


Figure B.12 Panel 1B: Fracture Line.

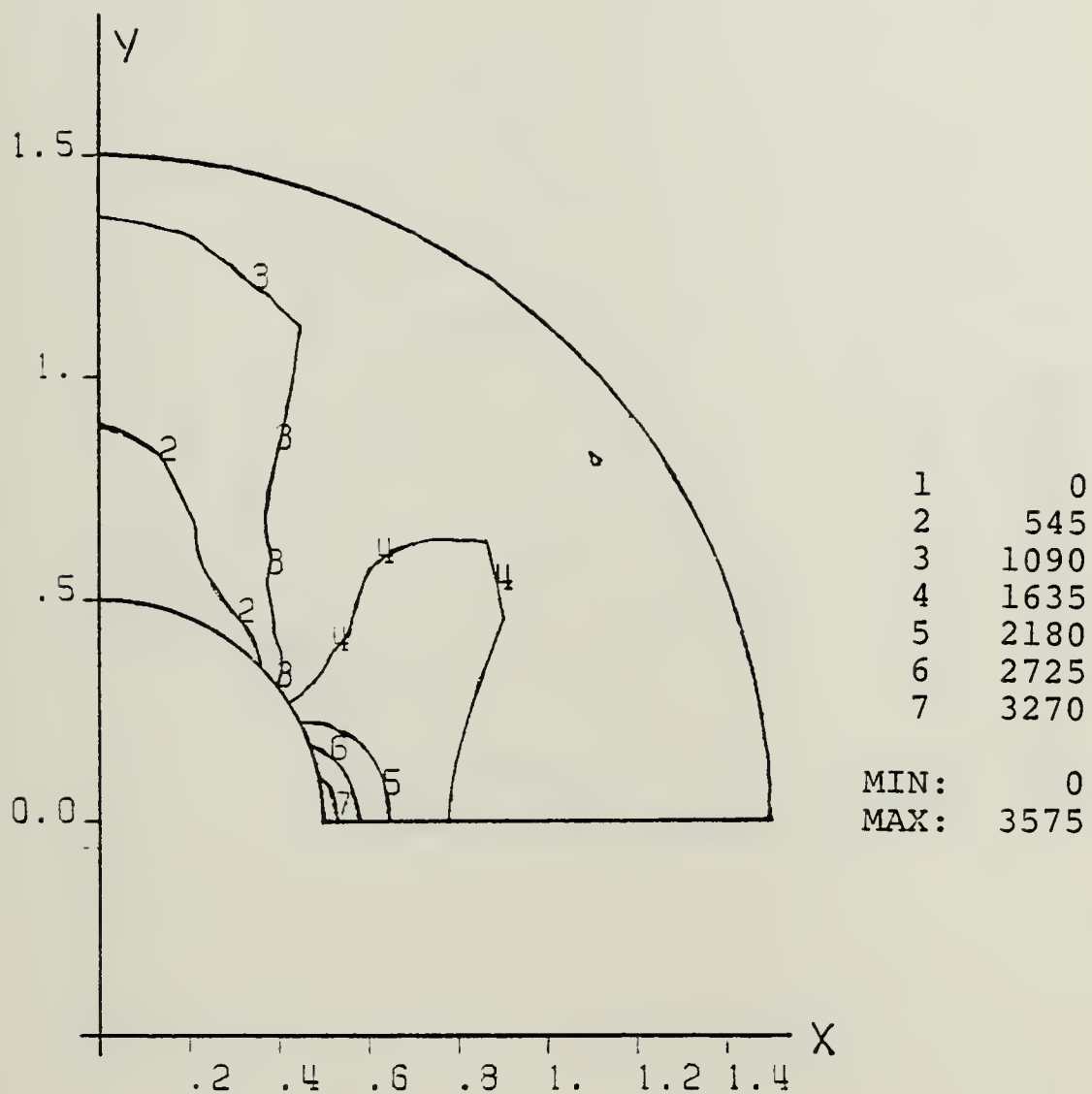


Figure B.13 Panel 1B: Eps-Y ($\times 10^6$) Contours Near Cutout.

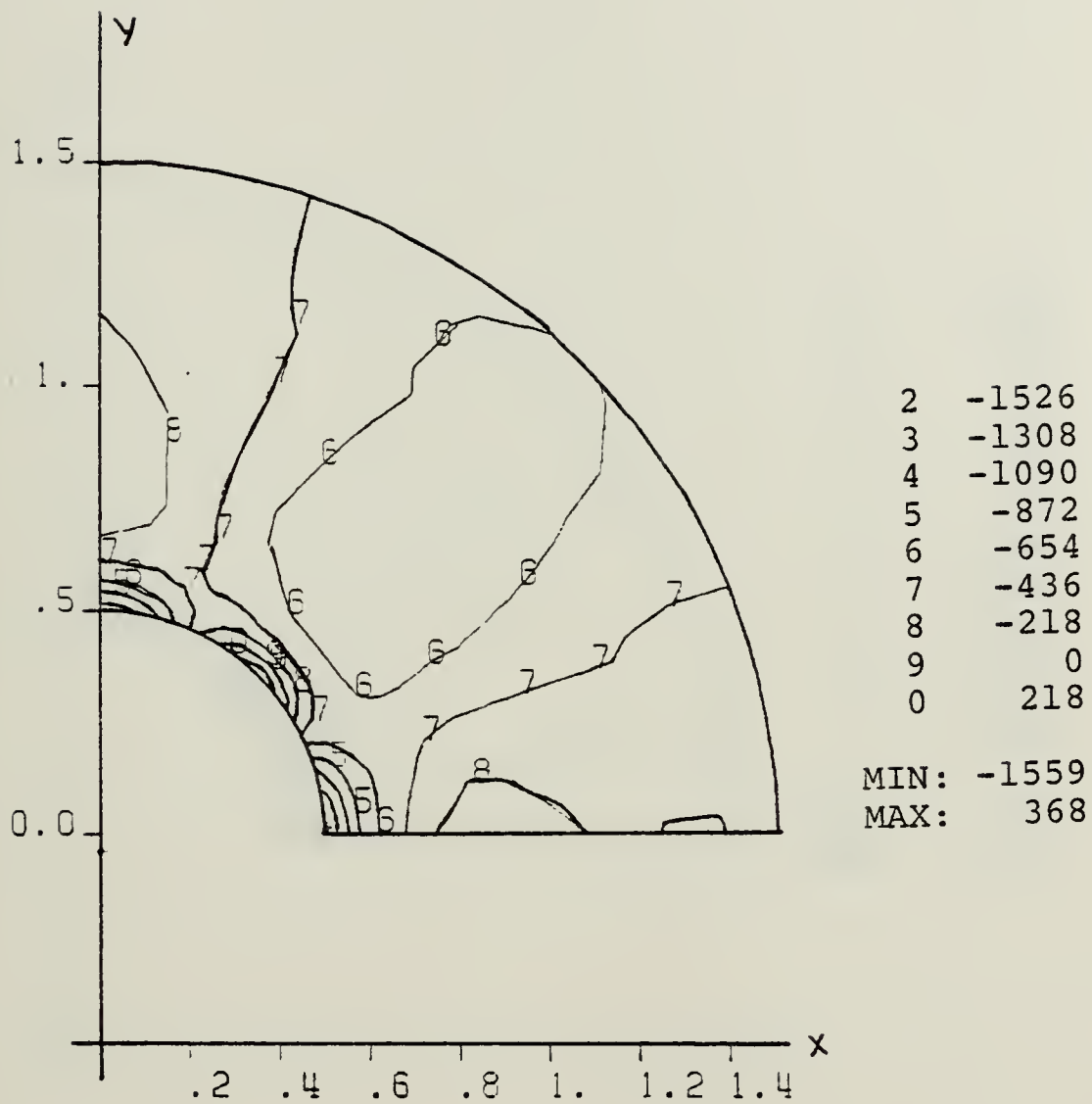


Figure B.14 Panel 1B: Eps-X ($\times 10^6$) Contours Near Cutout.

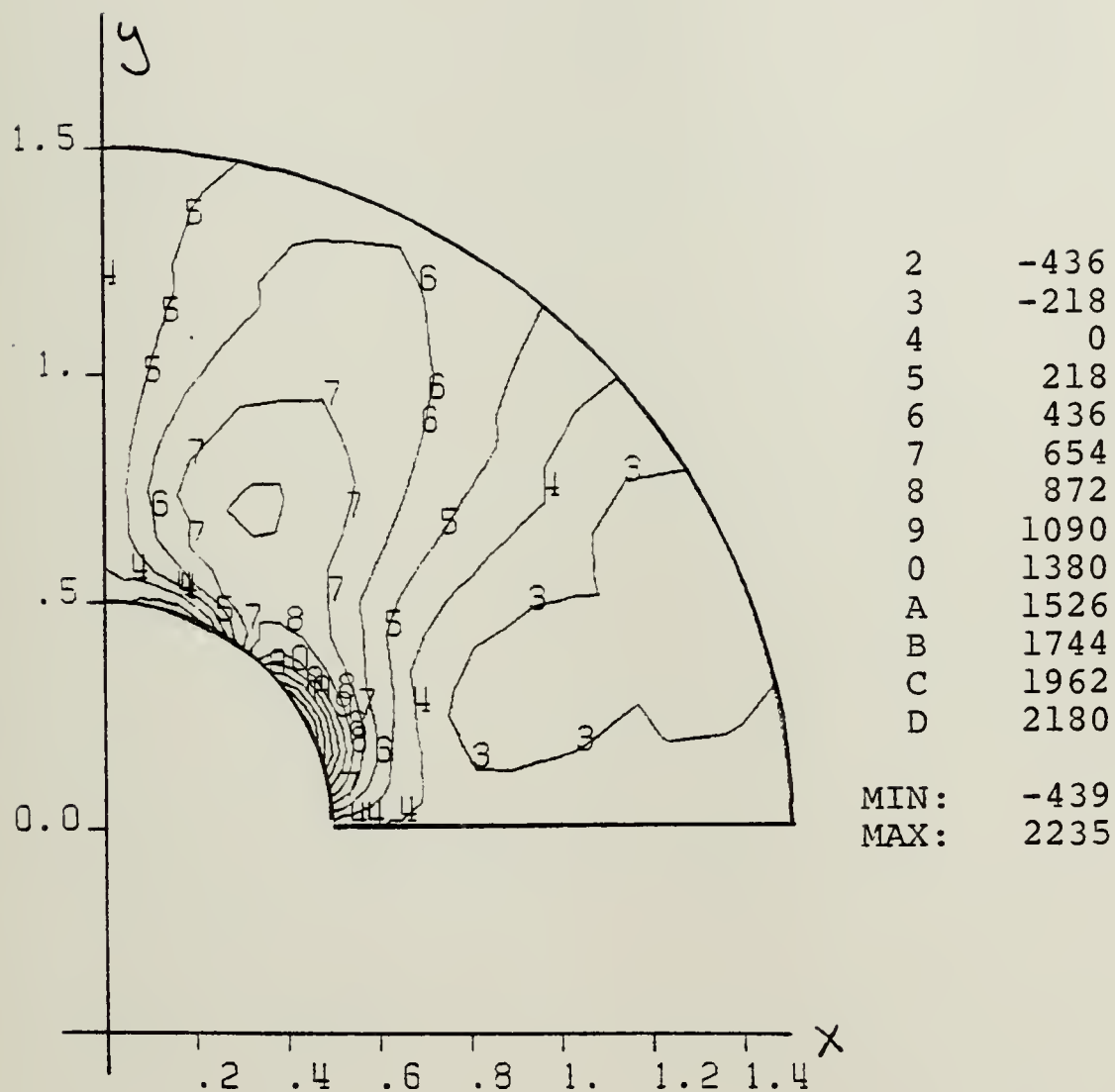


Figure B.15 Panel 1B: Eps-XY (x10⁶) Contours Near Cutout.

APPENDIX C
PANEL 2A

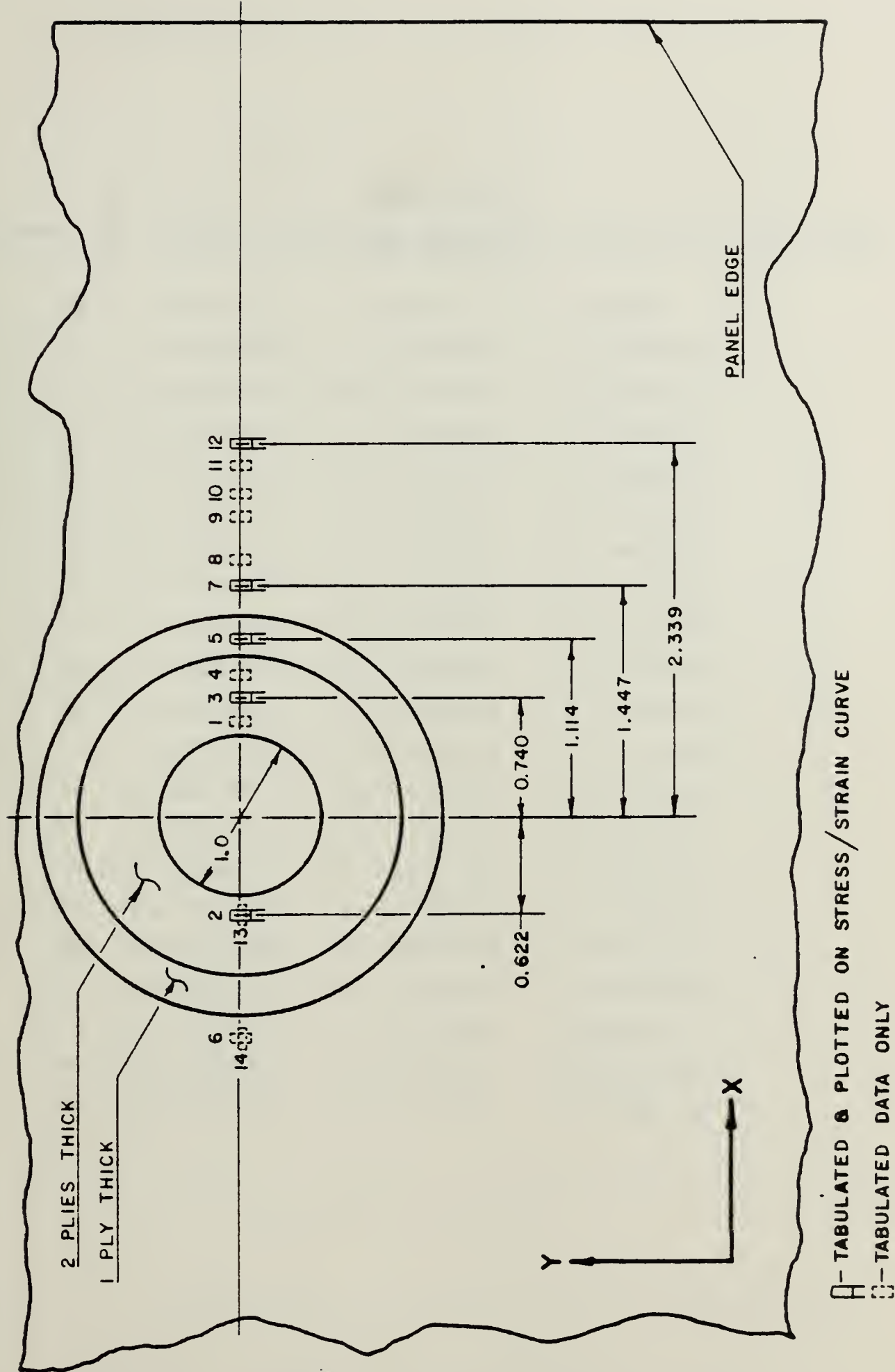


Figure C.1 Panel 2A: Strain Gage Locations.

TABLE VIII

Panel 2A: Strain Gage Locations and Strain at 10,000 psi
(Far Field)

G#	X-Coord.	Y-Coord.	Strain
01	0.5990E+00	-0.0025E+00	0.1715E-02
02	-0.6220E+00	-0.0115E+00	0.1784E-02
03	0.7400E+00	-0.0105E+00	0.1534E-02
04	0.8885E+00	-0.0225E+00	0.1162E-02
05	0.1114E+01	-0.0200E+00	0.1122E-02
06	-0.1386E+01	-0.0195E+00	0.1198E-02
07	0.1447E+01	-0.0105E+00	0.1181E-02
08	0.1604E+01	-0.0165E+00	0.1228E-02
09	0.1868E+01	-0.0155E+00	0.1265E-02
10	0.2023E+01	-0.0100E+00	0.1255E-02
11	0.2186E+01	-0.0060E+00	0.1321E-02
12	0.2339E+01	-0.0050E+00	0.1261E-02
13	-0.6220E+00	-0.0115E+00	-0.3200E-04
14	-0.1386E+01	-0.0195E+00	-0.1690E-03
15	-0.2060E+01	0.0010E+00	-0.3520E-03
16	-0.0030E+00	0.5630E+00	-0.4810E-03
17	0.0085E+00	-0.6420E+00	0.7200E-04
18	-0.1370E+00	-0.7039E+01	-0.3380E-03
19	-0.0695E+00	-0.6970E+01	0.4080E-03
20	-0.0025E+00	-0.6907E+01	0.1320E-02

Panel 2A: 0/90 Degree, 206 Percent Reinforcement
 Far Field 10,000 PSI Tensile Load (+Py)
 Micro-Strain Along Horizontal Axis of Symmetry

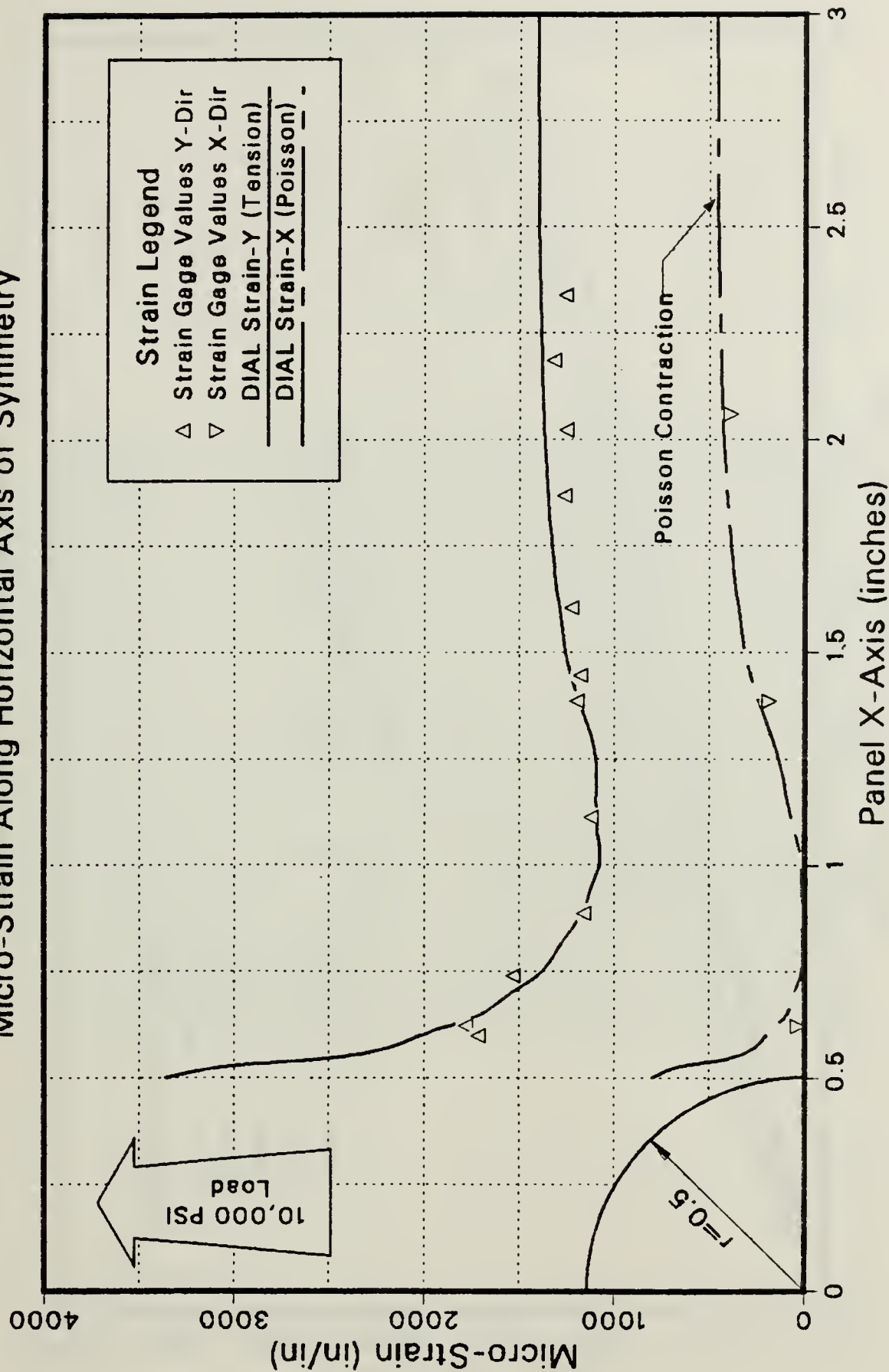


Figure C.2 Panel 2A: Strain Along X Axis at 10,000 psi.

Panel 2A: 0/90 Degree, 206 Percent Reinforcement Micro-Strain vs Tensile Load

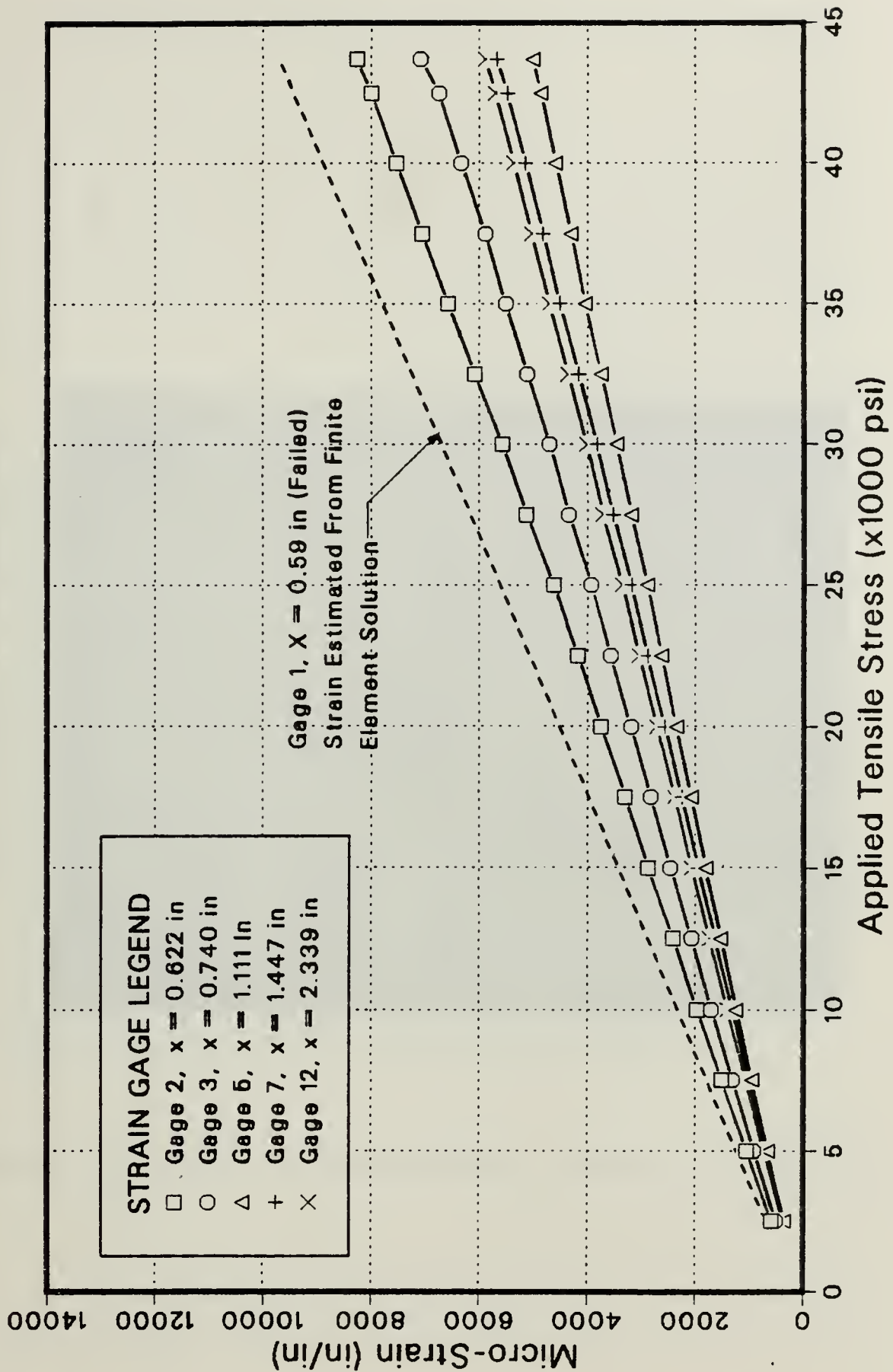


Figure C.3 Panel 2A: Microstrain vs. Tensile Load.

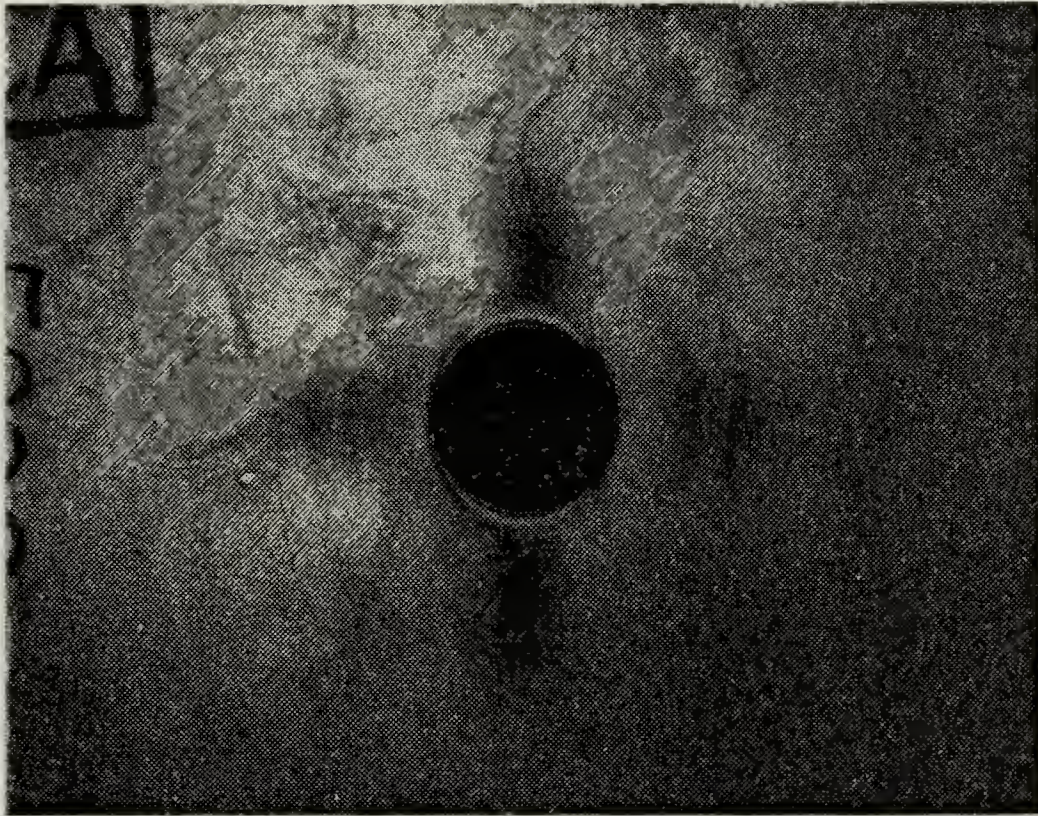


Figure C.4 Panel 2A: Photoelastic Panel at 5,000 psi.

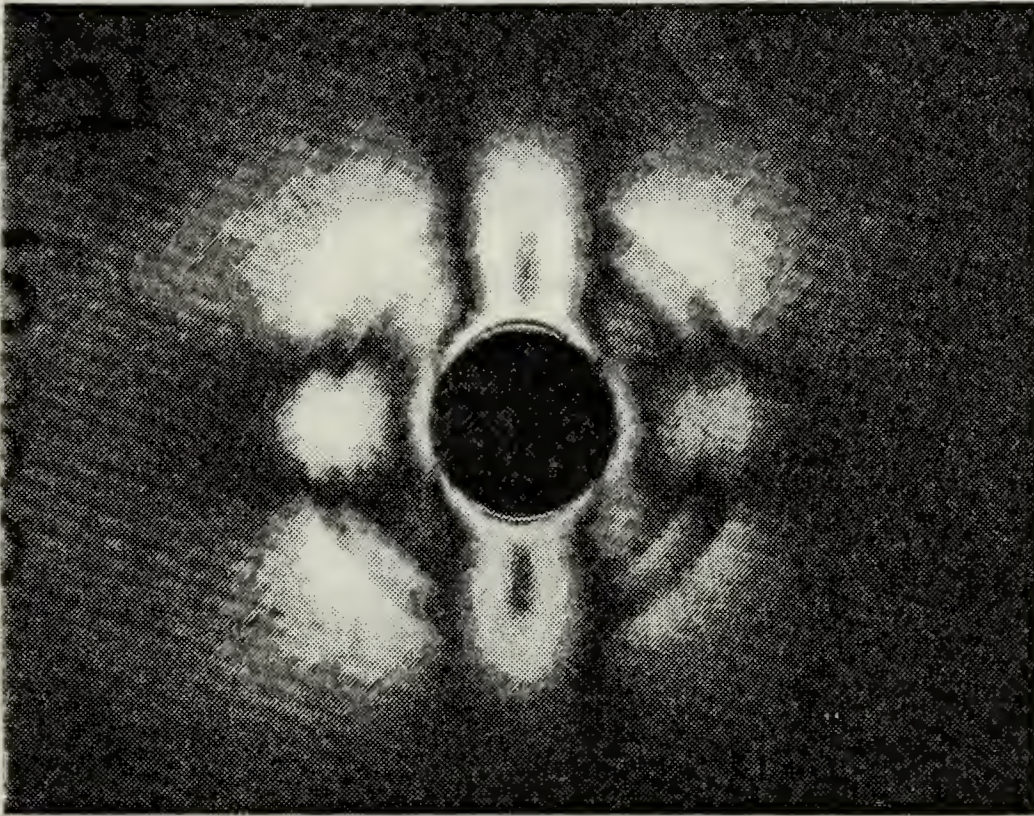


Figure C.5 Panel 2A: Photoelastic Panel at 10,000 psi.

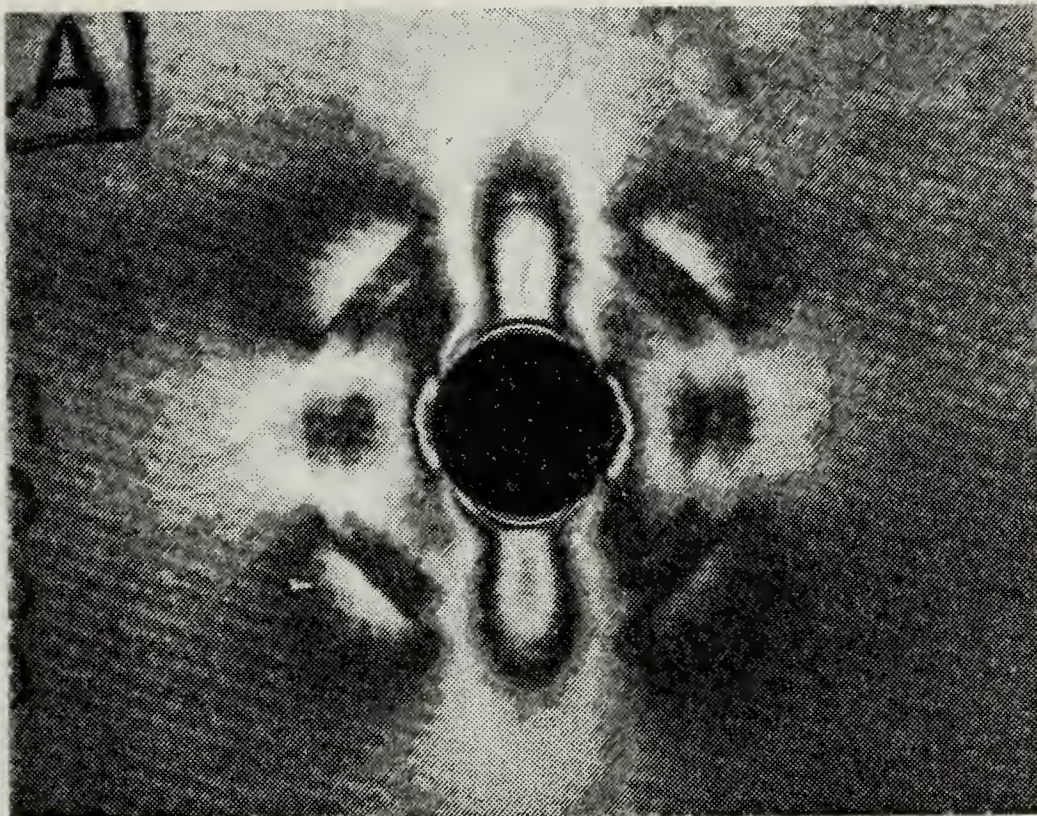


Figure C.6 Panel 2A: Photoelastic Panel at 15,000 psi.

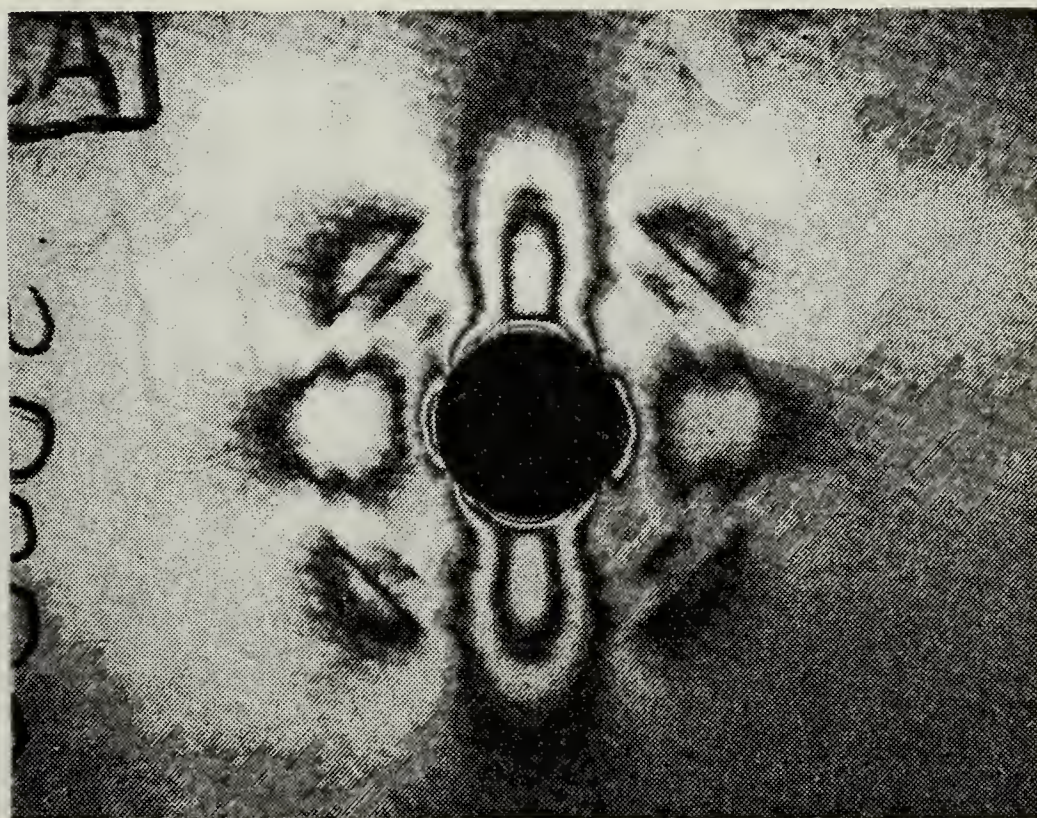


Figure C.7 Panel 2A: Photoelastic Panel at 20,000 psi.

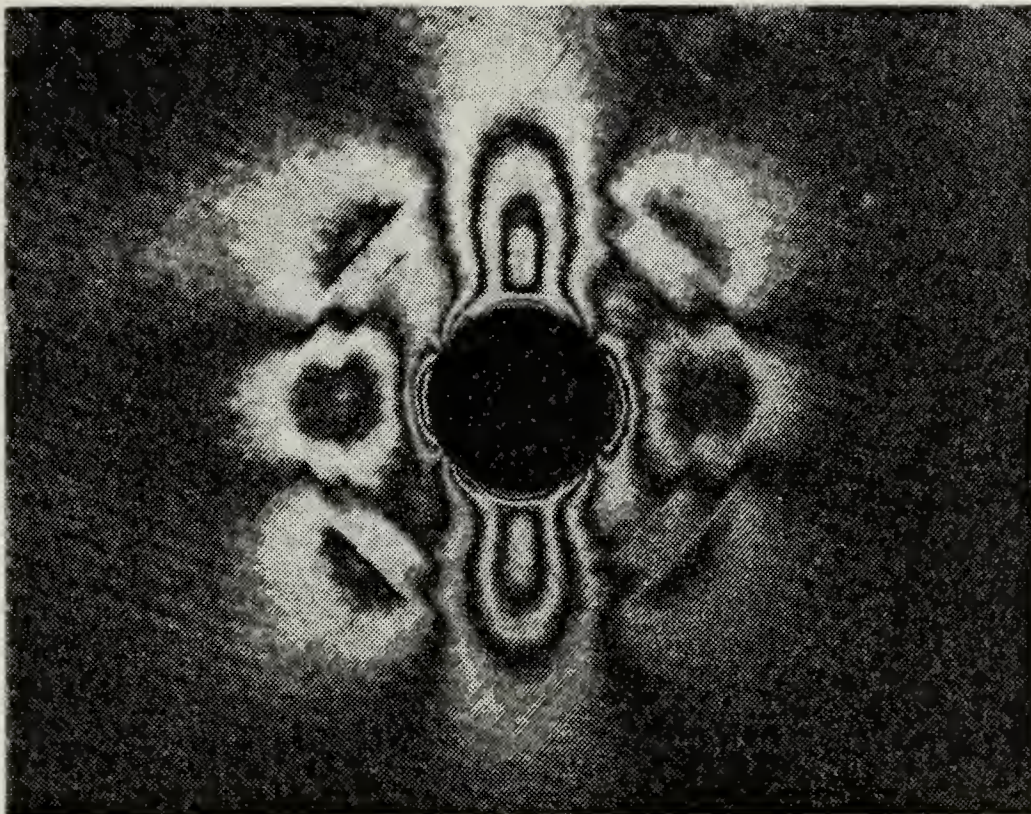


Figure C.8 Panel 2A: Photoelastic Panel at 25,000 psi.

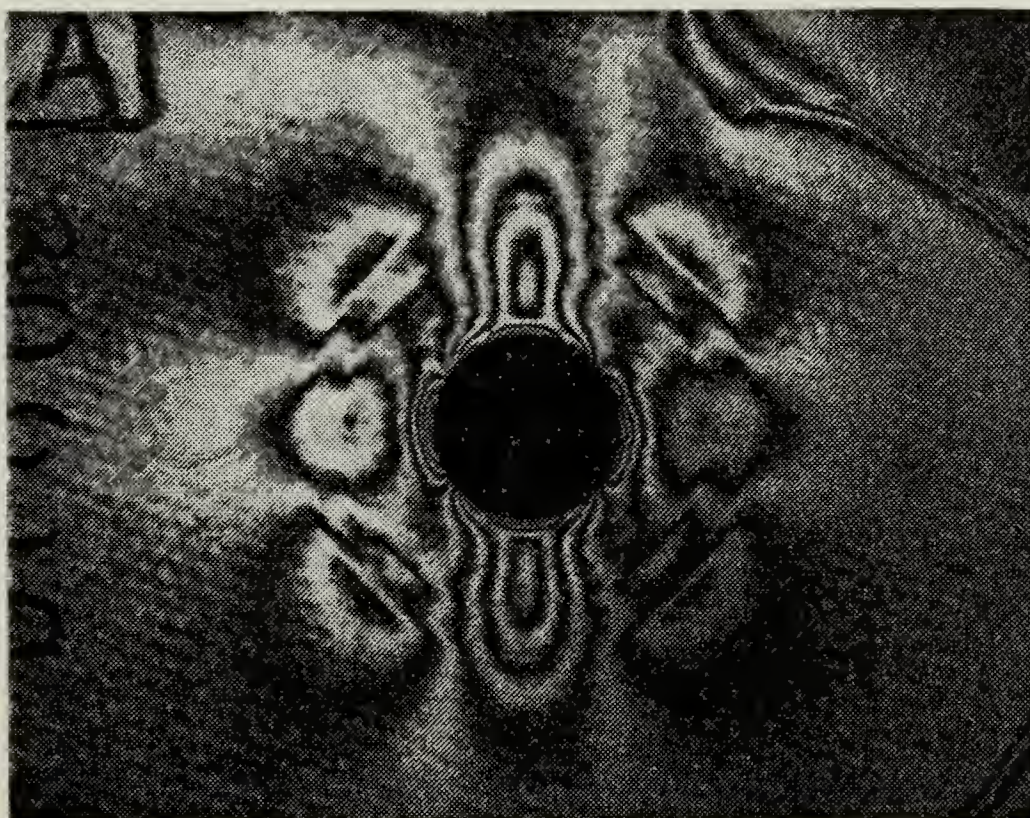


Figure C.9 Panel 2A: Photoelastic Panel at 30,000 psi.

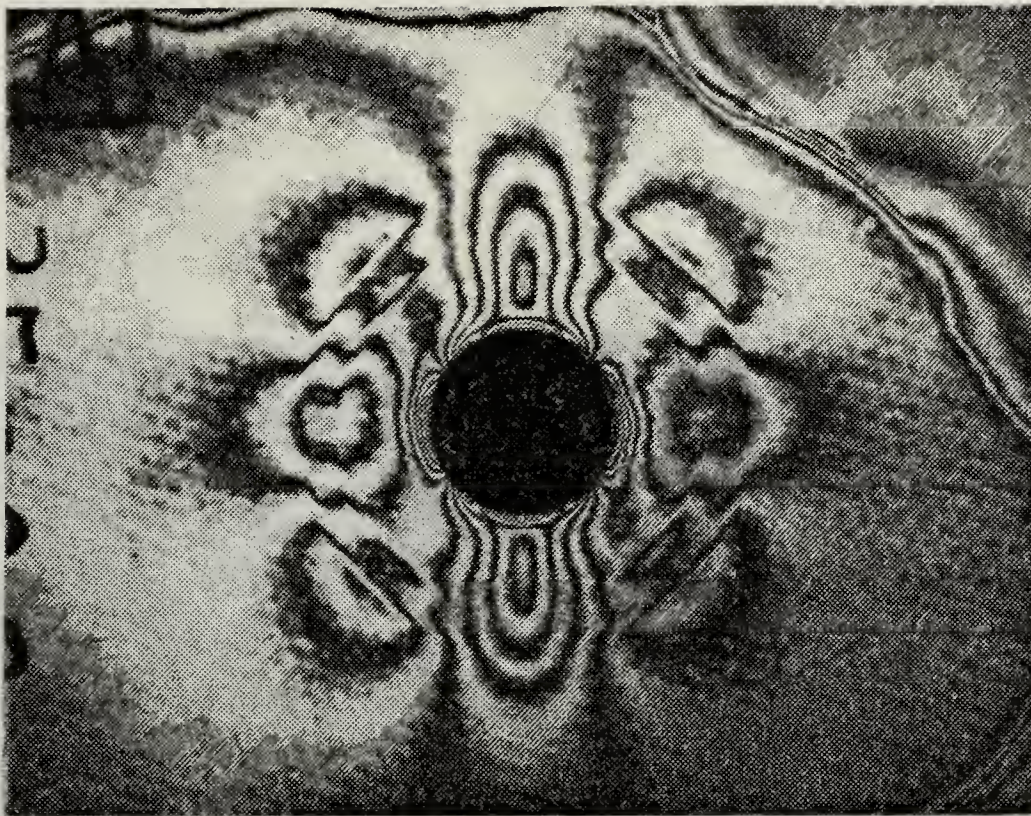


Figure C.10 Panel 2A: Photoelastic Panel at 35,000 psi.

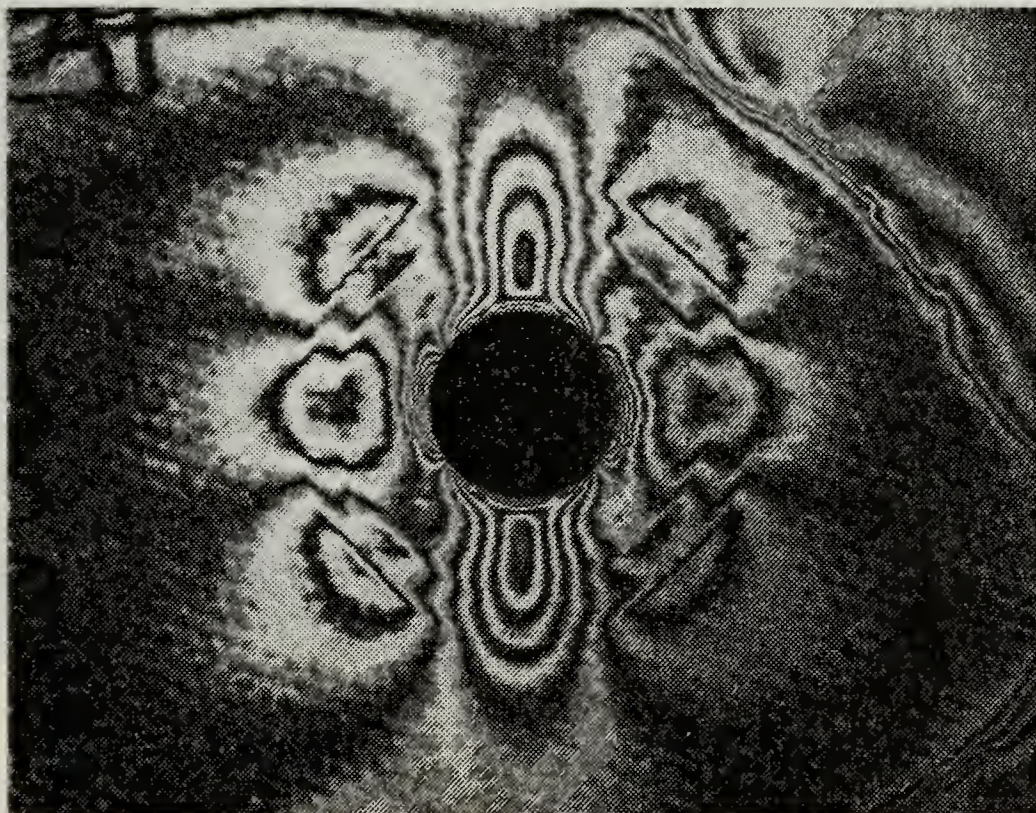


Figure C.11 Panel 2A: Photoelastic Panel at 40,000 psi.

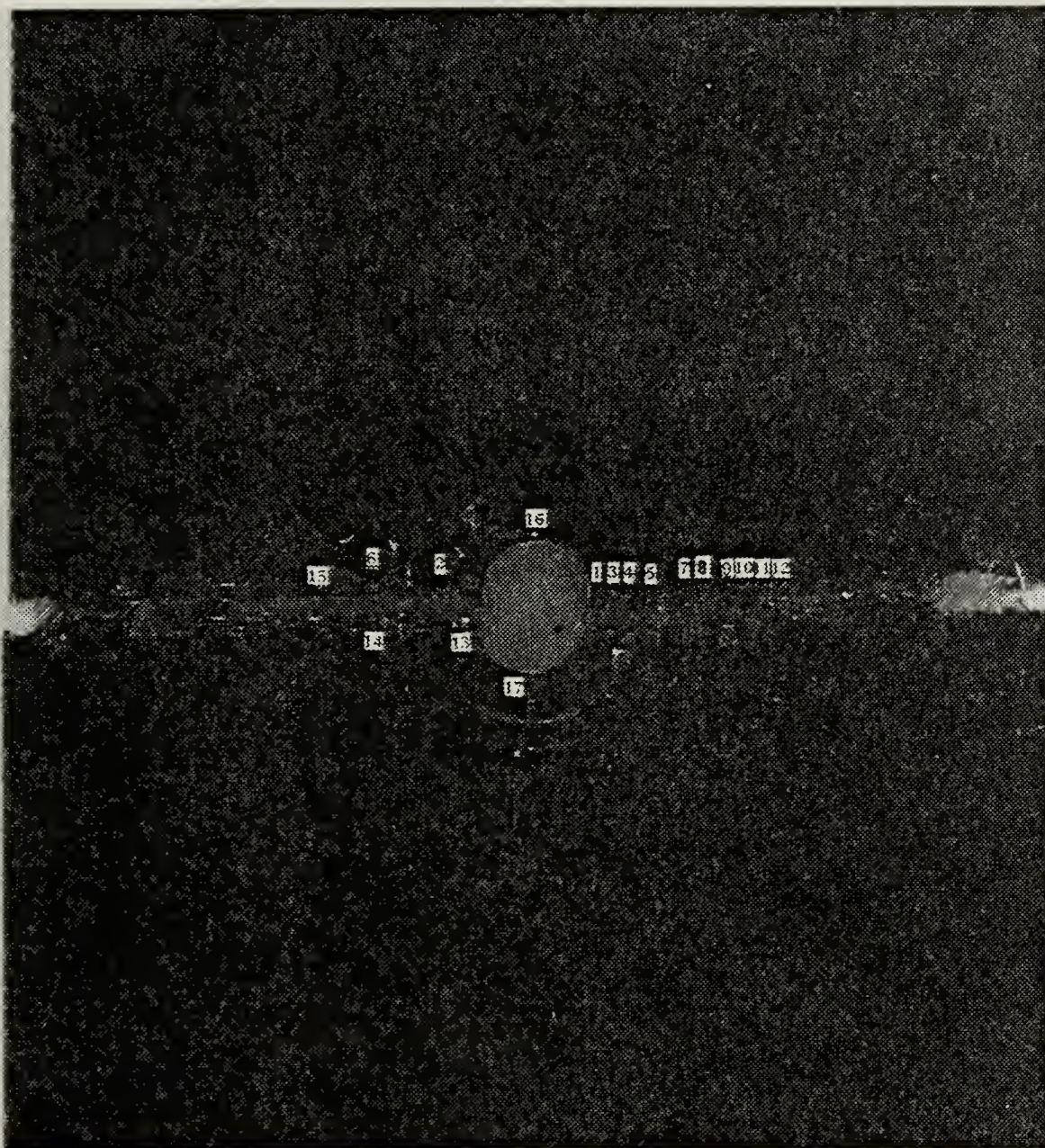


Figure C.12 Panel 2A: Fracture Line.

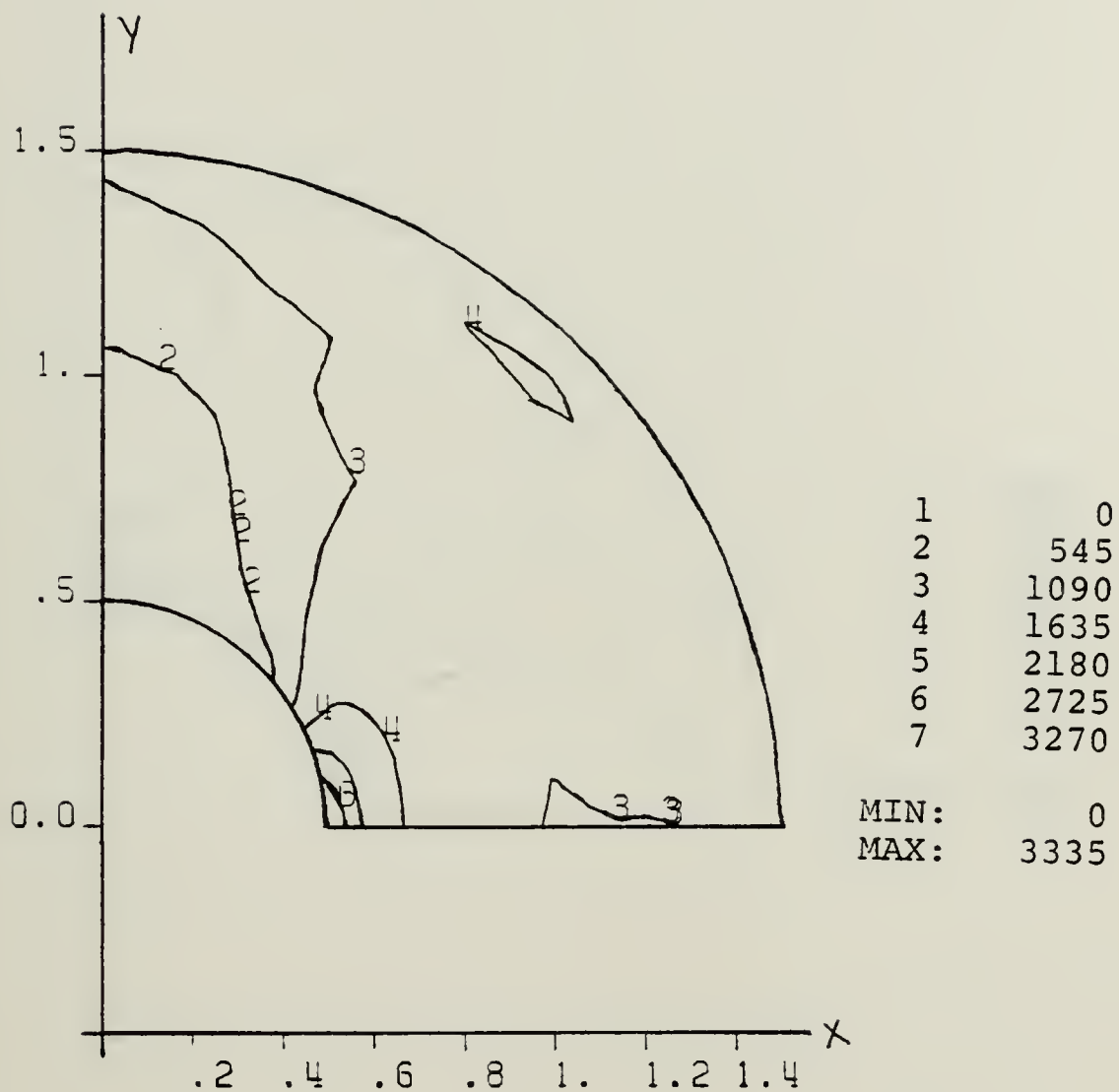


Figure C.13 Panel 2A: Eps-Y ($\times 10^6$) Contours Near Cutout.

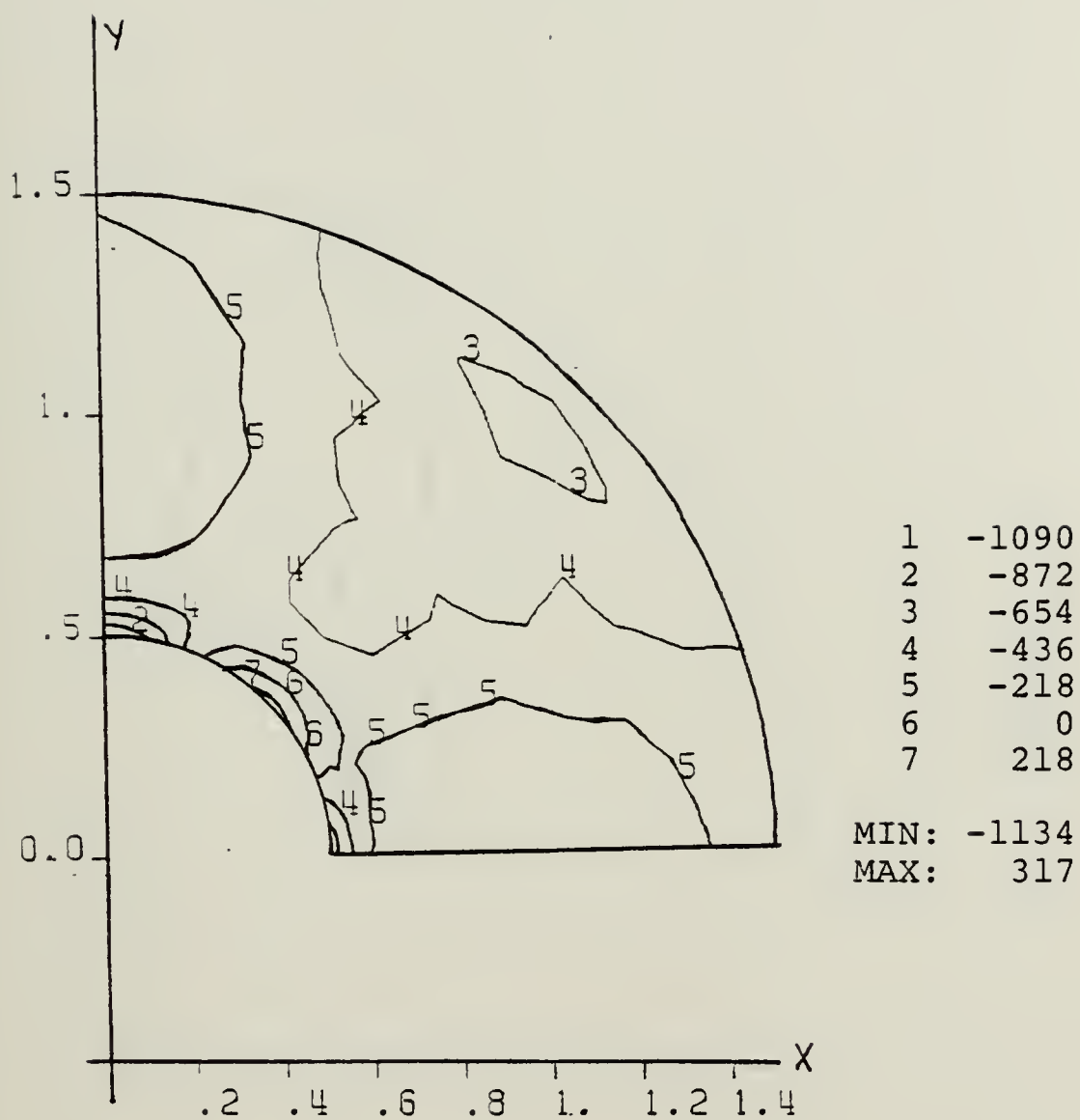


Figure C.14 Panel 2A: Eps-X ($\times 10^6$) Contours Near Cutout.

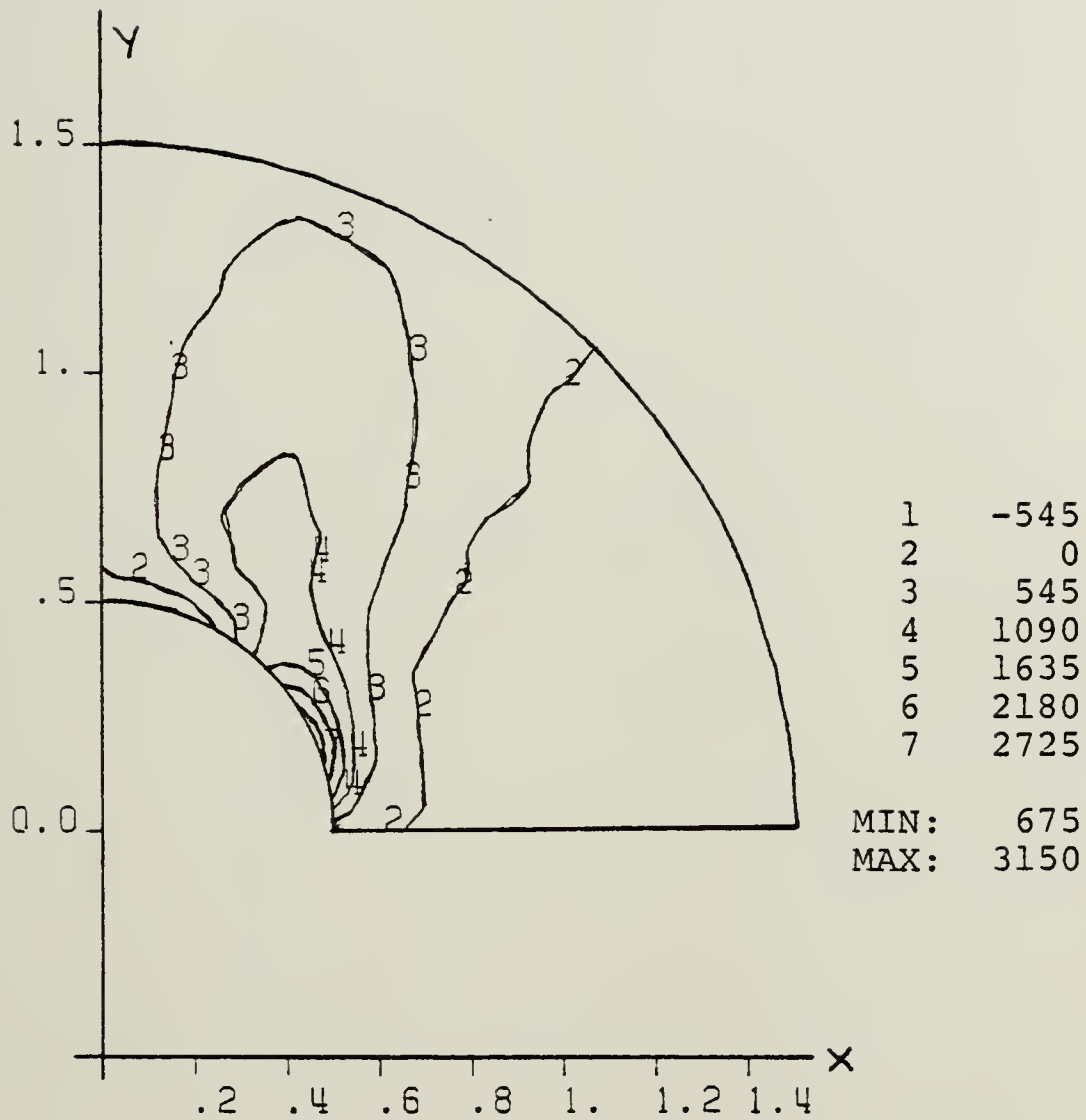


Figure C.15 Panel 2A: Eps-XY ($\times 10^6$) Contours Near Cutout.

APPENDIX D
PANEL 2B

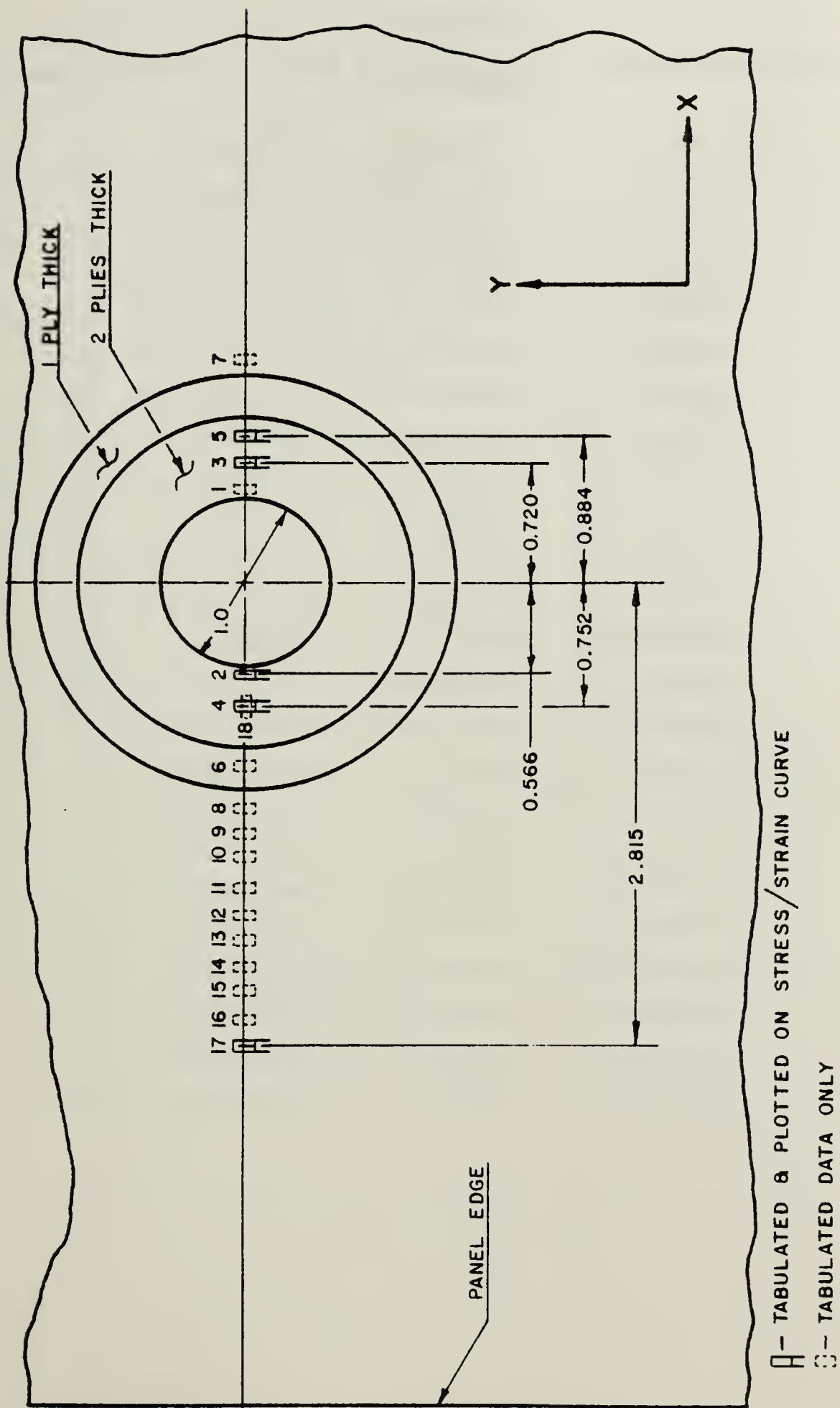


Figure D.1 Panel 2B: Strain Gage Locations.

TABLE IX

Panel 2B: Strain Gage Locations and Strain at 10,000 psi
(Far Field)

G#	X-Coord.	Y-Coord.	Strain
01	0.5645E+00	-0.0065E+00	0.2697E-02
02	-0.5665E+00	0.0085E+00	0.2840E-02
03	0.7200E+00	0.0010E+00	0.1779E-02
04	-0.7520E+00	0.0130E+00	0.1739E-02
05	0.8845E+00	-0.0070E+00	0.1365E-02
06	-0.1128E+01	0.0015E+00	0.1135E-02
07	0.1335E+01	0.0055E+00	0.1262E-02
08	-0.1374E+01	0.0245E+00	0.1058E-02
09	-0.1533E+01	0.0240E+00	0.1111E-02
10	-0.1697E+01	0.0230E+00	0.1107E-02
11	-0.1852E+01	0.0165E+00	0.1164E-02
12	-0.2019E+01	0.0165E+00	0.1082E-02
13	-0.2170E+01	0.0165E+00	0.1160E-02
14	-0.2338E+01	0.0165E+00	0.1149E-02
15	-0.2492E+01	0.0165E+00	0.1144E-02
16	-0.2655E+01	0.0165E+00	0.1151E-02
17	-0.2815E+01	0.0165E+00	0.1121E-02
18	-0.7520E+00	0.0130E+00	-0.3070E-03
19	0.1710E+01	0.0100E+00	-0.2380E-03
20	0.0100E+00	-0.5915E+00	-0.6220E-03
21	-0.0080E+00	-0.7746E+01	0.1404E-02
22	-0.0790E+00	-0.7812E+01	0.6610E-03
23	-0.1475E+00	-0.7878E+01	-0.4060E-03

Panel 2B: 45 Degree, 206 Percent Reinforcement
 Far Field 10,000 PSI Tensile Load (+Py)
 Micro-Strain Along Horizontal Axis of Symmetry

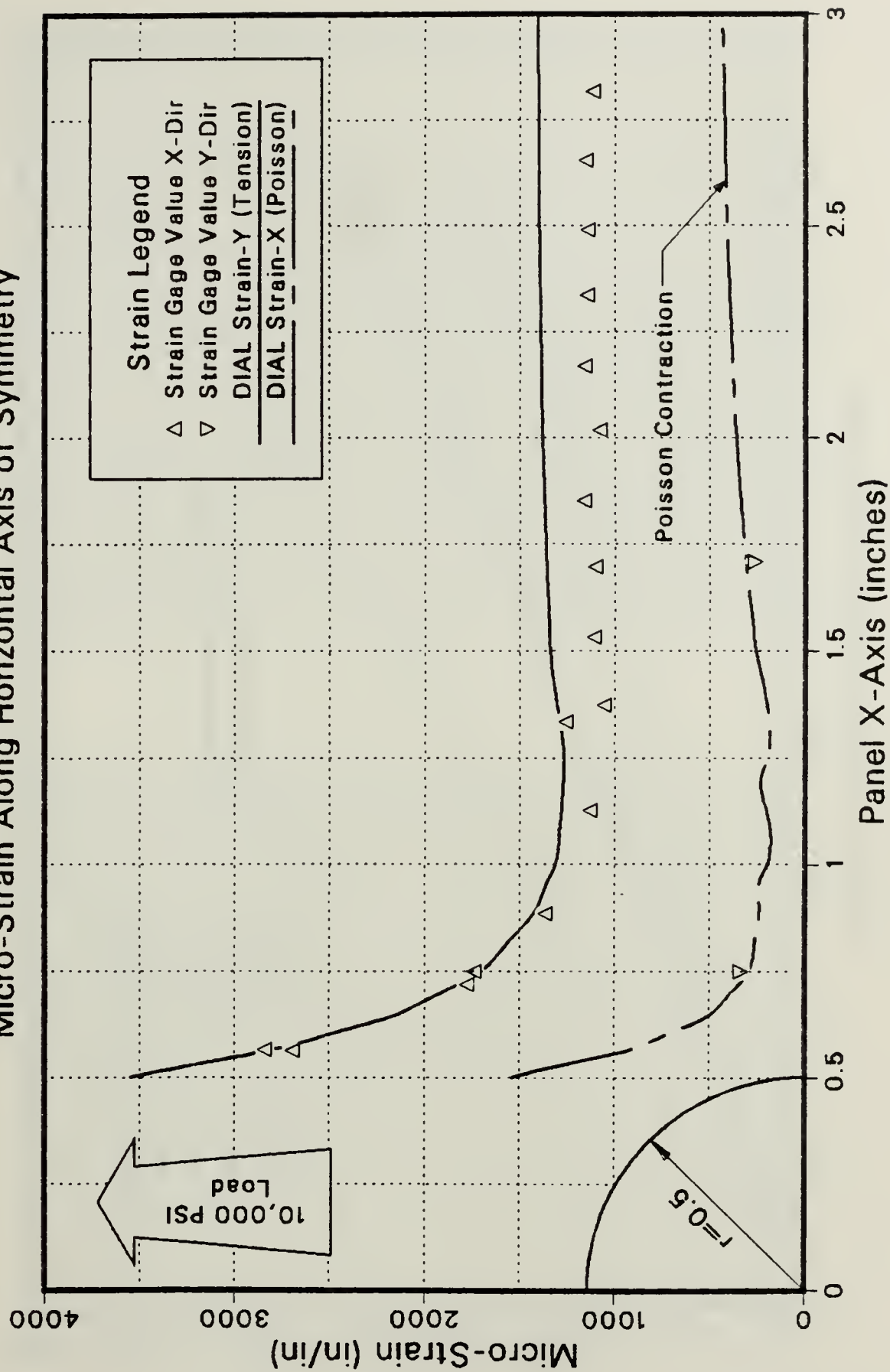


Figure D.2 Panel 2B: Strain Along X Axis at 10,000 psi.

Panel 2B: 45 Degree, 206 Percent Reinforcement

Micro-Strain vs Tensile Load

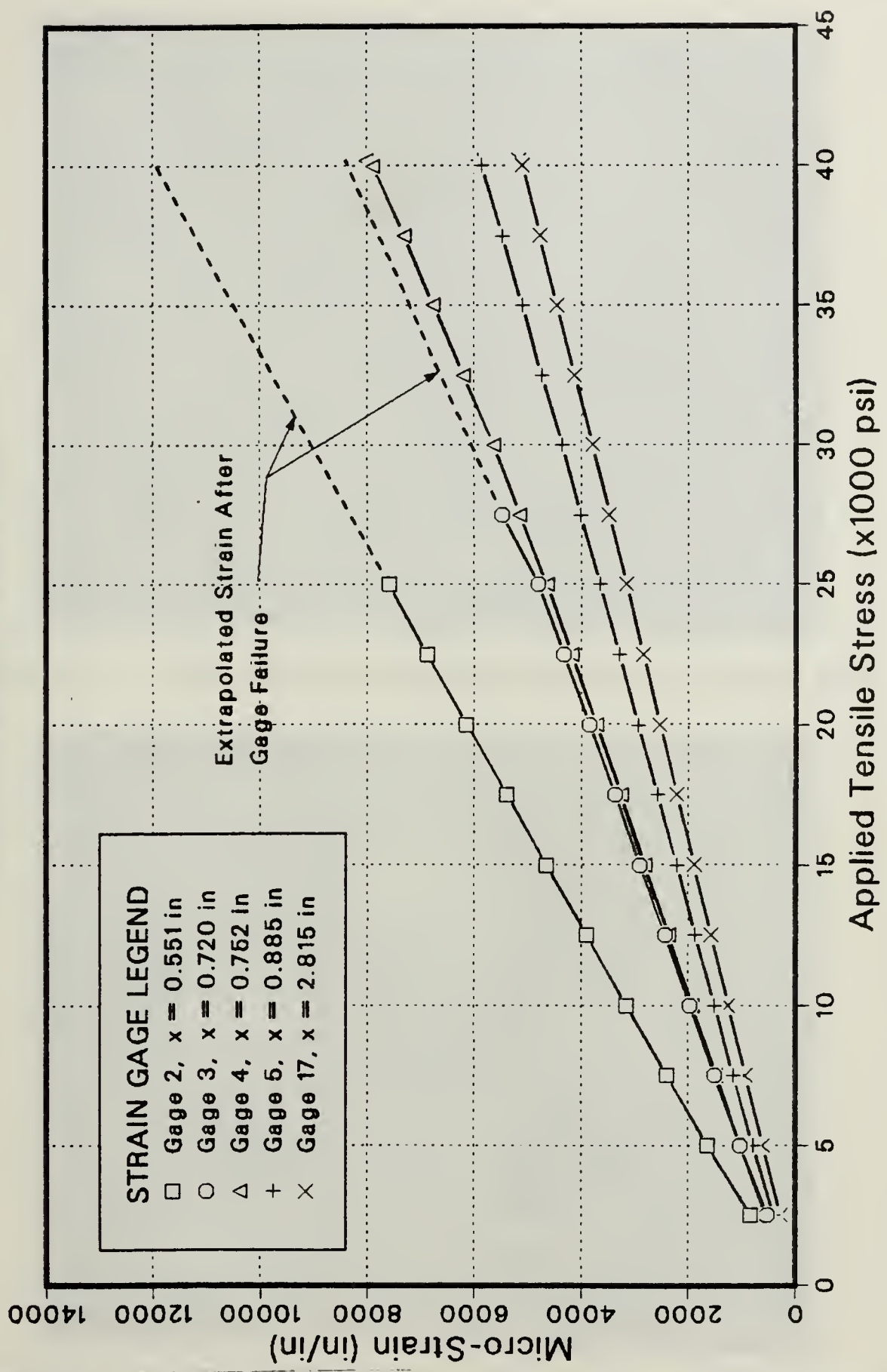


Figure D.3 Panel 2B: Microstrain vs. Tensile Load.

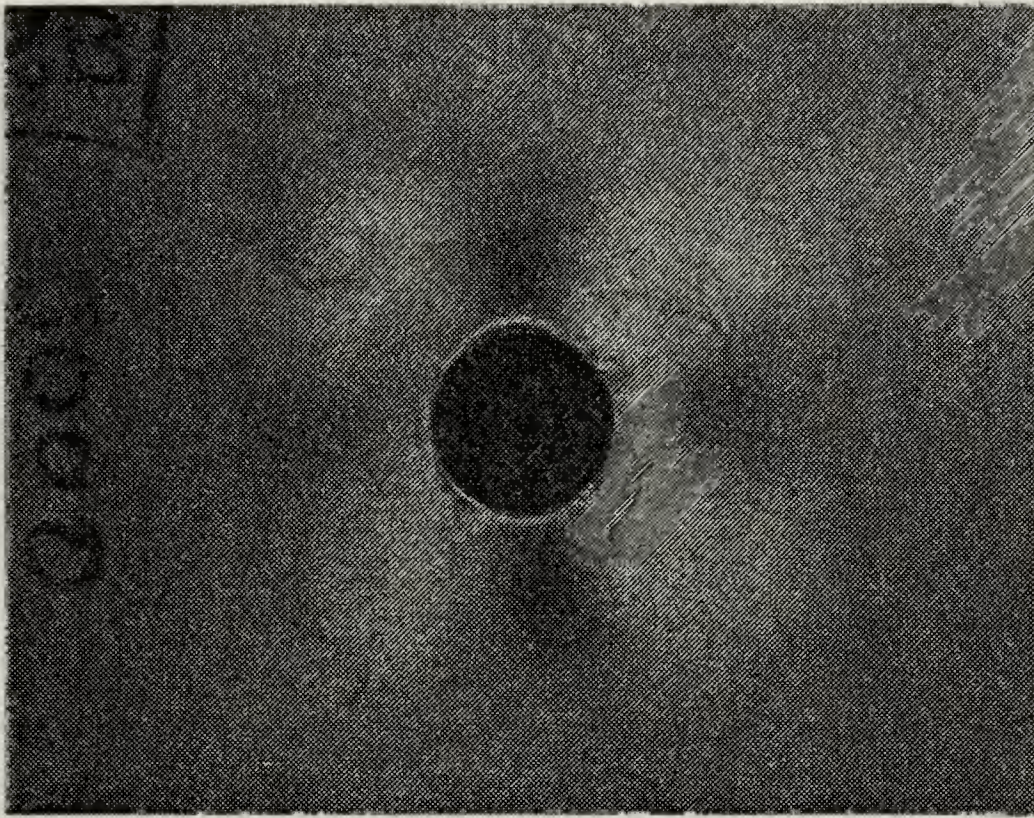


Figure D.4 Panel 2B: Photoelastic Panel at 5,000 psi.

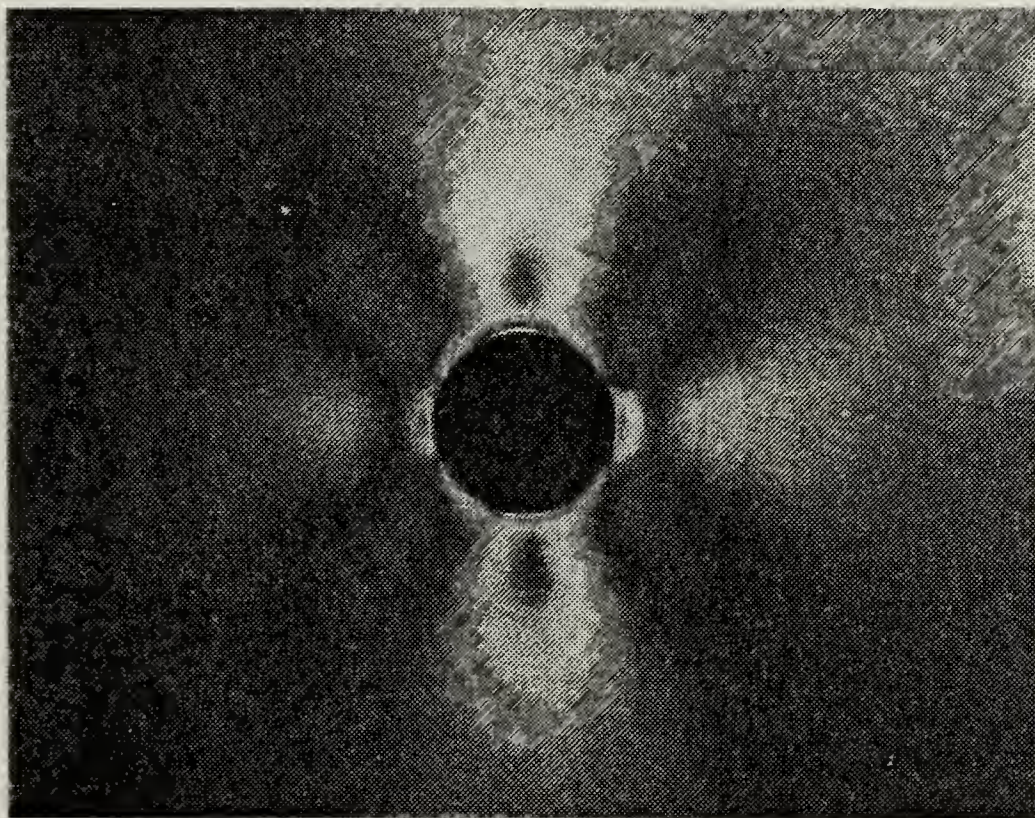


Figure D.5 Panel 2B: Photoelastic Panel at 10,000 psi.

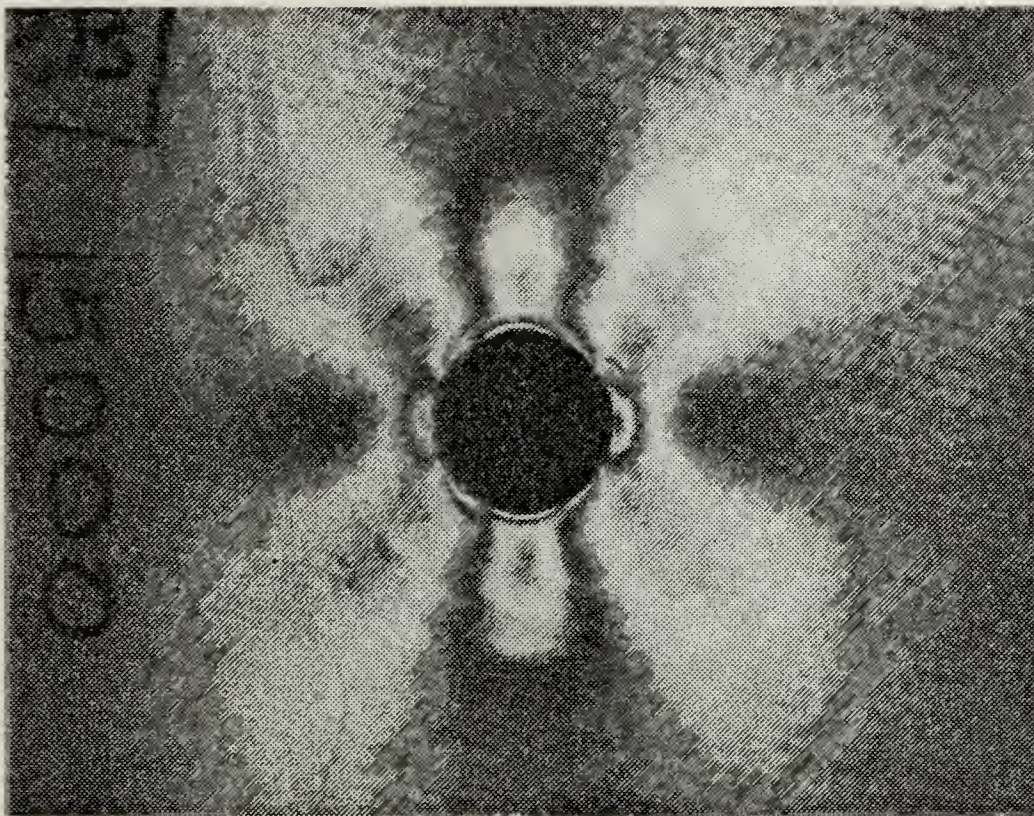


Figure D.6 Panel 2B Photoelastic Panel at 15,000 psi.

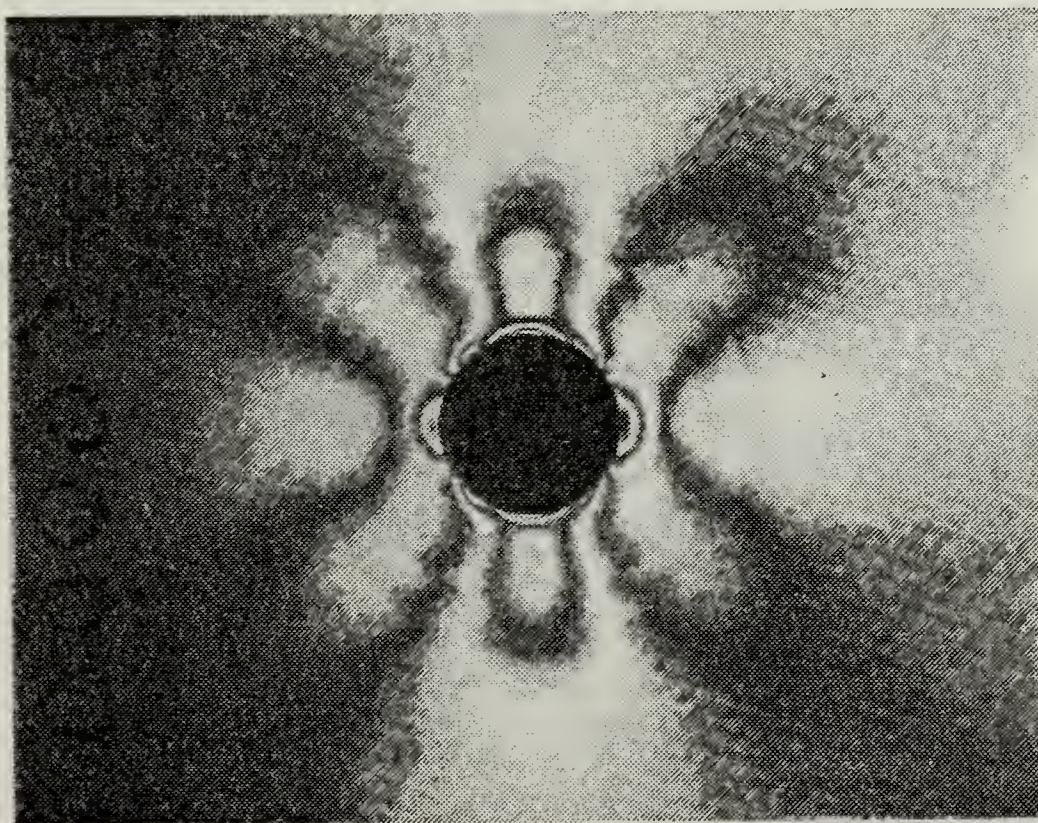


Figure D.7 Panel 2B Photoelastic Panel at 20,000 psi.

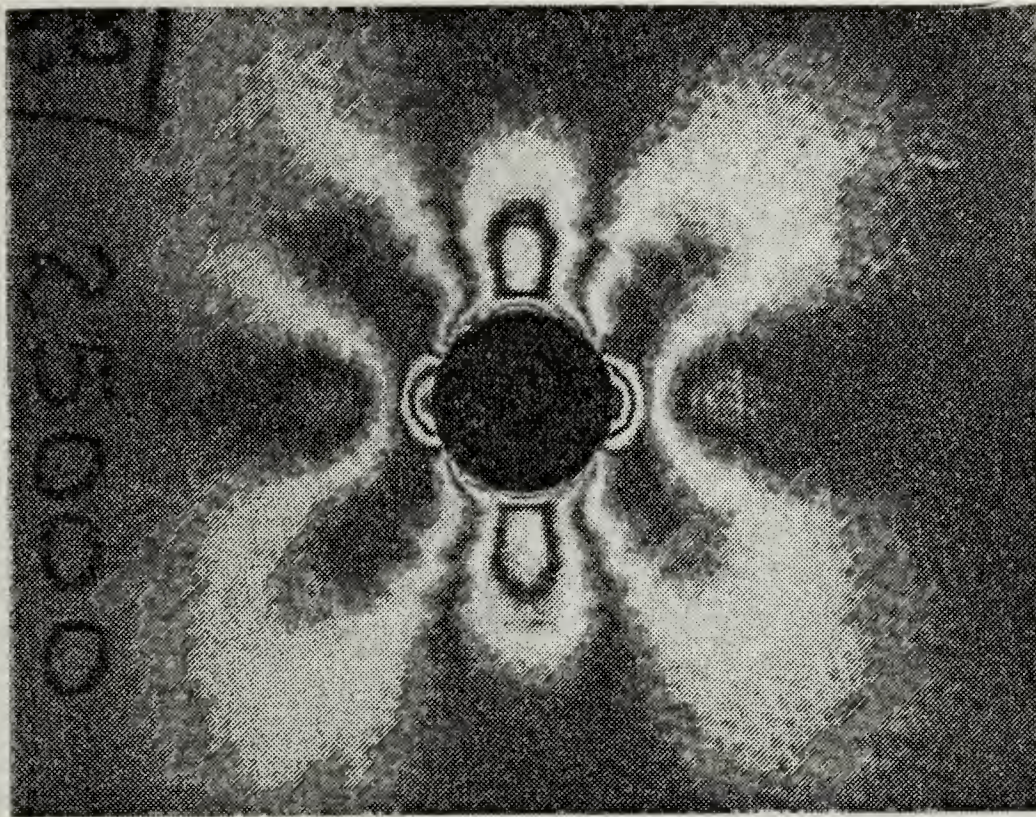


Figure D.8 Panel 2B Photoelastic Panel at 25,000 psi.

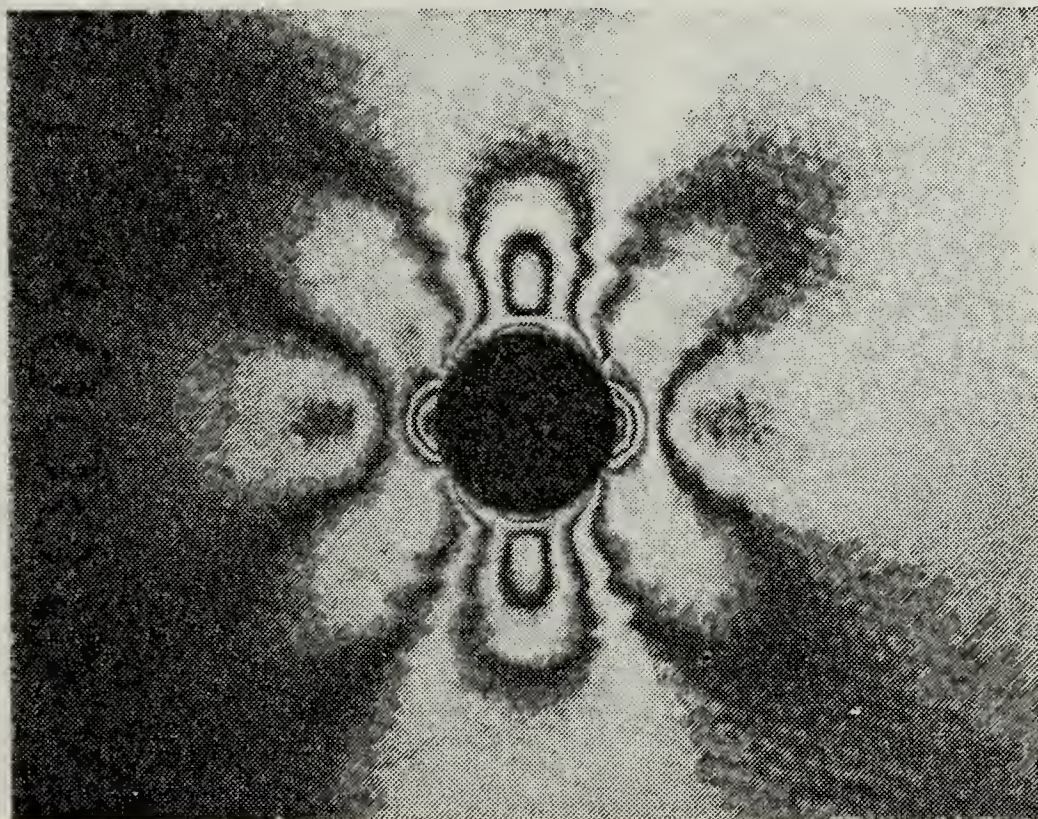


Figure D.9 Panel 2B: Photoelastic Panel at 30,000 psi.

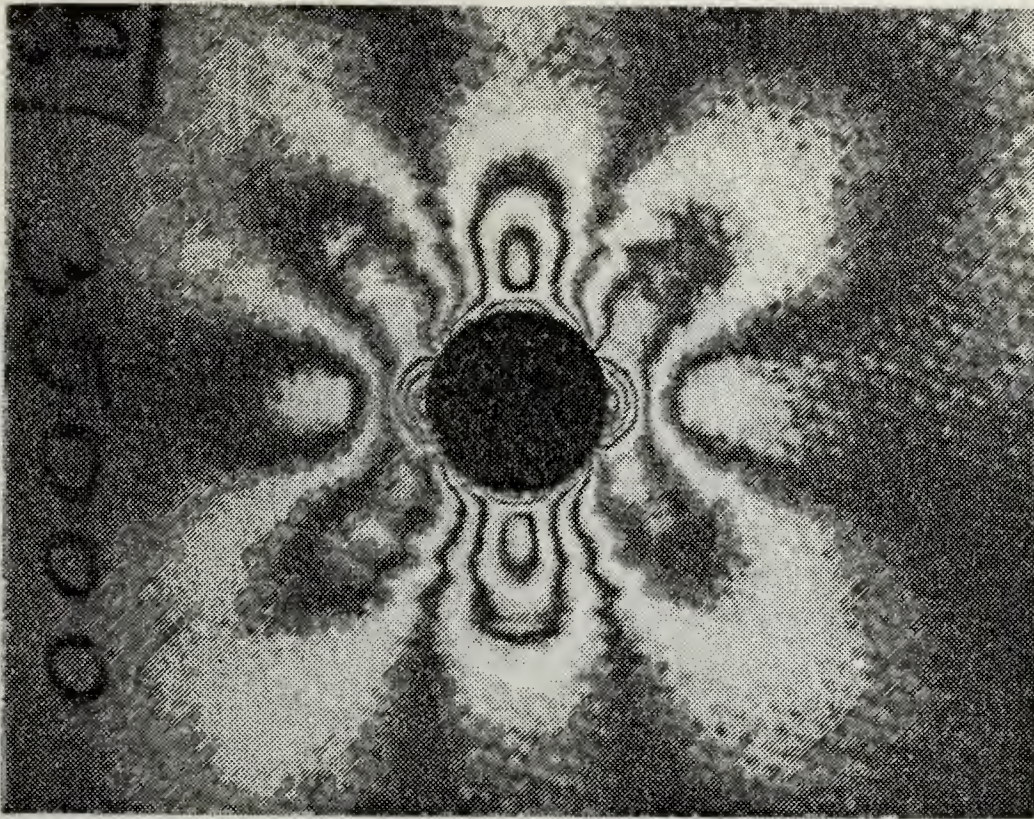


Figure D.10 Panel 2B: Photoelastic Panel at 35,000 psi.

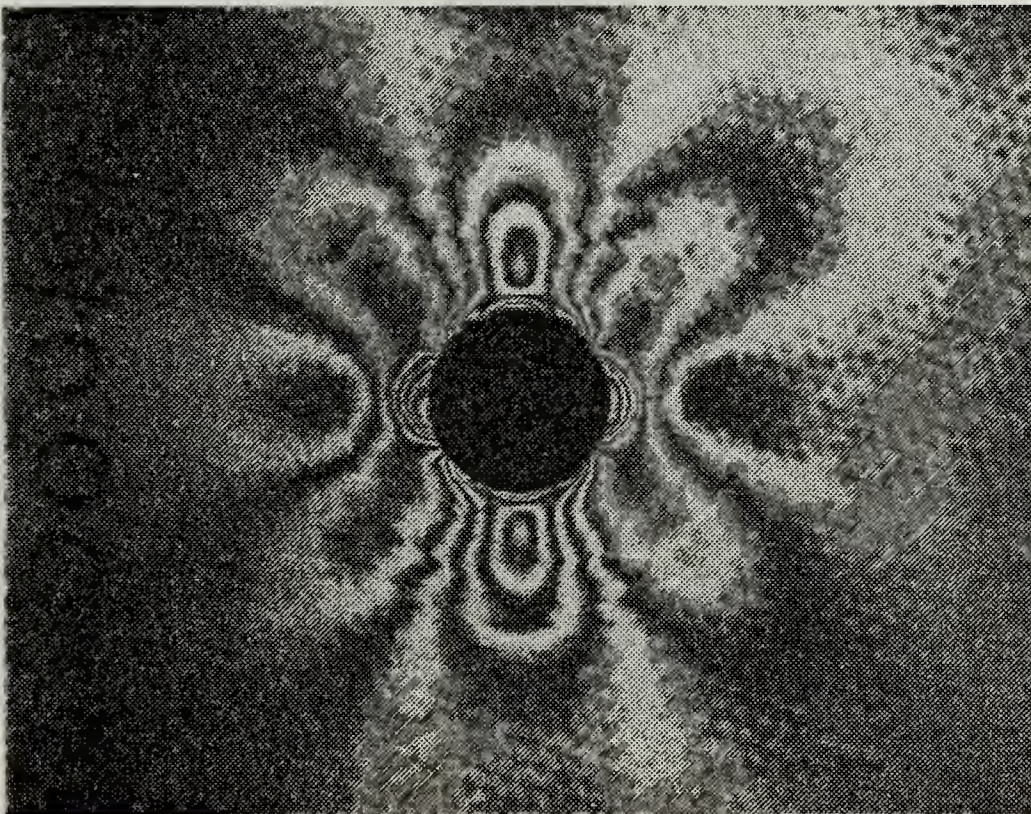


Figure D.11 Panel 2B: Photoelastic Panel at 40,000 psi.

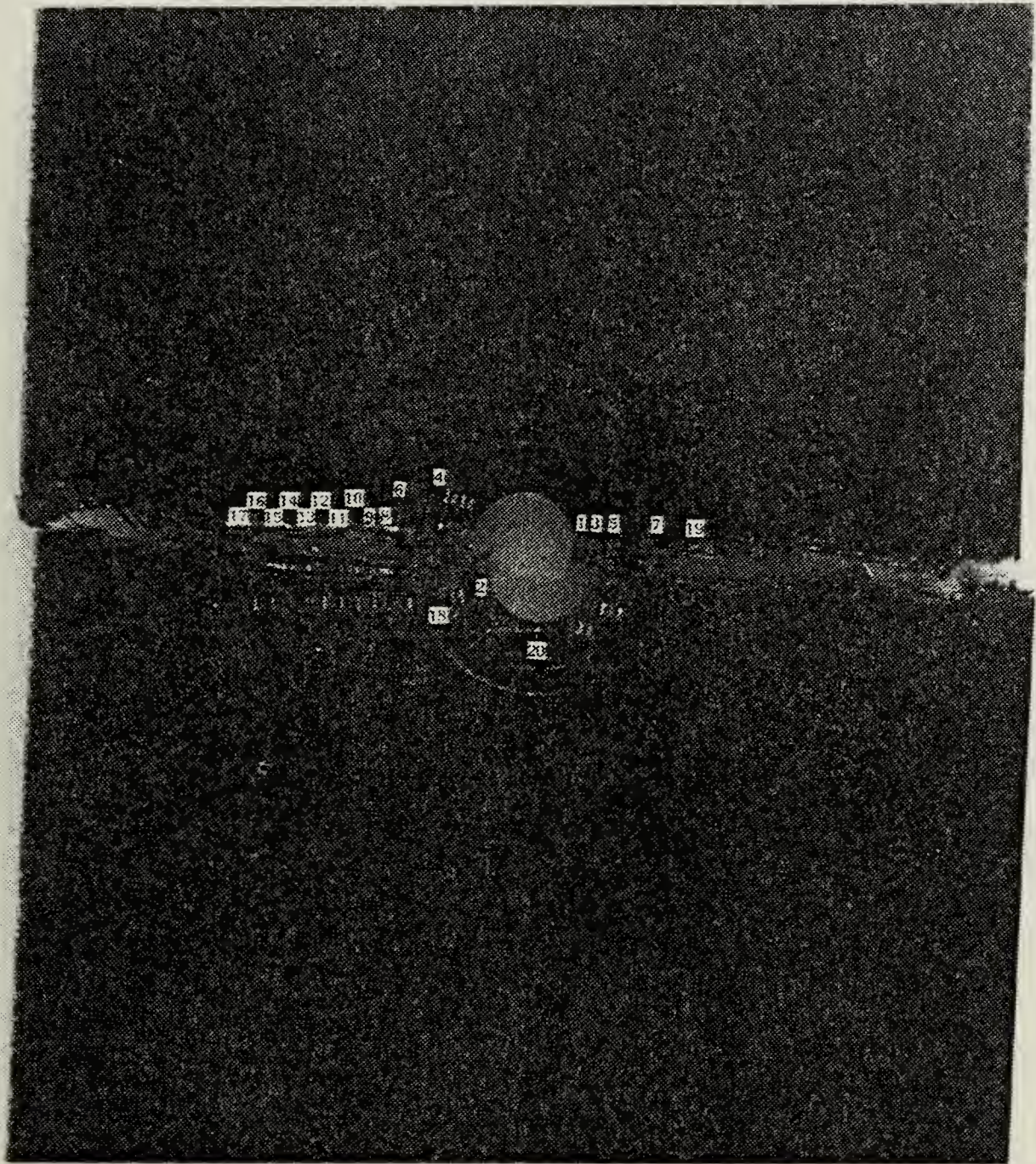


Figure D.12 Panel 2B: Fracture Line.

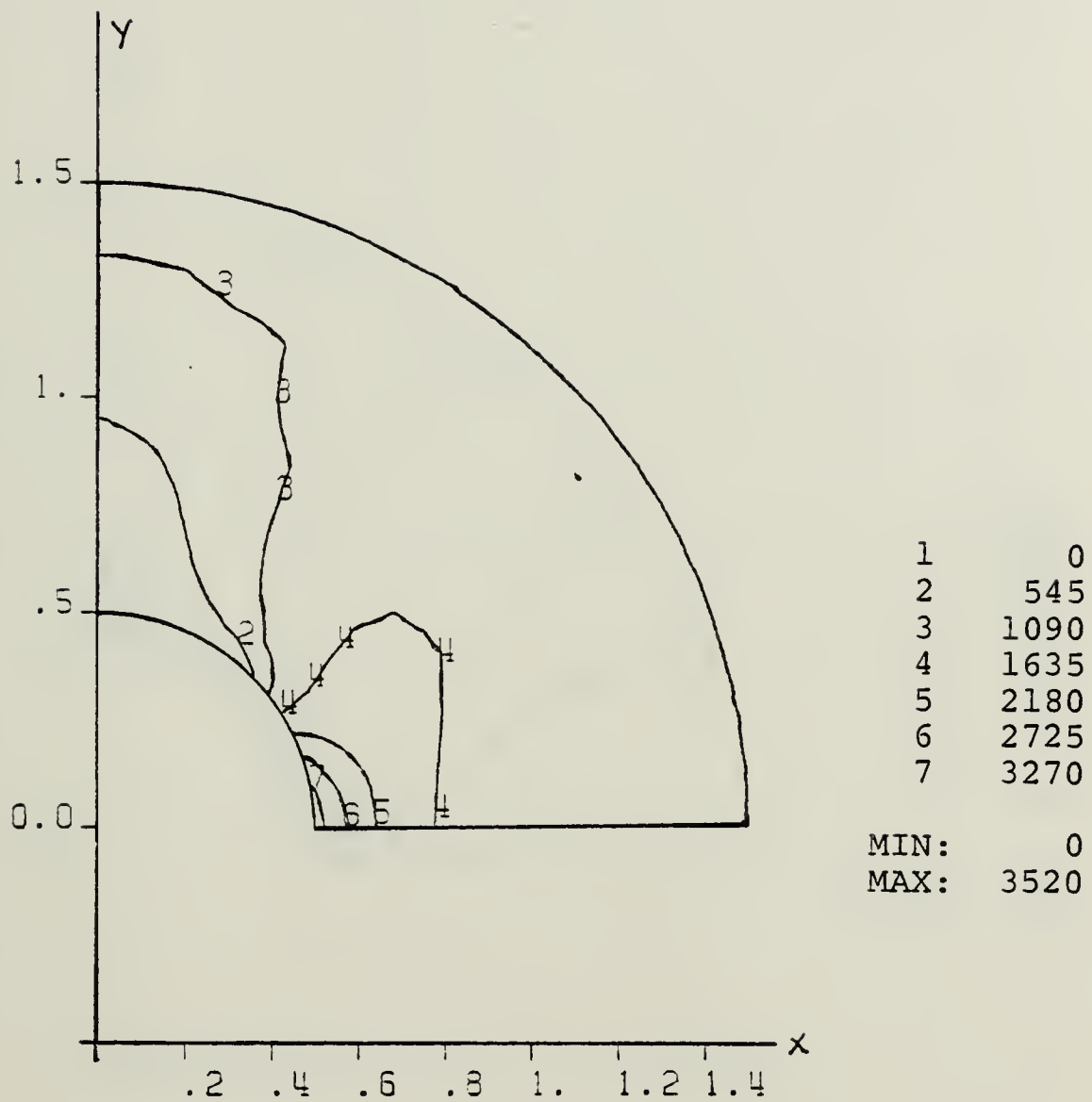


Figure D.13 Panel 2B: Eps-Y ($\times 10^6$) Contours Near Cutout.

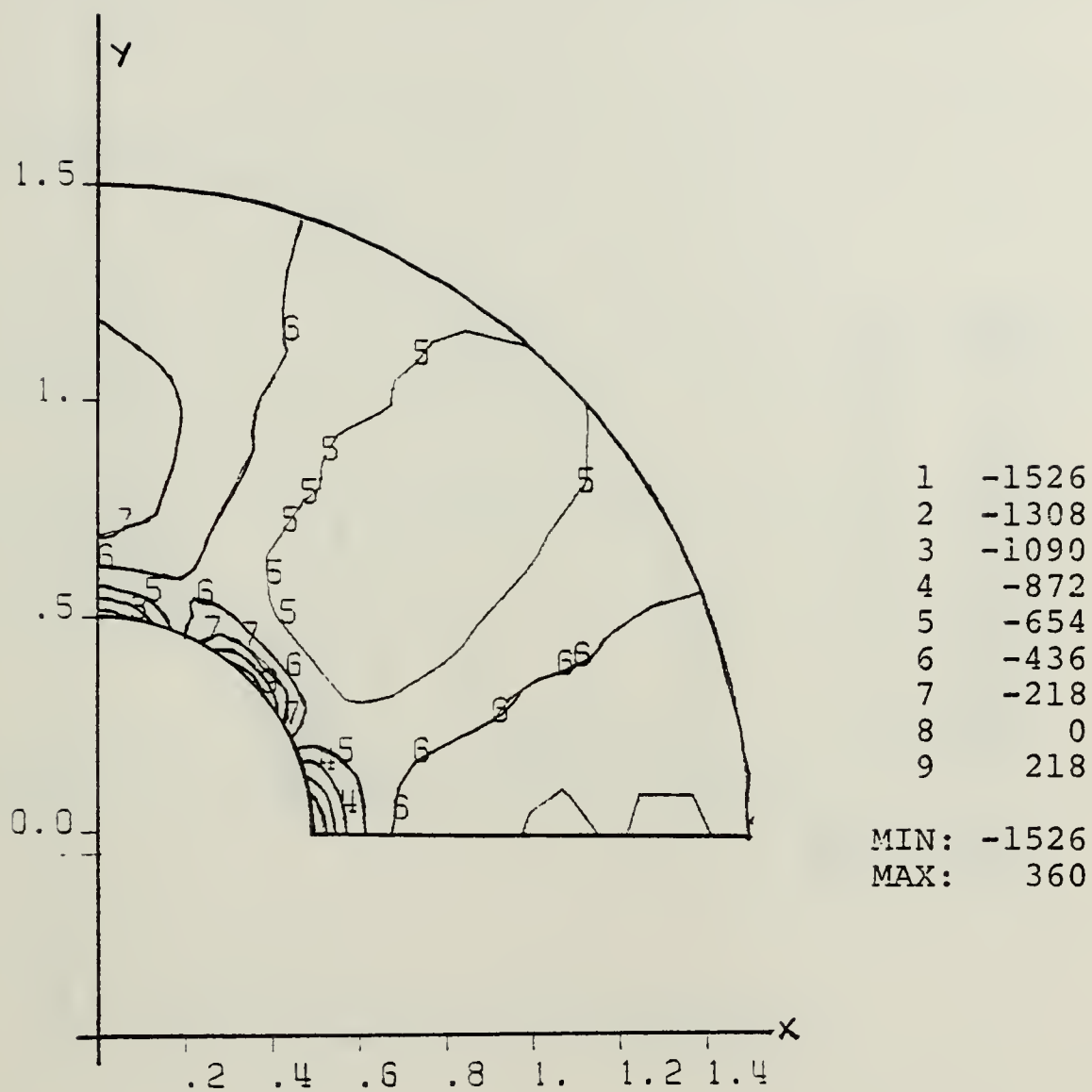


Figure D.14 Panel 2B: Eps-X ($\times 10^6$) Contours Near Cutout.

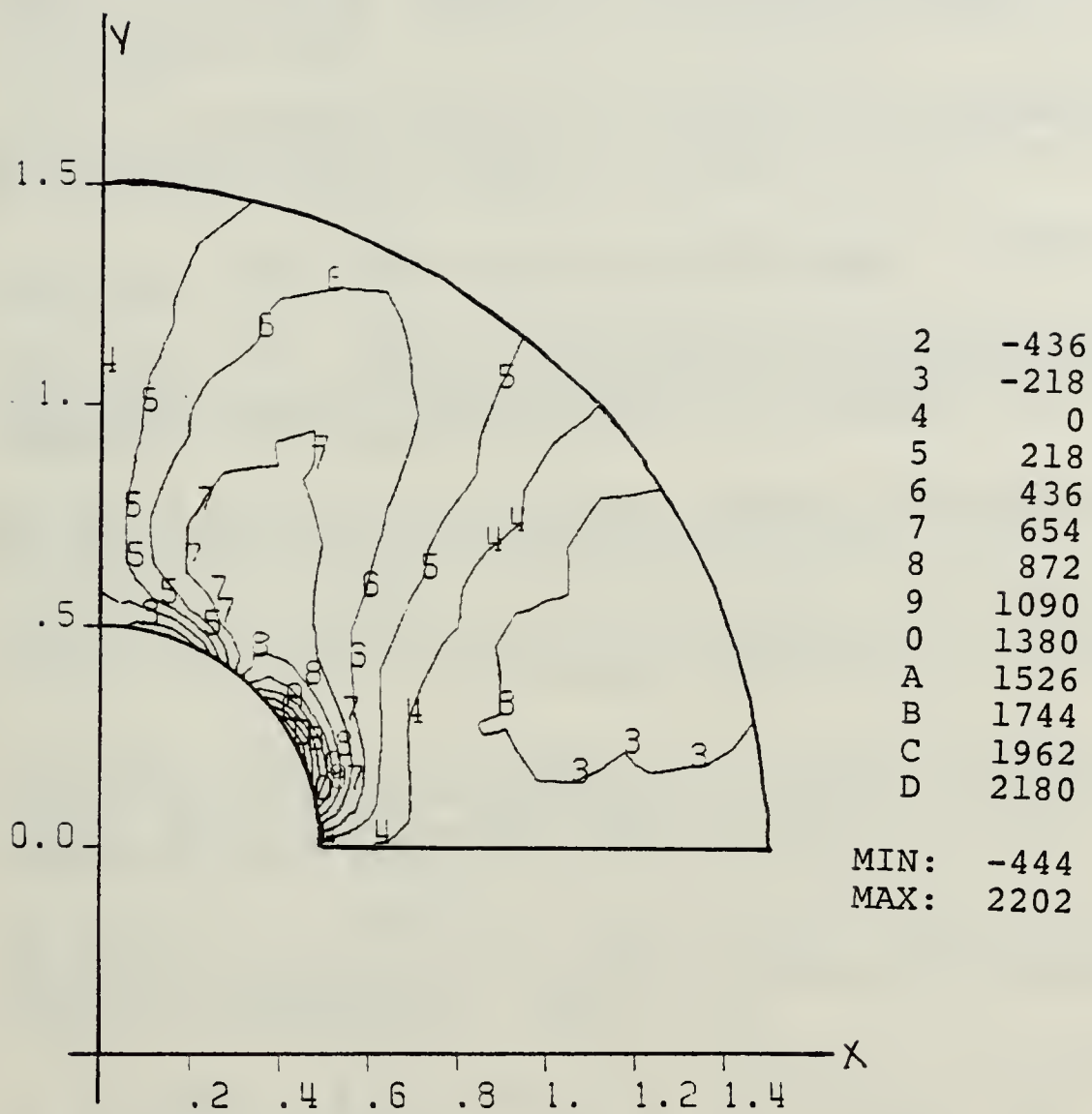


Figure D.15 Panel 2B: Eps-XY ($\times 10^6$) Contours Near Cutout.

LIST OF REFERENCES

1. Delmonte, J., Technology of Carbon and Graphite Fiber Composites, Van Nostrand Reinhold Co., 1981
2. Applied Technology Laboratory, TR 80-D-36A, Advanced Composite Airframe Program - Preliminary Design, v. 1 - Basic Report (Part 1), by R. J. Ford, and others, p. 43 - 92, December 1981.
3. Applied Technology Laboratory, TR 80-D-39A, Advanced Composite Airframe Program - Preliminary Design, v. 1 - Basic Report (Part 2), by R. E. Goodall and R. E. Head, p. 383 - 396, January 1982.
4. Tsai, S. W. and Hahn, R. H., Introduction to Composite Materials, Technomic Publishing Co., 1980.
5. Air Force Wright Aeronautical Laboratories Technical Report 81-3041, Effect of Variances and Manufacturing Tolerances on the Design Strength and Life of Mechanically Fastened Composite Joints, Vol 1-3, by Garbo, S.P. and Ogonowski, J.M., April 1981
6. Air Force Materials Laboratory, Advanced Composites Design Guide, Air Force Systems Command, Wright-Patterson AFB, Ohio, Vol II, Section 2.5.1, 1973.
7. Daniel, I.M., Rowlands, R.E., Whiteside, J.B., "Effects of Material and Stacking Sequence on Behavior of Composite Plates with Holes", Experimental Mechanics, Jan. 1974, p. 1.
8. Rowlands, R.E., I. M. Daniel, and J. B. Whiteside, "Geometric and Loading Effects on Strength of Composite plates with Cutouts", Composite Materials: Testing and Design (Third Conference), ASTM STP 546, American Society for Testing and Materials, p. 361, 1974.
9. Daniel, I. M., Rowland, R. E., and Whiteside, J. B., "Deformation and Failure of Boron-Epoxy Plate with Circular Hole", Analysis of the Test Methods for High Modulus Fibers and Composites, ASTM STP 521, American Society for Testing and Materials, August 1973.
10. Konish, H.J. and Whitney, J.M., "Approximate Stresses in an Orthotropic Plate Containing a Circular Hole", Journal of Composite Materials, Vol. 9, pp. 157-166, Apr. 1975.
11. Waddoups, M.E., Eisenmann, J.R. and Kaminski, B.E., "Macroscopic Fracture Mechanics of Advanced Composite Materials", Journal of Composite Materials, Vol. 5, pp. 446-454, Oct. 1971.
12. Garbo, S.P. and Ogonowski, J.M., "Strength Predictions of Composite Laminates with Unloaded Fastener Holes", AIAA Journal, Vol. 18, pp. 585-589, May 1980.
13. Whitney, J.M. and Nuismer, R.J., "Stress Fracture Criteria for Laminated Composites Containing Stress Concentrations", Journal of Composite Materials, Vol. 8, pp. 253-265, July 1974.

14. Bailie, J.A., Duggan, M.F., Fisher, L.M., and Yee, R.C., "Effects of Holes on Graphite Cloth Epoxy Laminates Tension Strength", Journal of Aircraft Vol. 19, pp. 559-566, July 1982.
15. Kim, R.Y., and Hahn, H.T., "Effect of Curing Stresses on the First ply-failure in Composite Laminates", Journal of Composite Materials, Vol. 13, pp. 2-16, Jan. 1979.
16. McKenzie, D. O., The Analysis of Reinforced Holes in Carbon Fiber Plates, Ph.D. Thesis, University of Bristol, February 1976.
17. O'Neill, G. S., Asymmetric Reinforcement of a Quasi-Isotropic Graphite-Epoxy Plate Containing a Circular Hole, M.S. and Engineer Degree Thesis, Naval Postgraduate School, Monterey, California, June 1982.
18. Ferguson, G.H., Cyr, N., DIAL User's Manual, Lockheed Missiles and Space Co., Sunnyvale, CA, 1982.
19. Sullivan, P.D., Composite Laminate Analysis Program (RSO), Naval Postgraduate School, Monterey CA, (to be published).
20. Ferguson, G.H., Cyr, N., DIAL Finite Element System, Paper presented at 3rd International Seminar on Finite Element Systems., Sept 23-25, 1981, Southampton University, UK.
21. Sullivan, P. D., Analysis of Symmetric Reinforcement of Graphite/Epoxy Honeycomb Sandwich Panels with a Circular Cutout under Uniaxial Compressive Loading, Aeronautical Engineer's (A. Eng.) Thesis, Naval Postgraduate School, Monterey, California, December 1983.
22. "Accurate Strain Gage Measurements at Stress Concentrations", Epsilonics Vol. 1, pp. 10-11, July 1982.
23. Photolastic Inc., Bulletin P-1120-2 Materials for: Photoelastic Coatings/Photoelastic Models, Raleigh, North Carolina.
24. Photolastic Inc., Instruction Manual for 030 Series Reflection Polariscopes, Raleigh, North Carolina.

BIBLIOGRAPHY

Agarwal, B.D., Broutman, L.J., Analysis and Performance of Fiber Composites, John Wiley and Sons, New York, N.Y., 1980.

Crossman, F.W. and Wang, A.S.D., "Stress Field Induced by Transient Moisture Sorption in Finite-Width Composite Laminates," Journal of Composite Materials, Vol. 12, pp. 2-18, Jan. 1978.

Dally, J. W. and Riley, W. F., Experimental Stress Analysis, McGraw-Hill, 1965

De Jong, T., "Stresses Around Pin-Loaded Holes in Elasticity Orthotropic or Isotropic Plates," Journal of Composite Materials, Vol. 11, pp. 313-331, July 1977.

England, A. H., Complex Variable Methods in Elasticity, Wiley-Interscience, 1971

Hahn, H. T. and Pagano, N. J., "Curing Stresses in Composite Laminates," Journal of Composite Materials, Vol. 9, pp. 91-106, Jan. 1975.

Hahn, H. T. and Tsai, S. W., "On behavior of Composite Laminates After Initial ply Failure" Journal of Composite Materials, Vol. 8, pp. 288-305, July 1974.

Jennings, A., Matrix Computation for Engineers and Scientists, Wiley-Interscience, 1977.

Jones, R.M., "Stress-Strain Relations for Materials with Different Moduli in Tension and Compression", AIAA Journal, Vol. 15, pp. 16-22, Jan 1977.

Kuske, A. and Robertson, G., Photoelastic Stress Analysis, Wiley, 1974

Lekhnitskii, S.G., Theory of Elasticity of An Anisotropic Elastic Body, (Translated by P.Fern), Holden-Day, 1963

Loos, A.C., and Springer, G.S., "Effects of Thermal Spiking on Graphite-Epoxy Composites", Journal of Composite Materials, Vol. 13, pp. 17-34, Jan. 1979.

McKenzie, D.O., The Analysis fo Reinforced Holes in Carbon Fibre Plates, Ph.D. Thesis, University of Bristol, Feb. 1976.

Nuismer, R.J., Labor, J.D., "Applications of the Average Stress Failure Criterion: Part I-Tension," Journal of Composite Materials, Vol. 12 (July 1978), p. 238.

Pagano, N.J., "On the Calculation of Interlaminar Normal Stress in Composite Laminate," Journal of Composite Materials, Vol. 8, pp. 65-81, Jan. 1974.

Pagano, N.J. and Rybicki, E.F., "On the Significance of Effective Modulus Solutions for Fibrous Composites", Journal of Composite Materials, Vol. 8, pp. 214-228, July 1974.

Peterson, R.E., Stress Concentration Design Factors Wiley-Interscience, 1974.

Predecki P., and Barrett, C.S., "Stress Measurement in Graphite/Epoxy Composites By X-Ray Diffraction from Fillers"

Journal of Composite Materials, Vol. 13, pp. 61-71, Jan. 1979.

Przemienicki, J. S., Theory of Matrix Structural Analysis, McGraw-Hill Book Co., New York, N.Y., 1968. Chapter 4.

Rowlands, R.E., Daniel, I.M., Whiteside, J.B., "Stress and Failure Analysis of a Glass-Epoxy Plate with a Circular Hole", Experimental Mechanics, Jan. 1973, p.31.

Royal Aeronautical Society, "Stress Concentration Data", issued September 1965.

Tang, S., "A Boundary Layer Theory - Part I: Laminated Composites in Plane Stress", Journal of Applied Mechanics, Vol. 9, pp. 33-41, Jan. 1975.

Tang, S., "Interlaminar Stresses around Circular Cutouts in Composite plates under Tension", AIAA Journal, Vol. 15, pp. 1631-1637, Nov. 1977.

Tang, S., "Interlaminar Stresses of Uniformly Loaded Rectangular Composite Plates", Journal of Composite Materials, Vol. 10, pp. 69-78, Jan. 1975.

Timoshenko, S. P., Strength of Materials, Part II, Van Nostrand Co., Princeton, N.J.

Timoshenko, S. P. and Goodier, A. A., Theory of Elasticity, Second Edition, McGraw-Hill Book Co., New York, 1951.

Ugural, A. C. and Fenster, S. K., Advanced Strength and Applied Elasticity, Elsevier, 1981.

Wang, A.S.D. and Crossman, F.W., "Some New Results on Edge Effect in Symmetric Composite Laminates", Journal of Composite Materials, Vol. 11, pp. 92-106, Jan. 1977.

Wang, S.S. and Choi, I., "Boundary-Layer Effects in Composite Laminates: Part 1 - Free-Edge Stress Singularities", Journal of Applied Mechanics, Vol. 19, pp. 541-548, Sep. 1982.

Wang, S.S. and Choi, I., "Boundary-Layer Effects in Composite Laminates: Part 2 - Free-Edge Stress Solutions and Basic Characteristics", Journal of Applied Mechanics, Vol. 19, pp. 549-560, Sep. 1982.

Waddoups, M.E., Eisenmann, J.R. and Kaminski, B.E., "Macroscopic Fracture Mechanics of Advanced Composite Materials", Journal of Composite Materials, Vol. 5, pp. 446-454, Oct. 1971.

INITIAL DISTRIBUTION LIST

	No. Copies
1. Defense Technical Information Center Cameron Station Alexandria, Virginia 22314	2
2. Library, Code 0142 Naval Postgraduate School Monterey, California 93943	2
3. Department Chairman, Code 67 Department of Aeronautics Naval Postgraduate School Monterey, California 93943	1
4. Professor Milton H. Bank, Code 67Bt Department of Aviation Safety Naval Postgraduate School Monterey, California 93943	8
5. Dr. J.A. Bailie Organization 81-12, Building 154 Lockheed Missiles and Space Company PO Box 504 Sunnyvale, California 90486	5
6. Composite Materials Laboratory, Code 67 Department of Aeronautics Naval Postgraduate School Monterey, California 93943	5
7. CDR P.D. Sullivan, USN 9226 Whitney Street Silver Spring, Maryland, 20901	1
8. Cpt. D.H. Pickett, USA U. S. Army Safety Center Fort Rucker, Alabama 32326	5
9. LCDR G.H. O'Neill, USN Operations Department USS Okinawa (LPH 3) FPO, San Francisco 96625	1

297416

Thesis

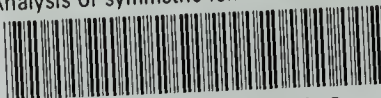
P488 Pickett

c.1 Analysis of symmetric
reinforcement of Quasi-
Isotropic Graphite-Epoxy
plates with a circular
cutout under uniaxial
tensile loading.



thesP488

Analysis of symmetric reinforcement of Q



3 2768 001 92383 2
DUDLEY KNOX LIBRARY